

**NUMERICAL ANALYSIS OF PRECAST RUBBERIZED  
LIGHTWEIGHT CONCRETE WALL PANEL**

**LAI JIN MING**

**A project report submitted in partial fulfilment of the  
requirements for the award of Bachelor of Engineering  
(Honours) Civil Engineering**

**Lee Kong Chian Faculty of Engineering and Science  
Universiti Tunku Abdul Rahman**

**May 2021**

**DECLARATION**

I hereby declare that this project report is based on my original work except for citations and quotations which have been duly acknowledged. I also declare that it has not been previously and concurrently submitted for any other degree or award at UTAR or other institutions.

Signature :  \_\_\_\_\_

Name : Lai Jin Ming


ID No. : 1604805

Date : 07 May 2021

**APPROVAL FOR SUBMISSION**

I certify that this project report entitled “**NUMERICAL ANALYSIS OF PRECAST RUBBERIZED LIGHTWEIGHT CONCRETE WALL PANEL**” was prepared by **LAI JIN MING** has met the required standard for submission in partial fulfilment of the requirements for the award of Bachelor of Engineering (Honours) Civil Engineering at Universiti Tunku Abdul Rahman.

Approved by,

Signature :  \_\_\_\_\_

Supervisor : Dr. Lau See Hung

Date : 07 May 2021

The copyright of this report belongs to the author under the terms of the copyright Act 1987 as qualified by Intellectual Property Policy of Universiti Tunku Abdul Rahman. Due acknowledgement shall always be made of the use of any material contained in, or derived from, this report.

© 2021, LAI JIN MING. All right reserved.

## **ACKNOWLEDGEMENTS**

I would like to thank everyone who had contributed to the successful completion of this project. I would like to express my gratitude to my research supervisor, Dr. Lau See Hung for her invaluable advice, guidance and her enormous patience throughout the development of the research.

In addition, I would also like to express my gratitude to my loving parents and friends who had helped and given me encouragement for this research project.

## ABSTRACT

Precast concrete wall panels are common prefabricated building components used to replace conventional burnt clay bricks as non-load bearing walls. Recent researches focused on lightweight concrete wall panel due to its low density which would lead to the reduction in total building load. This research aimed to evaluate the engineering properties of precast rubberized lightweight concrete wall panel subjected to compressive loading through numerical analysis software, ABAQUS. Concrete smeared cracking was used to model the behaviour of concrete. A comparative study was conducted to examine the differences between the control sample and rubberized concrete wall panel under compressive strength. Next, separate rubberized concrete wall panel with calcium silicate board and concrete capping were modelled to evaluate the confining effect. Lastly, a combined wall panel was modelled, which comprises three single rubberized concrete wall panels to assess its actual behaviour in real-life practice. At 7.5 % crumb rubber replacement, the ultimate compressive strength reduced by 13 %, followed by an improvement in ultimate strain by 5 %. Both concrete capping and calcium silicate board did not cause any significant impact on the ultimate compressive strength but drop in ultimate strain by 11 % and 5 %, respectively. The numerical results underlined that the ultimate strain for the combined rubberized concrete wall panel had significantly improved from 0.0018 to 0.0027. Further research could be carried out with a higher crumb rubber replacement rate and different slenderness ratio.

## TABLE OF CONTENTS

<b>DECLARATION</b>		<b>i</b>
<b>APPROVAL FOR SUBMISSION</b>		<b>ii</b>
<b>ACKNOWLEDGEMENTS</b>		<b>iv</b>
<b>ABSTRACT</b>		<b>v</b>
<b>TABLE OF CONTENTS</b>		<b>vi</b>
<b>LIST OF TABLES</b>		<b>x</b>
<b>LIST OF FIGURES</b>		<b>xi</b>
<b>LIST OF SYMBOLS / ABBREVIATIONS</b>		<b>xv</b>
<b>CHAPTER</b>		
<b>1</b>	<b>INTRODUCTION</b>	<b>1</b>
1.1	General Introduction	1
1.2	Problem Statement	2
1.3	Aim and Objectives	3
1.4	Scope and Limitation of the Study	3
1.5	Importance of the Study	4
1.6	Layout of Thesis	4
<b>2</b>	<b>LITERATURE REVIEW</b>	<b>6</b>
2.1	Introduction	6
2.2	Lightweight Concrete	7
2.2.1	Lightweight Aggregate Concrete	7
2.2.2	Aerated Concrete	7
2.2.3	Foamed Concrete	8
2.2.4	No-fines Concrete	8
2.3	Rubberized Concrete	8
2.4	Classification of Rubber	10
2.4.1	Rubber Chips	10
2.4.2	Ground Rubber Powder	11
2.4.3	Crumb Rubber	11

2.5	Application of Crumb Rubber	11
2.6	Crumb Rubber Lightweight Foamed Concrete	12
2.7	Fresh Properties of Rubberized Concrete	13
	2.7.1 Workability	13
2.8	Hardened Properties of Rubberized Concrete	14
	2.8.1 Density	14
	2.8.2 Compressive Strength	15
	2.8.3 Splitting Tensile Strength	16
	2.8.4 Young's Modulus	17
2.9	Finite Element Analysis	18
	2.9.1 Constitutive Model for Concrete	18
	2.9.2 Numerical Analysis of Rubberized Concrete	19
2.10	Summary	21
<b>3</b>	<b>METHODOLOGY</b>	<b>22</b>
3.1	Introduction	22
3.2	Research Flowchart	22
3.3	Modelling Considerations	24
3.4	System of Units	25
3.5	Extraction of Material Properties from Past Literature	25
3.6	Construct Geometry Model	26
3.7	Flowchart for Defining Material Properties	32
3.8	Material Properties for Plain Concrete and Rubberized Concrete	34
	3.8.1 Elastic Behaviour	34
	3.8.2 Plastic Behaviour	35
	3.8.2.1 Concrete Smearred Cracking	36
	3.8.2.2 Failure Ratios	38
	3.8.2.3 Tension Stiffening	40
3.9	Material Properties for Calcium Silicate Board	42
	3.9.1 Elastic Behaviour	42
	3.9.2 Extended Finite Element Method (XFEM)	43
	3.9.2.1 Damage Initiation Criteria	43



	3.9.2.2	Damage Evolution	44
3.10		Specify Steps and Field Output Request	45
3.11		Specify Interactions	48
	3.11.1	General Contact	48
	3.11.2	Tie Constraint	50
	3.11.3	Define Enriched Region for XFEM	51
3.12		Specify Boundary Conditions	52
3.13		Specify Loading Conditions	54
3.14		Meshing	56
3.15		Summary	57
<b>4</b>		<b>RESULTS AND DISCUSSION</b>	<b>58</b>
4.1		Introduction	58
4.2		Control Sample for Concrete Wall Panel	58
	4.2.1	Influence of Slenderness Ratio	58
	4.2.2	Compressive Strength	59
4.3		Precast Rubberized Lightweight Concrete Wall Panel	63
	4.3.1	Influence of Slenderness Ratio	63
	4.3.2	Compressive Strength	64
4.4		Precast Rubberized Lightweight Concrete Wall Panel with Calcium Silicate Board	68
	4.4.1	Influence of Slenderness Ratio	68
	4.4.2	Compressive Strength	68
4.5		Comparative Study between Control-Wall, 7.5 % Crumb-Wall and 7.5 % Crumb-Wall + CS	73
	4.5.1	Suitability of Concrete Constitutive Model	73
	4.5.2	Compressive Stress-Strain Behaviour	75
	4.5.3	Stress Distribution	76
4.6		Precast Rubberized Lightweight Concrete Wall Panel with Concrete Capping	79
	4.6.1	Influence of Slenderness Ratio	79
	4.6.2	Compressive Strength	79
4.7		Combination of Three Precast Rubberized Lightweight Concrete Wall Panel	83

4.7.1	Influence of Slenderness Ratio	83
4.7.2	Compressive Strength	84
4.8	Summary	87
<b>5</b>	<b>CONCLUSION AND RECOMMENDATIONS</b>	<b>88</b>
5.1	Conclusion	88
5.2	Limitations and Recommendations for Future Research	90
	<b>REFERENCES</b>	<b>91</b>

**LIST OF TABLES**

Table 3.1:	List of consistent units in ABAQUS.	25
Table 3.2:	Designation and description for each simulation model.	27
Table 3.3:	Young's Modulus for plain concrete and rubberized concrete (Siringi, 2012).	34
Table 3.4:	Absolute compressive stress and plastic strain for plain concrete beyond elastic range (Siringi, 2012).	37
Table 3.5:	Absolute compressive stress and plastic strain for rubberized concrete beyond elastic range (Siringi, 2012).	37
Table 3.6:	Definition of each failure ratios.	38
Table 3.7:	Default value for failure ratio 1, 3 and 4.	39
Table 3.8:	Values for failure ratio 2 (Siringi, 2012).	39
Table 3.9:	Tension stiffening values (Siringi, 2012).	40
Table 4.1:	Percentage difference between numerical and theoretical value for ultimate compressive stress and ultimate strain.	74
Table 4.2:	Summary of numerical and theoretical value in terms of ultimate compressive stress and ultimate strain.	74

## LIST OF FIGURES

Figure 3.1:	Flowchart for methodology	23
Figure 3.2:	Compressive load test based on ASTM E72-15 (American Society for Testing and Materials, 2015).	24
Figure 3.3:	Standard dimension of 1500 mm x 600 mm x 63 mm for Control-Wall and 7.5 % Crumb-Wall.	27
Figure 3.4:	Illustration for third model, 7.5 % Crumb-Wall + CS.	28
Figure 3.5:	Modelling for fourth model, 7.5 % Crumb-Comb Wall in ABAQUS.	28
Figure 3.6:	Definition of wall panel as three-dimensional, deformable solid elements under part module.	29
Figure 3.7:	Definition of wall panel as homogenous solid in property module.	29
Figure 3.8:	The use of face-to-face constraint to align calcium silicate board to the surface of core panel.	30
Figure 3.9:	The use of face-to-face constraint to position concrete capping to the top surface of panel.	31
Figure 3.10:	The use of face-to-face constraint to align the wall panels side by side.	31
Figure 3.11:	Flowchart for defining material properties in ABAQUS.	33
Figure 3.12:	Input parameters for elastic behaviour of control concrete wall panel.	34
Figure 3.13:	Input parameters for elastic behaviour of rubberized concrete wall panel.	35
Figure 3.14:	Input values for concrete smeared cracking to simulate non-linear behaviour of control concrete wall panel.	37
Figure 3.15:	Input values for concrete smeared cracking to simulate non-linear behaviour of rubberized concrete wall panel.	38
Figure 3.16:	Defining failure ratios for control concrete wall panel.	39
Figure 3.17:	Defining failure ratios for rubberized concrete wall panel.	40

Figure 3.18:	Defining tension stiffening for control concrete wall panel.	41
Figure 3.19:	Defining tension stiffening for rubberized concrete wall panel.	41
Figure 3.20:	Input parameters for elastic behaviour of calcium silicate board.	42
Figure 3.21:	MAXPS value for calcium silicate board.	44
Figure 3.22:	Defining damage evolution for calcium silicate board using fracture energy criterion.	45
Figure 3.23:	Both static, general and Nlgeom have been defined in step module.	46
Figure 3.24:	The increment size has been kept small with automatic control being selected.	46
Figure 3.25:	PHILSM, PSILSM and STATUSXFEM have been requested to output database.	48
Figure 3.26:	Input value for friction coefficient between concrete capping and wall panel.	49
Figure 3.27:	Definition of normal behaviour as hard contact between concrete capping and wall panel.	49
Figure 3.28:	Defining tie constraint for tying wall panels side-by-side.	50
Figure 3.29:	Defining tie constraint between the surfaces of calcium silicate board and core panel.	51
Figure 3.30:	Specifying enriched region for calcium silicate board.	52
Figure 3.31:	Defining ENCASTRE for bottom surface of wall panel.	53
Figure 3.32:	Defining top surface of wall panel as pinned support.	54
Figure 3.33:	Applying maximum value of uniform pressure load on top surface of wall panel with linear ramp pattern.	55
Figure 3.34:	Specifying C3D8R as mesh elements under mesh module.	56
Figure 3.35:	Defining seeding size of 0.03 for wall panel.	57
Figure 4.1:	Failure mode for Control-Wall and the location of concrete bulging.	59

Figure 4.2:	Numerical compressive stress-strain graph for Control-Wall.	60
Figure 4.3:	Contour plot for Control-Wall at the yield point.	61
Figure 4.4:	Magnified view for showing the location of critical yield strain for Control-Wall.	62
Figure 4.5:	Contour plot for Control-Wall before failure.	63
Figure 4.6:	Failure mode for 7.5 % Crumb-Wall and the location of concrete bulging.	63
Figure 4.7:	Numerical compressive stress-strain graph for 7.5 % Crumb-Wall.	64
Figure 4.8:	Contour plot for 7.5% Crumb-Wall at the yield point.	65
Figure 4.9:	Magnified view for showing the location of critical yield strain for 7.5% Crumb-Wall.	66
Figure 4.10:	Contour plot for 7.5 % Crumb-Wall before failure.	67
Figure 4.11:	Failure mode for 7.5 % Crumb-Wall + CS and the location of concrete bulging.	68
Figure 4.12:	Numerical compressive stress-strain curve for 7.5 % Crumb-Wall + CS.	69
Figure 4.13:	Contour plot for the calcium silicate board of 7.5 % Crumb-Wall + CS at the yield point.	70
Figure 4.14:	Contour plot for the rubberized concrete core panel of 7.5 % Crumb-Wall + CS at the yield point.	71
Figure 4.15:	Contour plot for the calcium silicate board of 7.5 % Crumb-Wall + CS before failure.	72
Figure 4.16:	Contour plot for the rubberized concrete core panel of 7.5 % Crumb-Wall + CS before failure.	72
Figure 4.17:	Numerical compressive stress-strain graph for Control-Wall, 7.5 % Crumb-Wall and 7.5 % Crumb-Wall + CS.	75
Figure 4.18:	Contour plot of von Mises stress for each model at the yield point.	77
Figure 4.19:	Contour plot of von Mises stress for each model before failure.	78

Figure 4.20: Failure model for 7.5 % Crumb-Wall + CAP and the location of concrete bulging.	79
Figure 4.21: Numerical compressive stress-strain curve for 7.5 % Crumb-Wall and 7.5 % Crumb-Wall + CAP.	80
Figure 4.22: Contour plot for 7.5 % Crumb-Wall + CAP at the yield point.	81
Figure 4.23: Contour plot for 7.5 % Crumb-Wall + CAP before failure.	82
Figure 4.24: Contour plot of ultimate von Mises stress before failure.	83
Figure 4.25: Failure mode for 7.5 % Crumb-Comb Wall and the location of concrete bulging.	83
Figure 4.26: Numerical compressive stress-strain curve for 7.5 % Crumb-Wall and 7.5 % Crumb-Comb Wall.	85
Figure 4.27: Contour plot for 7.5 % Crumb-Comb Wall at the yield point.	86
Figure 4.28: Contour plot for 7.5 % Crumb-Comb Wall before failure.	86

## LIST OF SYMBOLS / ABBREVIATIONS

$E$	Young's modulus
$f_{ck, cube}$	Characteristic cube compressive strength
$f_{ck}$	Characteristic cylinder compressive strength
$f_{tol}$	Predefined tolerance
$U_o$	Displacement for tension stiffening
$\nu$	Poisson's ratio
$\sigma_{max}$	Principal stress
$\sigma^o_{max}$	Maximum allowable principal stress
ASTM	American Society of Testing and Materials
AAC	Autoclave aerated concrete
BI	Brittleness index
CDP	Concrete damaged plasticity
CRLFC	Crumb rubber lightweight foamed concrete
C-S-H	Calcium silicate hydrate
C3D8R	8-node linear hexahedral meshing element
FEA	Finite element analysis
FEM	Finite element method
H/t	Slenderness ratio
IBS	Industrialised building system
LE	Logarithmic strain
LWA	Lightweight aggregates
MAXPS	Maximum principal stress
NAAC	Non-autoclave aerated concrete
XFEM	Extended Finite Element Method



## CHAPTER 1

### INTRODUCTION

#### 1.1 General Introduction

The Government of Malaysia had launched several initiatives to promote prefabricated construction or Industrialised Building System (IBS) within the construction industry to cope with the rising housing market. This is because the existing conventional in-situ construction method relies heavily on foreign labour. The associated productivity is very low, which is inefficient to fulfill the rapidly rising demand for housing. According to Vaghei, et al. (2014), precast concrete wall panel is the most common prefabricated building components used in Malaysia. In general, precast concrete wall panel is often made up of lightweight concrete to replace conventional burnt clay bricks as non-load bearing walls. Thus, a project's total cost can be reduced significantly as both superstructure and substructure elements can be designed with smaller dimensions due to the lower self-weight imposed.

Since concrete is known to be a brittle material, several kinds of research were conducted on the possible replacement of concrete substituents to improve ductility behaviour while retaining its high compressive strength. Ductility is a favourable structural behaviour for both non-load bearing and load-bearing precast concrete wall panel because it allows redistribution of stress and provides early warning signs of failure upon reaching ultimate stress. Rubberized concrete is one of the most studied concrete types, and it is made up of partial replacement of mineral aggregates with rubber aggregates. Duarte, et al. (2017) reported that rubberized concrete has higher ductility and lower unit weight than normal-weight aggregate concrete. Thus, rubberized concrete is suitable for non-load bearing precast wall panel, whereby high energy absorption is obligatory and high strength is unnecessary.

It should be underlined that most of the previous studies on precast rubberized lightweight concrete wall panel are fundamental of an experimental nature. However, there is a lack of numerical studies on the precast rubberized lightweight concrete wall panel's engineering properties. Before commercializing the use of precast rubberized lightweight concrete wall panel,

it is vital to perform numerical analysis to investigate the effects of rubber aggregates on precast concrete wall panel. Besides, it is crucial to define appropriate boundary conditions and sheathing materials in the modelling, which closely resembles the wall panel's actual condition in use. In this research, ABAQUS, a type of finite element analysis (FEA) software, is utilized to study the compressive behaviour of precast rubberized lightweight concrete wall panel.

## **1.2 Problem Statement**

Researchers suggested that waste rubber could replace mineral aggregates in producing lightweight concrete due to its lower unit weight than mineral aggregates, such as sand and gravel. Several research studies reported that rubberized concrete could be utilized as the raw material for producing precast concrete wall panel. This is because rubberized concrete has a higher ductility, which allows the panel to have a larger capacity to deform and sustain higher loads. Even though most of the research studies had already covered the effects of rubber aggregates on concrete structural properties through experimental tests, none of them demonstrated the complete stress distribution within the concrete matrix as the loading increases. Therefore, it is impossible to understand the failure mechanism of precast rubberized lightweight concrete wall panel as the location of critical stress and strain is unknown.

To date, there were only a few published works on numerical analysis of rubberized concrete, and none of the studies analyzed the effects of incorporating rubberized concrete for producing precast concrete wall panel. Besides, most of the existing numerical studies do not resemble the actual condition of wall panels used in the industry. Moreover, the existing numerical studies do not take into account the presence of insulation materials and the actual boundary conditions. Thus, it can be concluded that the numerical study on precast rubberized lightweight concrete wall panel was still lacking.

### **1.3 Aim and Objectives**

This research aims to evaluate the engineering properties of precast rubberized lightweight concrete wall panel subjected to compressive loading. The objectives are as follows:

1. To determine suitable constitutive model for simulating actual mechanical behaviour of precast rubberized lightweight concrete wall panel.
2. To study the effect of crumb rubber as partial fine aggregate replacement on the compressive strength of precast concrete wall panel.
3. To evaluate the confinement effect on precast rubberized lightweight concrete wall panel.
4. To evaluate the mechanical behaviour of combined precast rubberized lightweight concrete wall panels.

### **1.4 Scope and Limitation of the Study**

This research comprises five different models for comparison purposes. The boundary and loading conditions for the simulation models are based on compressive loading test under ASTM E72-15. The first model is a plain concrete wall panel with a 1500 mm x 600 mm x 63 mm dimension, which acts as the control sample for this fundamental research. The second model is made up of concrete with 7.5 % of crumb rubber as partial fine aggregates replacement with the same dimension as the control sample. Next, separate rubberized concrete wall panels with concrete capping and calcium silicate board are modelled for the third and fourth model, respectively. The last model is a combination of three single rubberized concrete wall panels.

The author of this study adopted the material properties for both plain concrete and rubberized concrete from Siringi (2012), limiting to 7.5 % crumb rubber replacement only. Besides, each simulation model has a similar dimension, thus having the same slenderness ratio.

## **1.5 Importance of the Study**

To resolve the environmental issues attributed to the disposal of waste tires and mining of natural aggregates, this research aims to explore the possibility of crumb rubber serving as a partial replacement of fine aggregates in precast concrete wall panel. It is worth noting that rubberized concrete is heterogeneous as crumb rubber behaves differently from the concrete matrix. It is essential to understand the interaction mechanism between these two materials and how they influence rubberized concrete's overall behaviour. However, the experimental test cannot evaluate the complete stress distribution of concrete specimens under loading; thus, it is impossible to fully understand the precast rubberized lightweight concrete wall panel's failure mechanism. Thus, the outcome of this research is to evaluate the stress-strain behaviour of precast rubberized lightweight concrete wall panel through the use of finite element method (FEM), which is a numerical technique to simulate the stress concentration within the concrete matrix.

## **1.6 Layout of Thesis**

### **Chapter 1: Introduction**

Brief information on precast rubberized lightweight concrete wall panel is discussed in this particular chapter. Besides that, the aim and objectives, scope and limitations and significance of this study will enable readers to have a general view of this study.

### **Chapter 2: Literature Review**

Several research and journals have been reviewed on types of lightweight concrete available in the current market and types of rubber to be incorporated to produce rubberized concrete. Besides, this chapter reviews the existing experimental works carried out to investigate the fresh and hardened properties of rubberized concrete. Lastly, several journals on the topic of FEM for simulating rubberized concrete have been reviewed.

**Chapter 3: Methodology**

This chapter covers the detailed steps in implementing the finite element method for precast rubberized lightweight concrete wall panels from geometry modelling to meshing in ABAQUS.

**Chapter 4: Results and Discussion**

In this chapter, the numerical results for precast rubberized lightweight concrete wall panel are generated and presented. Complete discussion on the compressive stress-strain behaviour is presented.

**Chapter 5: Conclusion and Recommendations**

Chapter 5 concludes the effect of incorporation crumb rubber as partial fine aggregate replacement in precast concrete wall panel. Besides that, recommendations are proposed to improve the existing flaws or limitations of the current study.

## CHAPTER 2

### LITERATURE REVIEW

#### 2.1 Introduction

Concrete can be classified based on respective unit density and application, such as normal strength concrete, high-density concrete, high-strength concrete and lightweight concrete. Generally, the compressive strength of normal strength concrete ranges from 20 MPa to 40 MPa and the basic ingredients are cement, sand, aggregates and water. As the name implies, the density of high-density concrete is about 50 % greater than normal strength concrete, which ranges from 3360 kg/m<sup>3</sup> to 3840 kg/m<sup>3</sup>. Therefore, it is normally adopted for construction of nuclear power plant as it could reduce the radiation to weaker state by absorbing both neutrons and gamma rays. On the other hand, the compressive strength of high strength concrete is more than 40 MPa and it can be produced by lowering the water/cement ratio or through addition of superplasticizer. Next, lightweight concrete can be termed as a type of concrete containing partial or fully replacement of lightweight aggregates or even foaming agent, which has lower unit density (300 kg/m<sup>3</sup> to 1840 kg/m<sup>3</sup>) compared to normal strength concrete with density ranges from 2240 kg/m<sup>3</sup> to 2400 kg/m<sup>3</sup>. However, the compressive strength of lightweight concrete is much lower compared to normal strength concrete due to its porous structure. Hence, lightweight concrete is more suitable to be adopted for non-load bearing purpose.

Since disposal of waste rubber tire has become a major concern, the idea of incorporating waste rubber particles as synthetic aggregates in producing precast lightweight concrete wall panel will certainly aid in creating a sustainable environment. Several journals had been reviewed in terms of the mechanical properties of rubberized concrete as to provide a clear direction in identifying research gap.

## **2.2 Lightweight Concrete**

Lightweight concrete can be further classified into 3 different types based on types of aggregates being incorporated in the concrete mix: lightweight aggregate concrete, aerated concrete, foamed concrete and no-fines concrete (Newman and Choo, 2003).

### **2.2.1 Lightweight Aggregate Concrete**

Lightweight aggregate concrete contains aggregates with relatively low specific gravity, which is lower than the average specific gravity of 2.6 for aggregates used in conventional concrete mix. According to EN 12620:2016, lightweight aggregates (LWA) can be manufactured from natural sources or even industrial by-product, with density not exceeding 2000 kg/m<sup>3</sup>. Thus, it can be divided into two main categories, which are natural aggregates and synthetic aggregates. Lightweight natural aggregates such as tuff, pumice and scoria are the products of volcanic eruption and do not require any complex processing apart from general screening. On the other hand, expanded shale, clay and slag are considered as synthetic aggregates with low density due to the pore structure within the aggregates. During the process of heating, the temperature inside the rotary kiln can easily get up to 1180°C, thus allowing the gas within inside of the aggregate to expand (Hoff, 2002). This results in pore structure within the aggregates, contributing to lower density and specific gravity. In addition, synthetic aggregates can also be termed as recycled waste, such as waste tire rubber or even plastic.

### **2.2.2 Aerated Concrete**

Both aerated and foamed concrete contain intentionally entrained voids within concrete matrix, whereby it could be produced through addition of aluminium powder and foaming agent respectively. Aerated concrete is made up of cement, fine sand or fine aggregates, water and also aluminium powder. It can be further classified into two types depending on the curing methods, which is autoclave aerated concrete (AAC) and non-autoclave aerated concrete (NAAC) (Saand, et al., 2019). Unlike NAAC, AAC is cured under high pressure in autoclave chamber with temperature maintained at 180°C. On the other hand, NAAC is cured under normal room condition and the end product has lower

compressive strength compared to AAC as higher temperature will accelerate hydration process (Ekaputri, et al., 2013). Furthermore, Ekaputri, et al. (2013) stated that the density of aerated concrete generally does not exceed 1000 kg/m<sup>3</sup> due to the absence of coarse aggregates and it's widely adopted to replace traditional clay bricks.

### **2.2.3 Foamed Concrete**

Generally, foamed concrete is termed as mixture containing of cementitious binder, fine sand, water and preformed foam, whereby the air content within concrete matrix is over 25 % (Newman and Choo, 2003). Foaming agent is the main constituent material that facilitates the air entraining process by reducing the surface tension of concrete mix and it can be further divided into protein-based and synthetic based foaming agent (Panesar, 2013). According to Jalal, et al. (2017), the typical density of foamed concrete ranges from 300 kg/m<sup>3</sup> to 1600 kg/m<sup>3</sup>. Due to its high flowability and also low density, foamed concrete can be adopted for void filling purpose and also producing concrete block (Jalal, et al., 2017).

### **2.2.4 No-fines Concrete**

No-fines concrete does not contain any fine aggregates and it contains only cement binder, water and coarse aggregates which ranges from 9 mm to 20 mm. Absence of fine aggregates will result in large number of air voids exist within concrete body, thus contributing lower compressive strength and density compared to normal weight concrete. The aggregates used should not have irregular shape or sharp edges as it will increase the possibility of local crushing under applied load.

## **2.3 Rubberized Concrete**

Rubberized concrete can be considered as lightweight aggregate concrete as it contains partial replacement of combination of both coarse and fine aggregates with synthetic rubber scraps. The idea of incorporating rubber particles into concrete mix does not change the chemical behaviour or properties of concrete as rubber particles does not involve in hydration process. Hence, the presence of rubber will only affect the mechanical properties of concrete in terms of



compressive strength, splitting tensile strength, elastic modulus, energy absorption, ductility and impact resistance.

The waste tire needs to undergo special treatment, such as cryogenic process in order to eliminate entrapped air, which contributes to low compressive strength. Moreover, removal of constituent materials like filler, steel wire and other textile components from the waste tires need to be carried out as it might ends up affecting the desired properties of final product (Sgobba, et al., 2010). In fact, tires can be categorized into two different sources, which is car tires and truck tires and both tires have different percentage of constituent materials. It was reported that the car or motor vehicle tires have higher percentage of rubber, which is around 48 % and 43 % for truck tires. Furthermore, car tires contain about 5 % of textile component and 15 % of steel fibres while truck tires reported to have 0 % and 27 % respectively (Fiore, et al., 2014).

According to Fiore, et al. (2014), the mechanical properties of concrete, such as compressive strength, tensile strength and also elastic modulus will drop significantly with partial or full replacement of aggregates with waste rubber. Besides that, the workability of rubberized lightweight concrete will decrease proportionally to the percentage of rubber replacement due to the high viscosity nature of rubber. According to Segre and Joekes (2000), soaking of rubber in sodium hydroxide solution will produce more hydration products (C-S-H gel) on the surface of rubber, which aids in bonding with cement matrix surrounding and further increase the performance of rubberized concrete in terms of compressive strength by 10%.

Despite the drawbacks, rubberized concrete is much lighter compared to conventional concrete in terms of mass density depending on percentage of rubber replacement. Since rubberized concrete has high ductility and low brittleness index, it has the potential application for building elements that stress the importance of high energy or vibration absorption (Fiore, et al., 2014).

As a matter of fact, rubberized concrete had been used extensively in the application of pavement due to its high performance of energy absorption and impact resistance (Xu, et al., 2020). Nevertheless, the application of

rubberized lightweight concrete for structural purpose or support heavy loadings are still limited and not much research had been carried out. This is mainly due to the heterogenous properties of rubberized concrete as both rubber and concrete are highly different from each other in terms of mechanical properties. Unlike steel reinforcement which is great in tensile strength helps in compensating the weakness of concrete and thus producing concrete with all-round strength. However, presence of rubber induces significant drop in compressive strength of concrete, which is the main concern for engineers and respective authority. In view of the performance of rubberized concrete in energy absorption and impact resistance, it's much suitable to be used in non-load bearing purpose, such as wall panel which is much lighter than conventional brick-wall. Rubberized concrete wall panel will certainly aid in reducing the overall cost for each project due to its lightweight properties and able to sustain impact from surroundings.

## **2.4 Classification of Rubber**

Based on past researches and journals, waste rubber tires can be further processed into 3 different types: rubber chips, crumb rubber and ground rubber powder. Since each of these rubbers has different size and surface texture, it will induce significant effect on the final product of concrete.

### **2.4.1 Rubber Chips**

Rubber chips can be termed as crushed rubber and the surface texture is found to be very rough due to grinding and cutting process. Besides that, the size of rubber chips is in between the range of 4mm and 15mm, as a result, it's considered to be the largest among other types of rubber (Zheng, Huo and Yuan, 2008). Furthermore, Panda, Parhi and Jena (2012) explained that rubber chip is normally used to replace coarse aggregates instead of fine aggregates. Even though the cost for producing rubber chips tend to be lower, the reduction in compressive strength is too significant to be ignored. The most possible reason is that rubber chips cannot be distributed evenly during the mixing process as the size is too large to fit into interfaces between aggregates and concrete matrix (Zheng, Huo and Yuan, 2008).

### **2.4.2 Ground Rubber Powder**

Ground rubber particles has the smallest size among the other 3 types of rubber, which typically ranges from 0.075mm to 0.475mm (Panda, Parhi and Jena, 2012). Several studies had showed that concrete mix with ground rubber powder exhibited better performance compared to rubber chips in terms of compressive strength and also elastic modulus. Zheng, Huo and Yuan (2008) stated that the compressive strength for concrete mix with ground rubber powder decreased from 53.8 MPa to 27.3 MPa at 45 % of rubber content, which is equivalent to almost 50% of strength reduction. However, the reduction in strength for rubber chips is more than 50 % due to uneven distribution of rubber particles within concrete matrix. Sofi (2018) highlighted that ground rubber powder could be used as a type of filler material to replace cement content and it could only be produced through micro-milling process.

### **2.4.3 Crumb Rubber**

Generally, crumb rubber can be used as replacement for sand or fine aggregates and it can be manufactured through milling process, whereby big chunk of rubber is processed into smaller size of particles (Azmi, et al., 2015). Panda, Parhi and Jena (2012) highlighted that the size of crumb rubber is in between rubber chips and ground rubber powder, which ranges from 0.425 mm to 4.75 mm. Crumb rubber can be produced through a series of mechanical process, such as granulation process, cracker milling process and lastly magnetic separation process to remove inorganic materials such as steel wire. In fact, the first two process are responsible to cut waste rubber into smaller particles based on specific requirement.

## **2.5 Application of Crumb Rubber**

Crumb rubber from waste tires had been widely used in construction of pavement since last century (Ibrahim, et al., 2013). It was reported that rubber particles has the potential in improving the cracking resistance of asphaltic mix. The improvement is attributed to swelling process of rubber particles, which leads to higher viscosity of asphaltic mix. Ibrahim, et al. (2013) further reported that rubber particles can swell up to five times of its original size by

absorbing maltene, which is one of the major insoluble components of bitumen, leaving only asphaltene in the mix (Ibrahim, et al., 2013). Hofko, et al. (2016) further explained that higher proportion of asphaltene resulted in lower creep response, but increment in stiffness and viscosity of bituminous mix.

Besides that, crumb rubber had been adopted in construction of ballasted track in order to lower the degradation rate of ballast particles due to continuous impact force from moving train (Sol-Sánchez, et al., 2015). In fact, crumb rubber exhibits elastic properties and it was found out that it could reduce the settlement of ballast track by 50 % by replacing 10 % of ballast particles with crumb rubber. Therefore, it could improve the design life of ballast track, which leads to lower maintenance cost.

## **2.6 Crumb Rubber Lightweight Foamed Concrete**

In view of the benefits obtained by incorporating rubber and foaming agent in concrete, researchers had combined both materials in producing crumb rubber lightweight foamed concrete (CRLFC). Therefore, crumb rubber lightweight foamed concrete exhibits some of the properties of foamed concrete, which is lightweight and good fire resistance, not to mention it also exhibits good ductility and low brittleness index. Eltayeb, et al. (2020) had carried out an experiment to evaluate the effect of rubber content and water/cement ratio on the mechanical properties of CRLFC. As expected, the experiment showed decrement in density of concrete along with increasing of rubber content.

Wang, et al. (2019) highlighted that foamed concrete should not be mixed with large amount of crumb rubber particles as it will result in tremendous drop in compressive strength. Since rubber particles do not involve in the hydration process of cement, the bonding or adhesion force between rubber particles and concrete matrix is very weak (Wang, et al., 2019). Besides that, Wang, et al. (2019) stated that presence of rubber particles interrupts the capability of cement to wrap the foaming bubbles, as a result, the bubbles within concrete matrix tend to be unstable and eventually burst. Furthermore, it was reported that rubber particles tend to float to the top surface of foamed concrete mix due to its low density. In overview, it's not recommended to increase the rubber percentage more than 5 % as it will result

in poor pore structure within foamed concrete mix, which ultimately leads to deterioration of mechanical properties. However, increasing of rubber content increases the impact resistance of foamed concrete as rubber is good in absorbing impact energy and it allows larger deformation before fail (Eltayeb, et al., 2020). Thus, it gives signal to users to take actions before failure of structure occurs. Unlike crumb rubber lightweight foamed concrete, foamed concrete tends to exhibit brittle behaviour upon deformation. Therefore, Eltayeb, et al. (2020) concluded that improved impact resistance is one of the significant and useful properties for crumb rubber lightweight foamed concrete.

## **2.7 Fresh Properties of Rubberized Concrete**

Workability is one of the most important fresh properties that need to be paid attention as it determines how efficient is the placement and mixing of concrete. In addition, high workability indicates that the labour cost can be reduced as the cost for hiring extra labours and buying admixtures can be cut down.

### **2.7.1 Workability**

According to Fiore, et al. (2014), it was reported that the workability of concrete with 10 % and 20 % content of rubber particles is slightly higher compared to control sample or normal concrete. Bing and Ning (2014) explained that under the same water/cement ratio, the slump value of rubberized concrete will be higher due to non-polar characteristics of rubber particles, which has low water absorption capacity. However, decrement in workability of concrete mix can be observed once the replacement with rubber particles is up to 30 % or more as increasing percentage of rubber particles will cause the mix to become more viscous (Fiore, et al., 2014). According to Bing and Ning (2014), the spiky surface of rubber particles is the main reason that leads to reduction of slump. This is because it will result in high friction between the rubber particles and concrete mix, which ultimately reduces the flowability of concrete by its own weight.

## 2.8 Hardened Properties of Rubberized Concrete

For this particular study, the mechanical properties such as density, compressive strength, splitting tensile strength and Young's Modulus of rubberized lightweight concrete are investigated.

### 2.8.1 Density

Based on the experiment carried out by Fiore, et al. (2014), seven concrete mix with different rubber replacement percentage had been tested and coarse aggregates was being omitted in the mix samples. Thus, suitable amount of sand had been incorporated to produce concrete mix with good performance in workability. Fiore, et al. (2014) reported that the average unit weight of control sample decreased from 2137 kg/m<sup>3</sup> to 1939.5, 1815, 1669 and 1545 kg/m<sup>3</sup> with rubber replacement percentage at 10, 20, 30 and 40 % respectively. It was also reported that the density drops tremendously until 1154 kg/m<sup>3</sup> when the percentage of rubber is up to 50% or more.

On the other hand, Zheng, Huo and Yuan (2008) had prepared a few samples by replacing coarse aggregate in conventional concrete with different percentage of waste rubber particles. Besides that, there are two types of rubbers being adopted, which is ground rubber and crushed rubber or also known as rubber chips. Zheng, Huo and Yuan (2008) reported that the influence of rubber types is less significant on the unit weight of concrete mix. At 45 % of rubber content, it was being observed that the average density of concrete is 2006 kg/m<sup>3</sup> and 2046 kg/m<sup>3</sup> for ground rubber powder and crushed rubber respectively.

The reason behind reduction of density is the large air voids created by the angular shape of rubber particles, which leads to high porosity within the concrete mix. Ling (2011) also mentioned that rubber particles tend to entrap air from surroundings due to its non-polar behaviour, which in turn decreases the density of concrete mix. Bing and Ning (2014) also explained that rubber particles has lower density of 1150 kg/m<sup>3</sup> compared to normal coarse aggregates, which has higher average unit density of 1650 kg/m<sup>3</sup>. Therefore, rubberized concrete tend to have lower density compared to normal concrete. For a given rubber replacement percentage, Ling (2011) found out that the

density of rubberized concrete tend to increase along with increasing of water/cement ratio. Ling (2011) further explained that this phenomenon might be due to presence of free water, which fills up the pore or empty spaces within concrete matrix, thus increasing the density.

### **2.8.2 Compressive Strength**

Based on the experimental results carried out by Fiore, et al. (2014), it can be deduced that the compressive strength of concrete reduces in a constant rate with the increasing of rubber content. In addition, Fiore, et al. (2014) reported that the average compressive strength on 28th day decreased from 30 MPa to below 15 MPa at rubber percentage of 0 % and 30 % respectively. Thus, it can be deduced that concrete mix with 10 % and 20 % of rubber content has almost similar compressive strength as control sample, which is around 26 MPa to 28 MPa and it can be used for structural application with the addition of small amount of coarse aggregates. On the other hand, concrete mix with rubber content more than 30 % has very low compressive strength as well as density. Hence, it's much suitable to be used as non-load bearing application.

Kumaran, Mushule and Lakshmiopathy (2008) explained that the reason for strength reduction is due to the entrapped air, which increases with percentage of rubber particles incorporated. Therefore, it is advisable to add de-airing agent during the mixing process before casting. Ling (2011) observed that the compressive strength decreased from 42.5 MPa to 12.4 MPa when the percentage of rubber replacement is up to 50 % at constant water/cement ratio of 0.55. Ling (2011) further explained that the strength reduction is up to 70 % and it might be due to smooth surface texture of rubber particles, which will significantly degrade the adhesion or bonding force between rubber particles and concrete matrix.

Furthermore, Zheng, Huo and Yuan (2008) had studied the effects of rubber types on the compressive strength of rubberized concrete by carrying out cube and cylinder compressive test. It was reported that the reduction for both cube and cylinder compressive strength of rubberized concrete is more significant when rubber chips is being incorporated into the mix compared to ground rubber powder. It can be explained that small particle size of ground

rubber powder allows it to be distributed evenly within concrete matrix and fill up the existing pores, which leads to higher compressive strength (Zheng, Huo and Yuan, 2008).

### **2.8.3 Splitting Tensile Strength**

Generally, the tensile strength of a normal concrete is around 10 % of its targeted compressive strength, which is about 4 – 10 MPa. According to Batayneh, Marie and Asi (2008), both experimental compressive strength and tensile strength of lightweight concrete demonstrated linear relationship with rate of strength reduction as the rubber content increases. In fact, concrete is weak in tension and low bonding force between rubber particles and concrete matrix will only further deteriorate the tensile strength. Based on the indirect tensile test carried out by Duarte, et al. (2015), it can be observed that normal concrete without presence of rubber particles will release loud sound when breaking into halves. In fact, this is one of the characteristics for materials with brittle behaviour. On the other hand, rubberized concrete is found to be remain connected by rubber particles even though it breaks down into halves once reaching maximum tensile stress. Thus, it indicates that presence of rubber particles will change the behaviour of concrete from brittle to ductile behaviour. Ductile failure mode is indeed useful for both structural and non-structural application as it signals the users to take action for rectifying purpose.

Zheng, Huo and Yuan (2008) mentioned that brittleness index (BI) can be used as an indication of ductility. It was reported that the brittleness index of rubberized concrete is lower compared to normal conventional concrete, whereby low BI signifies good performance in terms of ductility and energy absorption capability. Next, it was reported that the brittleness index of rubberized concrete decreases linearly with increasing percentage of rubber particles. Thus, it signifies that higher rubber content will increase the ductility of concrete, which will lead to larger plastic deformation when fracture occurs. Zheng, Huo and Yuan (2008) stated that even though rubberized concrete with rubber chips yielded lowest BI compared to ground rubber powder with 45 % of rubber percentage but the BI for ground rubber was much lower than rubber



chips at both 15 % and 30 % rubber content. When it comes to choosing suitable rubber types to be incorporated in concrete mix, all mechanical aspect of rubberized concrete should be taking into consideration besides brittleness index. Thus, it would be wise to adopt ground rubber powder as the substitute of aggregates for rubberized concrete as it exhibits higher ductility at lower percentage of rubber content and the strength reduction is less drastic compared to rubber chips.

#### **2.8.4 Young's Modulus**

When it comes to designing a structural element for either load-bearing or non-load bearing purpose, both strength and stiffness of the element should be taken into consideration. Young's Modulus can be termed as material's resistance towards elastic deformation under applied load and it can be used to evaluate the stiffness of a material. Therefore, low Young's Modulus indicates an elastic material while stiff material has high Young's Modulus as more stress is required to produce considerable amount of strain. Strukar, et al. (2018) concluded that the Young's Modulus of concrete mix is inversely proportional to the percentage of rubber content. Therefore, higher percentage of rubber content will lead to lower elastic modulus, whereby it helps in reducing the brittleness of concrete structures (Li, Ruan and Zeng, 2014).

Furthermore, Li, Ruan and Zeng (2014) had performed an experiment to investigate stress-strain behaviour of rubberized concrete with five different percentage of rubber content and also five different size of rubber particles. It was reported that the elastic modulus of rubberized concrete decreases along with decreasing size of rubber particles under the same rubber percentage. Strukar, et al. (2018) highlighted that rubberized concrete will experience larger deformation or strain of that normal concrete under same applied loading condition, even though rubberized concrete exhibited decrement in compressive strength. Li, Ruan and Zeng (2014) also reported that ultimate strain capacity of rubberized concrete is inversely proportional to the size of rubber particles, which signifies that smaller rubber particles tend to increase the deformation capability and prevent cracks initiation. This is because smaller size of rubber particles can be distributed more evenly within the

concrete matrix and also the interfaces between aggregates and concrete matrix (Li, Ruan and Zeng, 2014). In overview, incorporation of smaller size of rubber particles will help to produce concrete with lower elastic modulus, which has higher strain deformation capacity.

## **2.9 Finite Element Analysis**

Experimental research is one of the most effective way adopted by past research journals to investigate the properties of rubberized concrete. However, the experimental results might not be that accurate due to unforeseen factors or circumstances, as a result, numerical analysis comes in to validate the experimental results without being influenced by surrounding external factors. Besides that, since rubberized concrete is a highly heterogenous material, numerical tools or finite element tools should be adopted to investigate the influence on overall concrete composite behaviour due to the presence of rubber particles.

Finite element analysis can be defined as computerized simulation process to predict the behaviour of real-world object subjected to given conditions with the aid of mathematical equations or FEM. The basic principle behind FEM is that a real object will be modelled by breaking down into finite number of small elements, whereby the individual behaviour of each element is defined by sets of mathematical equations. Respective individual behaviour of elements will then be added up to predict the actual behaviour of the object.

### **2.9.1 Constitutive Model for Concrete**

There are three constitutive models available in ABAQUS to simulate concrete's inelastic behaviour: concrete damaged plasticity (CDP), concrete smeared cracking and brittle cracking model. However, it should be noted that researchers seldom use brittle cracking model as it assumes that the concrete compressive behaviour is always linear elastic, which does not resemble the true nature of concrete.

According to the user manual of ABAQUS, CDP is primarily used to simulate the inelastic behaviour of concrete structures under cyclic loading. Next, CDP is the only constitutive model that can be used together with rebar

to analyze reinforced concrete structures. Moreover, CDP also considers the brittle failure mechanism of concrete, which is compression failure due to concrete crushing and cracking failure.

Concrete smeared cracking is fundamentally designed to simulate concrete's inelastic behaviour under monotonic loading (Siringi, 2012). However, it should be noted that concrete smeared cracking does not take into account the effect of bond-slip and dowel action when rebar is embedded inside the concrete structures. In other words, the concrete behaviour simulated under concrete smeared cracking is independent of the rebar. Thus, concrete smeared cracking is often used to simulate plain concrete structures only.

### **2.9.2 Numerical Analysis of Rubberized Concrete**

To date, there were only a few published works on numerical analysis of rubberized concrete. Duarte, et al. (2016) had carried out numerical analysis to assess the ductility and compressive strength of steel tubes filled with rubberized concrete. Based on the comparison between numerical and experimental results by Duarte, et al. (2016), it was confirmed that CDP could be extended to simulate rubberized concrete. Duarte, et al. (2016) had verified that concrete-filled steel tubes with 5 % and 15 % rubber replacement had relatively lower compressive strength and stiffness but higher ductility than normal concrete-filled steel tubes. Besides, Al-Shwaiter and Al-Gaboby (2019) had utilized ABAQUS to investigate the mechanical behaviour of rubberized concrete-filled steel tubes analytically. The numerical results were consistent with the experimental results, whereby the column capacity reduced with increasing rubber replacement percentage.

Thomas, Gupta and Panicker (2015) had performed numerical analysis to investigate the effect of crumb rubber replacement from 0 % to 20 % on the compressive strength and flexural strength of high strength concrete. CDP was utilized by Thomas, Gupta and Panicker (2015) for the simulation of rubberized concrete, and the analytical results were then verified back with experimental results. It was identified that the numerical results for both compressive strength and flexural strength of high strength concrete showed a

decreasing trend with the increase of crumb rubber replacement percentage. At 20 % crumb rubber replacement, both the compressive strength and flexural strength reduced by 71 % and 27 %, respectively. Besides, Al-Azzawi, Shakir and Saad (2018) had adopted CDP to investigate the effect of rubber fiber on the flexural strength of the concrete beam. It was reported that incorporating 0.5 % rubber fiber increased the flexural strength of rubberized concrete by 21 %, while the ultimate displacement increased by 37 %. However, there was a drop in the flexural strength by 4 % when the fiber content was increased to 1%. Thus, Al-Azzawi, Shakir and Saad (2018) highlighted that the numerical results were in good agreement with experimental results, whereby the optimum rubber fiber content was proved to be 0.5 %.

Instead of using CDP, Duarte, et al. (2017) had utilized Extended Finite Element Method (XFEM) to simulate the inelastic behaviour of rubberized concrete subjected to monotonic compressive loading. Unlike other published works, Duarte, et al. (2017) were the first to present the use of MATLAB Image Processing to model the rubberized concrete's actual geometry by considering the heterogeneous distribution of rubber aggregates. It is worth mentioning that other published works assumed that the developed rubberized concrete model is a homogenous solid without considering that rubberized concrete is a highly heterogeneous material. This is because the mechanical properties of concrete and rubber aggregates differ from each other. According to Duarte, et al. (2017), XFEM was capable of simulating cracks initiation and propagation. The research had also provided important insight, whereby high stresses tend to develop at the surrounding of rubber aggregates, leading to cracks initiation. Duarte, et al. (2017) explained that the high-stress concentration was due to rubber aggregates' low elastic modulus compared to the concrete matrix, which may be deemed voids.

In general, it can be deduced that most published researches on numerical analysis of rubberized concrete utilized CDP as the constitutive model for simulating the inelastic behaviour of concrete. It is worth noting that there is only one published work by Siringi (2012) that utilized concrete smeared cracking to investigate rubberized concrete's flexural strength. Siringi (2012) proved that the developed model with concrete smeared cracking

showed good agreement with experimental results, whereby at 7.5 % crumb rubber replacement, there was a 15 % drop in the flexural strength.

## **2.10 Summary**

This chapter had explained the most common types of lightweight concrete and their respective production process. Next, various types of rubber and their respective function were discussed in detail. Besides, this research also critically reviewed the existing experimental works carried out to test both fresh and hardened properties of rubberized concrete. Furthermore, the differences between each concrete constitutive model were reviewed. Ultimately, the last section of this chapter had reviewed existing numerical studies for assessing rubberized concrete behaviour. After going through the literature review by past research studies, it can be deduced that previous experimental works failed to address the complete stress distribution in rubberized concrete upon loading. Therefore, the failure mechanism of precast rubberized lightweight concrete wall panel is not well understood. Besides, it is discovered that the topics on the numerical study of precast rubberized lightweight concrete wall panel appear to be ill-defined. Therefore, this research aims to address the existing research gap by proposing FEA software, ABAQUS, to evaluate the compressive behaviour of precast rubberized lightweight concrete wall panel.

## CHAPTER 3

### METHODOLOGY

#### 3.1 Introduction

A three-dimensional finite element model for precast rubberized lightweight concrete wall panel is simulated using one of the renowned commercial FEA software, ABAQUS to investigate its engineering properties under compressive loading. Chapter 3 begins with illustration of a flowchart, that depicts the complete steps for numerical analysis of precast rubberized lightweight concrete wall panel. Next, the parameters such as configuration of model, material parameters, analysis steps, interaction properties, boundary conditions, loading conditions and lastly, meshing to be considered in the execution of numerical analysis using ABAQUS are discussed. A summary is drawn at the end of Chapter 3.

#### 3.2 Research Flowchart

Figure 3.1 shows the complete procedures for this entire research.

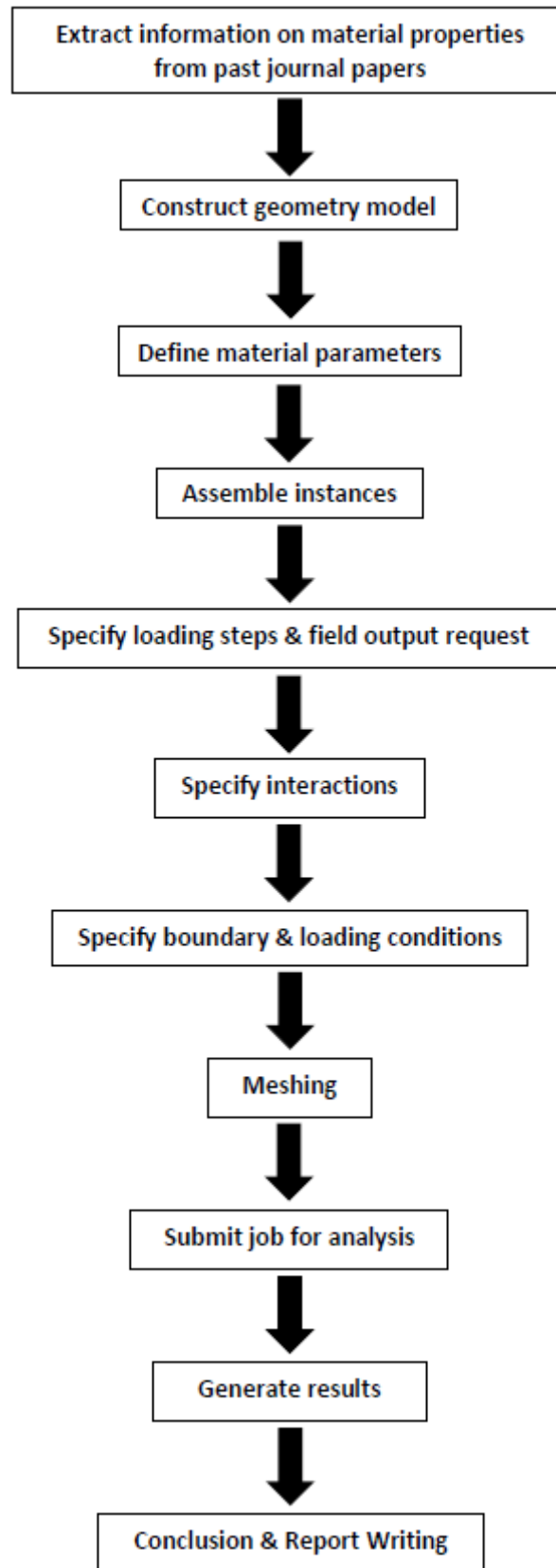


Figure 3.1: Flowchart for methodology

### 3.3 Modelling Considerations

In this research, all material properties that are defined in ABAQUS are extracted from past literature and the selection of parameters will be discussed in detail. The boundary and loading conditions for the simulation model are based on compressive loading test under ASTM E72-15 as shown in figure 3.2. ASTM E72-15 is a standard designed for testing the strength of wall panel made up of new material under various conditions that reflect those encountered during service, such as compressive load, tensile load, and transverse load due to wind action.

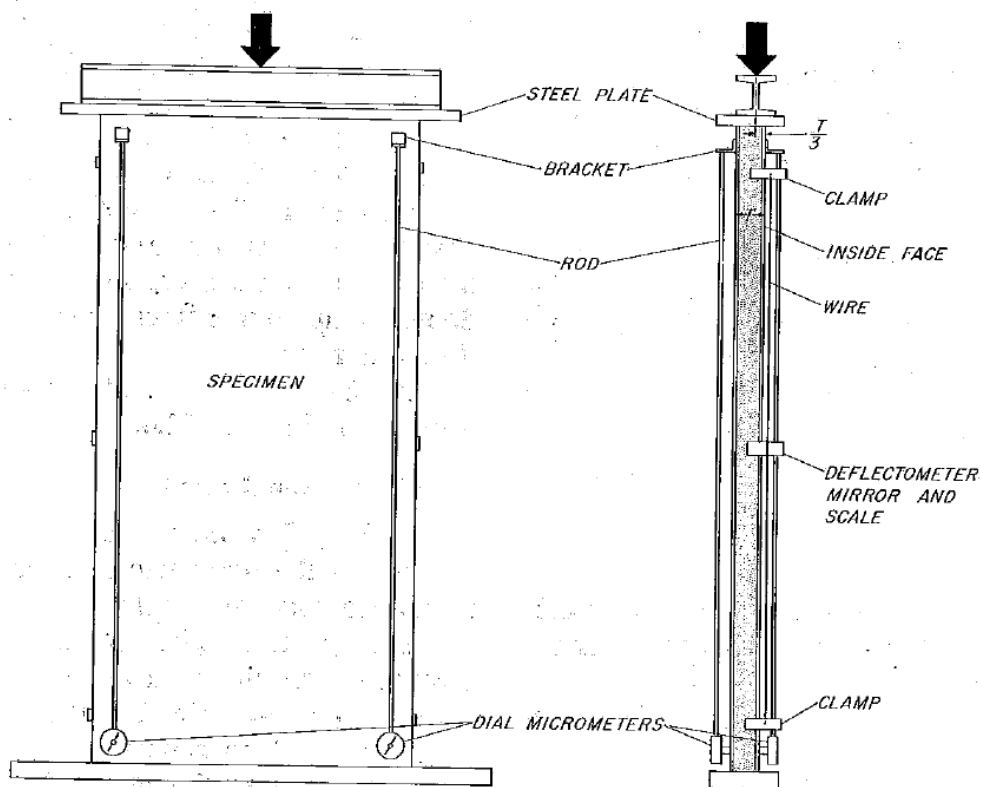


Figure 3.2: Compressive load test based on ASTM E72-15 (American Society for Testing and Materials, 2015).



### 3.4 System of Units

Before modelling, it is vital to decide which system of units to be adopted as ABAQUS does not have built-in units. Table 3.1 shows the common units and SI unit (in meter) is adopted throughout this research.

Table 3.1: List of consistent units in ABAQUS.

Quantity	SI	SI (mm)	US Unit (ft)	US Unit (inch)
Length	m	mm	ft	in
Force	N	N	lbf	lbf
Mass	kg	tonne ( $10^3$ kg)	slug	lbf s <sup>2</sup> /in
Time	s	s	s	s
Stress	Pa (N/m <sup>2</sup> )	MPa (N/mm <sup>2</sup> )	lbf/ft <sup>2</sup>	psi (lbf/in <sup>2</sup> )
Energy	J	mJ ( $10^{-3}$ J)	ft lbf	in lbf
Density	kg/m <sup>3</sup>	tonne / mm <sup>3</sup>	slug/ft <sup>3</sup>	lbf s <sup>2</sup> /in <sup>4</sup>

### 3.5 Extraction of Material Properties from Past Literature

It's vital to obtain the engineering properties of a material through experimental test or past literature before modelling in ABAQUS. In this study, the author adopted the latter approach in which all the input data for defining the material properties is extracted from Siringi (2012).

Siringi (2012) investigated the effect of crumb rubber and tire-derived aggregates on the flexural strength of concrete beam using ABAQUS. Siringi (2012) casted plain concrete, concrete containing 7.5% of crumb rubber as partial fine aggregate replacement and concrete containing 7.5 % of tire-derived aggregates as partial coarse aggregate replacement to evaluate the engineering properties of the material. Each concrete batch is then tested with compressive test and flexural test based on ASTM C39 and ASTM C78 respectively. The material properties obtained from the tests are then used by Siringi (2012) to design the concrete beam model subjected to four-point loading in ABAQUS.

Siringi (2012) verified the output of finite element model with experimental test and proved that the material properties defined in ABAQUS has high accuracy and reliability. Therefore, the material properties of both plain concrete and concrete containing 7.5 % crumb rubber are extracted by this research for simulation of wall panel subjected to compressive loading.

### **3.6 Construct Geometry Model**

Two different concrete batches are simulated, which are plain concrete acting as control sample and concrete containing 7.5% of crumb rubber as partial replacement of fine aggregates. A single wall panel with the standard dimension of 1500 mm x 600 mm x 63 mm is being constructed for each concrete batch and the designation for each model is shown in Table 3.2. Figure 3.3 shows the size for Control-Wall and 7.5 % Crumb-Wall in ABAQUS.

To further assess the confinement effect of sheathing material on rubberized concrete wall panel, third model is simulated with 7.5 % Crumb-Wall as the core panel with calcium silicate board acting as insulation layer. Figure 3.4 illustrates the concept for the third model with designation of 7.5 % Crumb-Wall + CS. The dimension of calcium silicate board is 1500 mm x 600 mm x 6 mm.

Since most of the precast wall panels in current practice are tied side by side for preventing collapsing inwards, fourth model is simulated by combining three single wall panel and each panel has similar material properties and dimension as the second model, 7.5 % Crumb-Wall. Figure 3.5 shows the modelling for fourth model, 7.5 % Crumb-Comb Wall.

Besides that, the last model is simulated with concrete capping on top of the surface of 7.5 % Crumb-Wall. The concrete capping is assigned with the material properties of plain concrete.

Table 3.2: Designation and description for each simulation model.

Model	Designation	Description
1	Control-Wall	Single wall panel made of plain concrete.
2	7.5 % Crumb-Wall	Single wall panel made of concrete containing 7.5 % of crumb rubber.
3	7.5 % Crumb-Wall + CS	Single wall panel made of concrete containing 7.5 % of crumb rubber with calcium silicate board as sheathing material.
4	7.5 % Crumb-Comb Wall	Combination of 3 single wall panels made of concrete containing 7.5 % of crumb rubber.
5	7.5 % Crumb-Wall + CAP	Single wall panel made of concrete containing 7.5 % of crumb rubber with concrete capping on top of panel.

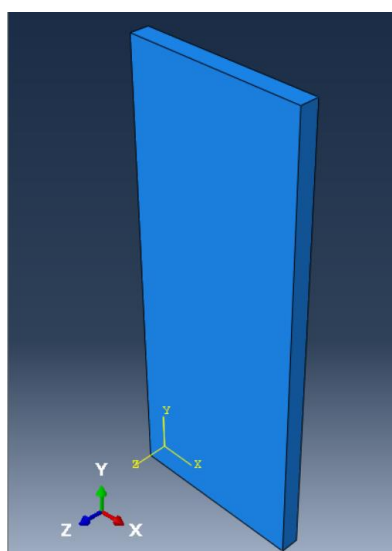


Figure 3.3: Standard dimension of 1500 mm x 600 mm x 63 mm for Control-Wall and 7.5 % Crumb-Wall.

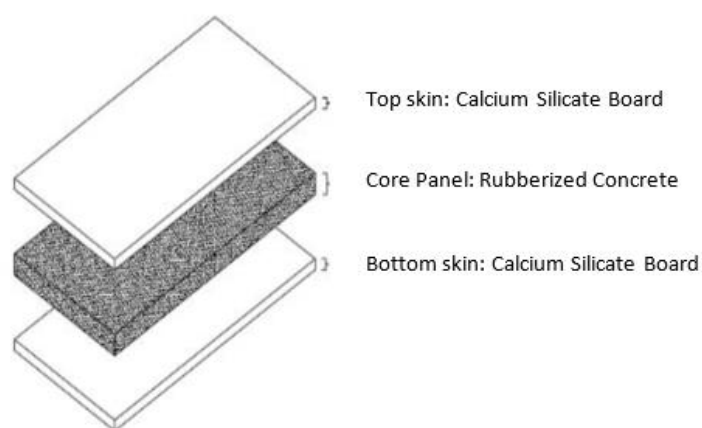


Figure 3.4: Illustration for third model, 7.5 % Crumb-Wall + CS.

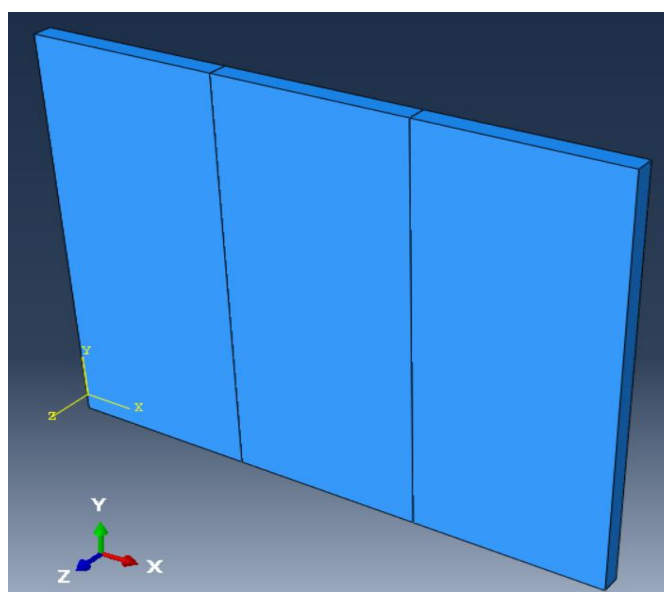


Figure 3.5: Modelling for fourth model, 7.5 % Crumb-Comb Wall in ABAQUS.

Each part of the model is defined as three-dimensional, deformable solid elements, including wall panel, calcium silicate board and concrete capping. Figure 3.6 shows that the wall panel is defined as three-dimensional, deformable solid elements under part module in ABAQUS. Even though concrete has high heterogeneity character, whereby its constituents, such as aggregates and crumb rubber particles pose different sizes and distributions, it's simulated as homogenous solid under property module as shown in Figure 3.7. The same goes for calcium silicate board.

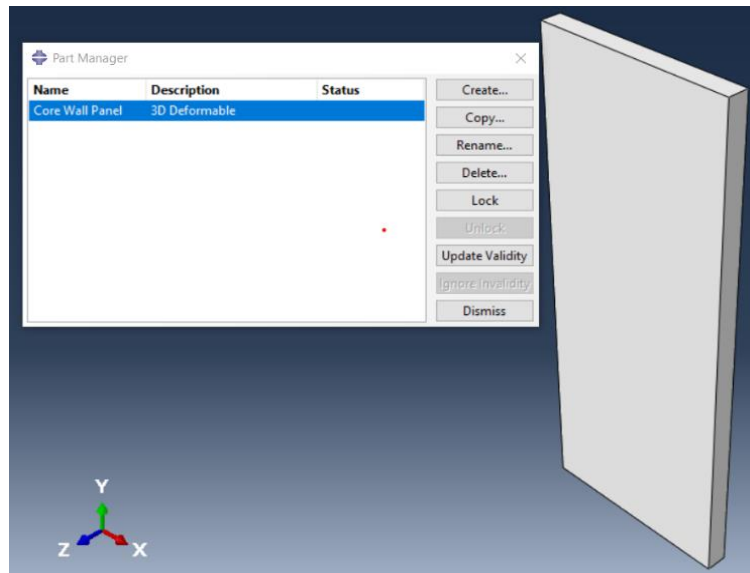


Figure 3.6: Definition of wall panel as three-dimensional, deformable solid elements under part module.

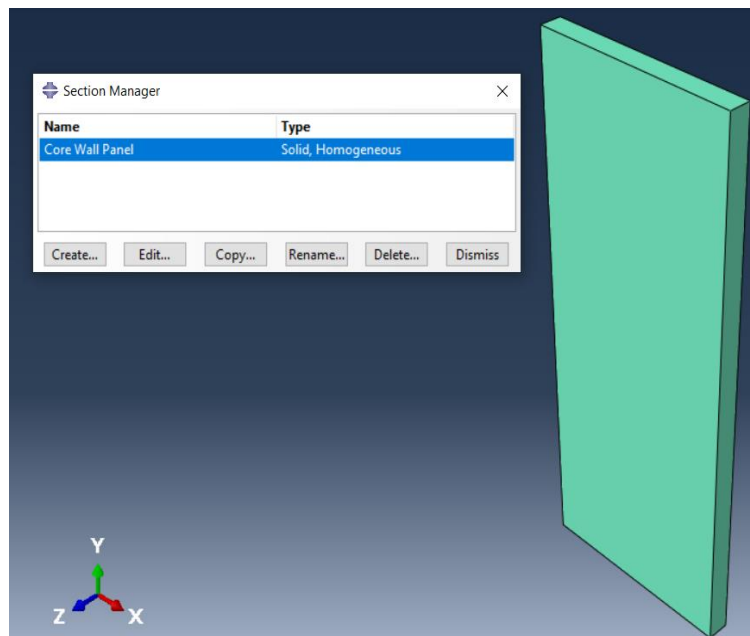


Figure 3.7: Definition of wall panel as homogenous solid in property module.

Before defining interactions, it's vital to position each part instance relative to each other by using position constraint feature that automatically align selected fixed or moveable faces in assembly module. Figure 3.8 introduces the use of face-to-face constraint feature to align calcium silicate board to the surface of core panel. In fact, the same feature can be applied for positioning concrete capping to the top surface of panel and aligning wall panels side by side as shown in Figures 3.9 and 3.10.

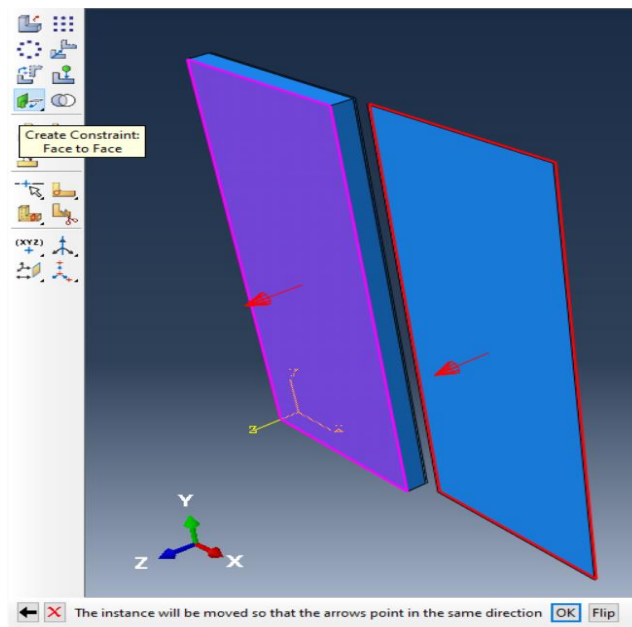


Figure 3.8: The use of face-to-face constraint to align calcium silicate board to the surface of core panel.

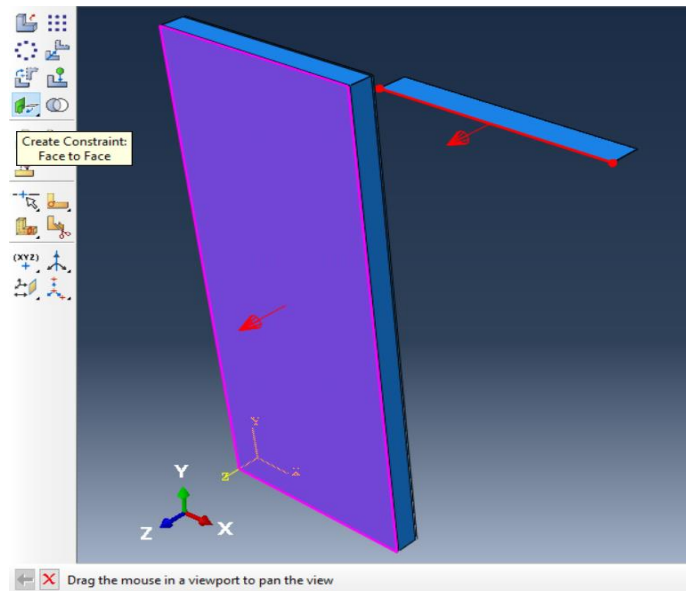


Figure 3.9: The use of face-to-face constraint to position concrete capping to the top surface of panel.

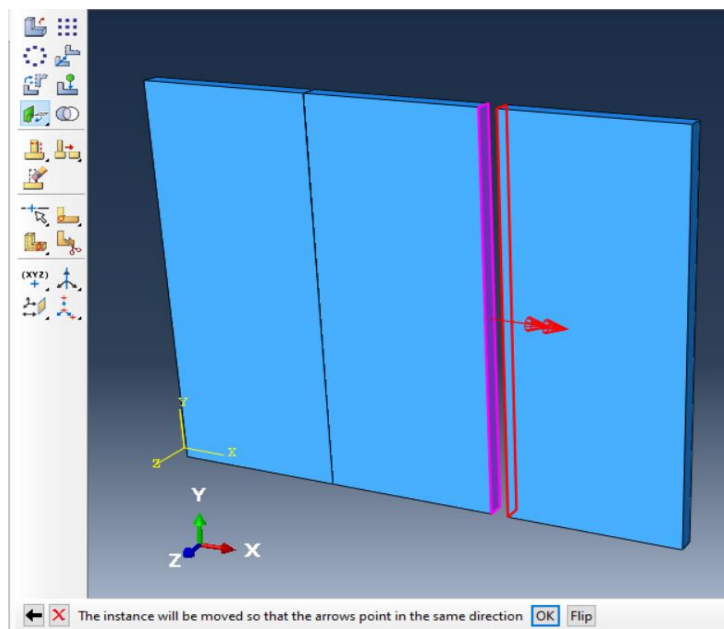


Figure 3.10: The use of face-to-face constraint to align the wall panels side by side.

### **3.7 Flowchart for Defining Material Properties**

Figure 3.11 illustrates the flowchart for defining material parameters for plain concrete, rubberized concrete and calcium silicate board in this research. When it comes to modelling concrete in ABAQUS, the material properties can be separated into both linear elastic and non-linear behaviour. In order to model highly non-linear behaviour of concrete under compressive loading, concrete smeared cracking model has been proposed in this research and it must be used in conjunction with both tension stiffening and failure ratios. Since ABAQUS does not have any built-in material model for calcium silicate, Extended Finite Element Method (XFEM) has been utilized to simulate plastic behaviour and failure of calcium silicate board.



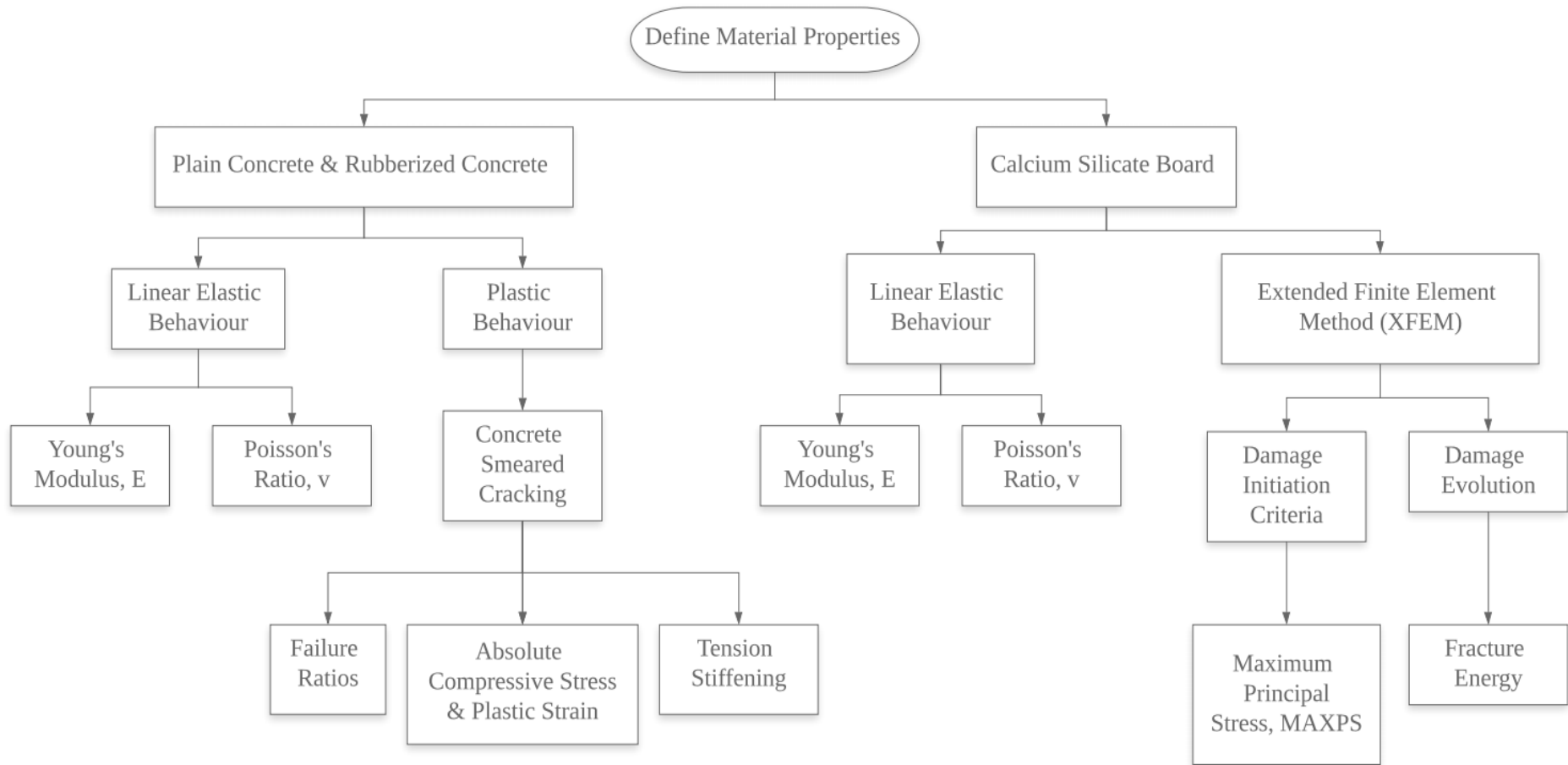


Figure 3.11: Flowchart for defining material properties in ABAQUS.

### 3.8 Material Properties for Plain Concrete and Rubberized Concrete

#### 3.8.1 Elastic Behaviour

To define elastic behaviour of a material, ABAQUS requires input data for both Young's Modulus,  $E$  and Poisson's Ratio,  $\nu$ . Table 3.3 shows the value of Young's Modulus adopted for plain concrete and rubberized concrete respectively. The Poisson's Ratio of concrete generally ranges from 0.15 to 0.20, thus an average value of 0.18 is being adopted for both plain concrete and rubberized concrete (Siringi, 2012). Figures 3.12 and 3.13 show the input parameters for elastic behaviour of plain concrete and rubberized concrete wall panel under property module, respectively.

Table 3.3: Young's Modulus for plain concrete and rubberized concrete (Siringi, 2012).

Material	Young's Modulus (N/m <sup>2</sup> )
Plain Concrete	2.47 E + 10
Rubberized Concrete (7.5% Crumb Rubber)	2.08 E + 10

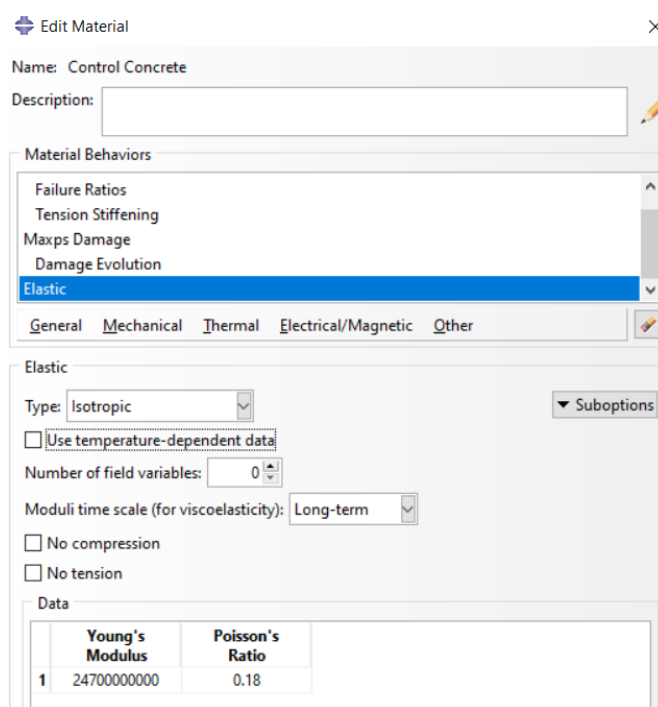


Figure 3.12: Input parameters for elastic behaviour of control concrete wall panel.

The screenshot shows the 'Edit Material' dialog box for a material named 'Core Wall Panel'. The 'Material Behaviors' list includes Failure Ratios, Tension Stiffening, Maxps Damage, Damage Evolution, and Elastic (which is selected). The 'Elastic' section is expanded, showing the following parameters:

- Type: Isotropic
- Use temperature-dependent data:
- Number of field variables: 0
- Moduli time scale (for viscoelasticity): Long-term
- No compression:
- No tension:

The 'Data' table is as follows:

	Young's Modulus	Poisson's Ratio
1	20800000000	0.18

Figure 3.13: Input parameters for elastic behaviour of rubberized concrete wall panel.

### 3.8.2 Plastic Behaviour

It is insufficient to model both plain concrete and rubberized concrete having only linear elastic behaviour as it's vital to examine its load-deformation behaviour when subjected to severe overload. Therefore, non-linear analysis has been introduced with the consideration of geometric non-linearity in this research and ABAQUS provides a list of constitutive models to define both linear and non-linear behaviour for different categories of material. Concrete is considered as brittle material and its inelastic behaviour can be modelled with three different plasticity models: concrete smeared cracking, brittle cracking model and concrete damaged plasticity.

### 3.8.2.1 Concrete Smeared Cracking

In this research, concrete smeared cracking was chosen to simulate the inelastic behaviour of concrete and it must be used in conjunction with tension stiffening and failure ratios. The main reason for choosing concrete smeared cracking is that it takes into account both cracking and post-cracking behaviour, whereby presence of cracks will affect subsequent stress and stiffness of the concrete. This modelling approach also does not require remeshing of the entire model after cracks occur, which aids in improving the computational efficiency (Gregori, et al., 2021).

Besides, Chaudhari and Chakrabarti (2012) reported that stress over-estimation tends to occur for concrete damaged plasticity model under coarser meshing size but smeared cracking model is able to provide desired results with relatively coarser mesh. Concrete damaged plasticity is designed for concrete structures subjected to cyclic or dynamic loading. Therefore, it is not compatible with the loading applied in ASTM E72-15, static monotonic loading. Brittle cracking model is also not suitable for this particular research as it assumes that respective material behaves linearly during compression, which does not reflect the true nature of concrete accurately (Dassault Systèmes, 2014).

Under concrete smeared cracking, the information required is the absolute value of compressive stress and respective plastic strain. In fact, Siringi (2012) stated that both compressive stress and plastic strain can be extracted from concrete cylinder compressive test based on ASTM C39. Tables 3.4 and 3.5 summarized the value of compressive stress and plastic strain adopted for both plain concrete and rubberized concrete wall panel respectively. It can be deduced that the initial value of compressive stress can be taken at initial yield point or 50 % of ultimate compressive strength, whereby the onset of plastic strain is zero. As for the second value, it can be estimated by taking compressive stress at 75 % of ultimate compressive strength while the third value denotes the maximum compressive strength for each concrete type. Figures 3.14 and 3.15 show the use of concrete smeared cracking to simulate non-linear behaviour of control concrete and rubberized concrete wall panel in ABAQUS.

Table 3.4: Absolute compressive stress and plastic strain for plain concrete beyond elastic range (Siringi, 2012).

	Compressive stress, $\sigma$ (N/m <sup>2</sup> )	Plastic strain, $\epsilon$
Plain Concrete	1.43 E + 07	0
	2.16 E + 07	0.00033
	2.86 E + 07	0.00079

Table 3.5: Absolute compressive stress and plastic strain for rubberized concrete beyond elastic range (Siringi, 2012).

	Compressive stress, $\sigma$ (N/m <sup>2</sup> )	Plastic strain, $\epsilon$
Rubberized Concrete (7.5 % Crumb Rubber)	1.24 E + 07	0
	1.91 E + 07	0.00038
	2.48 E + 07	0.00083

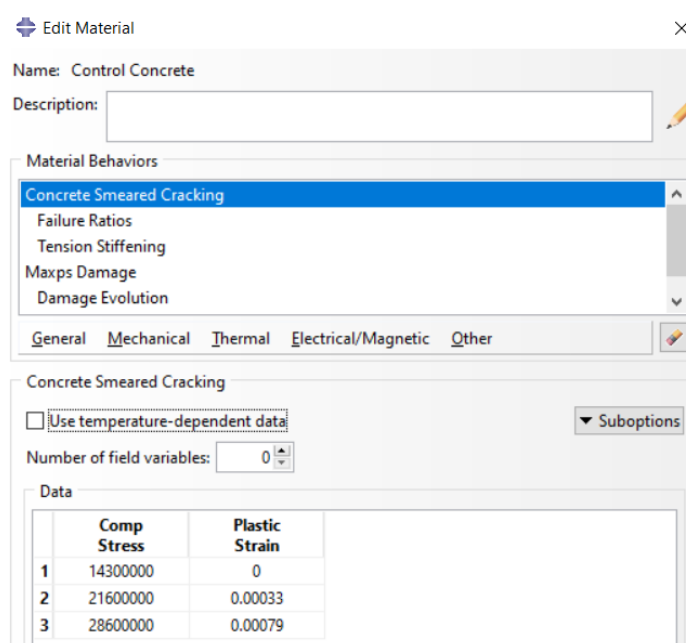


Figure 3.14: Input values for concrete smeared cracking to simulate non-linear behaviour of control concrete wall panel.

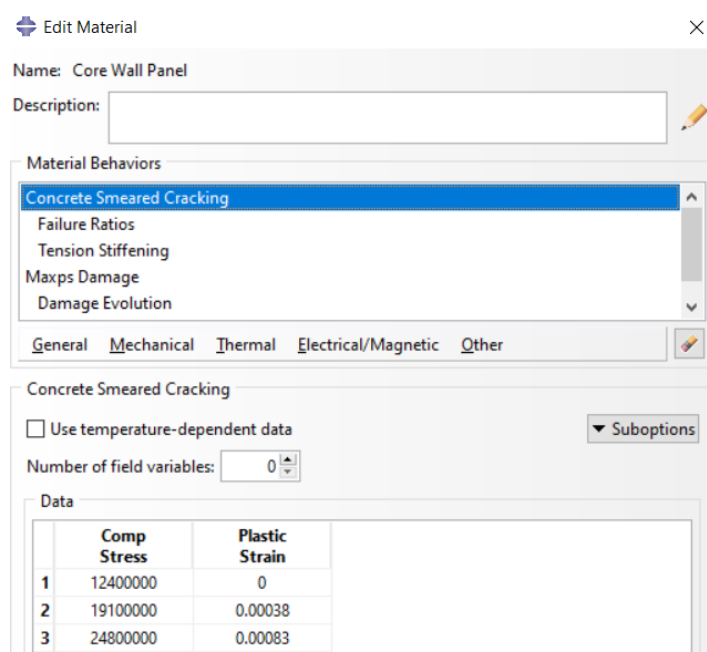


Figure 3.15: Input values for concrete smeared cracking to simulate non-linear behaviour of rubberized concrete wall panel.

### 3.8.2.2 Failure Ratios

Cracking will occur when the stress reaches the failure surface or crack detection surface. There are total four failure ratios to be specified for defining the shape of failure surface as described in Table 3.6.

Table 3.6: Definition of each failure ratios.

Ratio 1	Ratio of biaxial compressive stress to uniaxial compressive stress.
Ratio 2	Ratio of uniaxial tensile stress at failure to uniaxial compressive stress at failure.
Ratio 3	Ratio of principal plastic strain at ultimate stress for both biaxial compression and uniaxial compression.
Ratio 4	Ratio of the tensile principal stress value at cracking in plane stress to tensile cracking stress for uniaxial tension.

In overview, the parameters for ratio 1, 3 and 4 require biaxial tests to be conducted. However, the complexity of the test setup and high cost of triaxial machine are the reasons for limited information on biaxial experiment data (Chiew, et al., 2019). Therefore, the default value suggested by ABAQUS

for ratio 1, ratio 3 and ratio 4 have been adopted while ratio 2 can be calculated by having information from both compressive and tensile experimental test conducted by Siringi (2012). Table 3.7 illustrates the default value for ratio 1, 3 and 4 while Table 3.8 summarizes the value calculated by Siringi (2012) for failure ratio 2. Figures 3.16 and 3.17 show the value of each failure ratio for plain concrete wall panel and rubberized concrete wall panel, respectively.

Table 3.7: Default value for failure ratio 1, 3 and 4.

Ratio	Default value suggested by ABAQUS
1	1.16
3	1.28
4	0.333

Table 3.8: Values for failure ratio 2 (Siringi, 2012).

Ratio	Material	Calculated value
2	Plain Concrete	0.15
	Rubberized Concrete (7.5% Crumb Rubber)	0.17

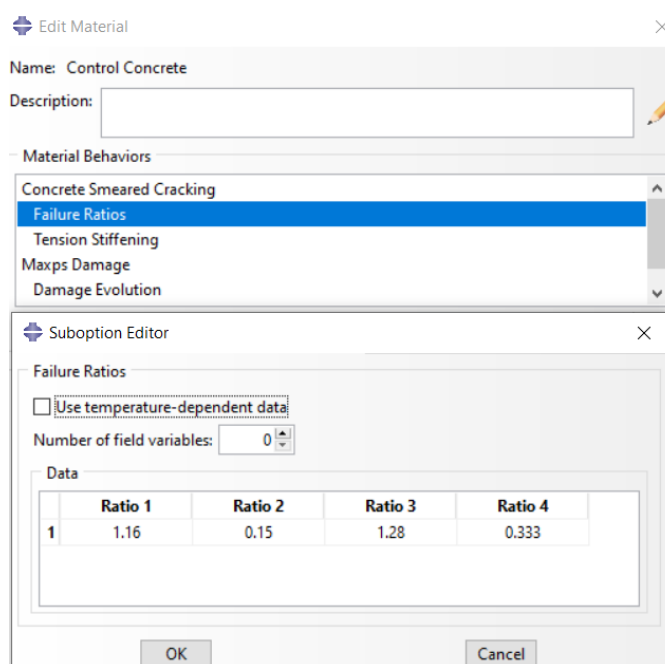


Figure 3.16: Defining failure ratios for control concrete wall panel.

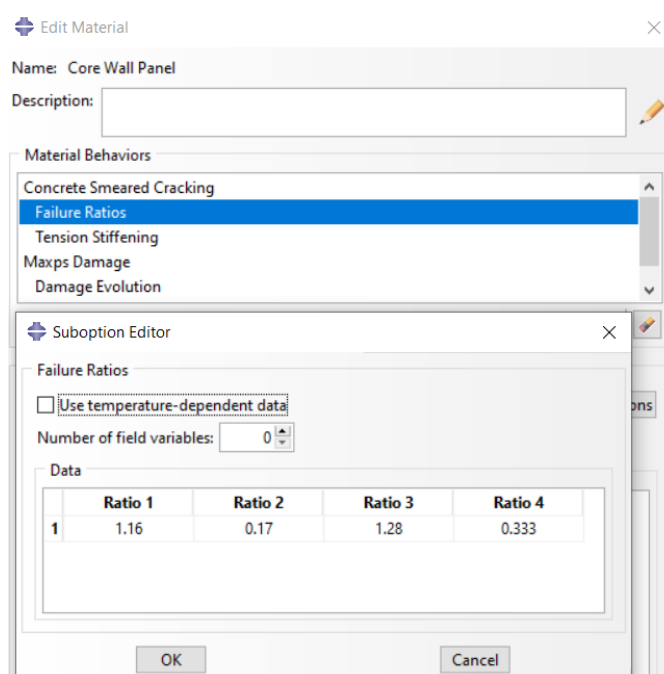


Figure 3.17: Defining failure ratios for rubberized concrete wall panel.

### 3.8.2.3 Tension Stiffening

Tension stiffening is an important parameter that can be used to model post-failure behaviour of concrete, which is termed as strain-softening whereby concrete experiences rapid declination in stress beyond peak value of stress followed by considerable deformation. Since there's no reinforcement being modelled, it's recommended to specify tension stiffening with fracture energy cracking criterion rather than post-failure stress-strain relation. This is because post-failure stress-strain relation will induce mesh sensitivity and convergence problem for concrete model with little or no reinforcement. Fracture energy cracking utilizes the concept of brittle fracture, whereby it's characterized by stress-displacement instead of stress-strain response. Thus, it requires the value of ultimate displacement,  $U_o$  for each concrete type under tension. Table 3.9 summarizes the value for ultimate displacement for both plain concrete and rubberized concrete in meter.

Table 3.9: Tension stiffening values (Siringi, 2012).

Material	Displacement, $U_o$ (meter)
Plain Concrete	0.000254
Rubberized Concrete (7.5% Crumb Rubber)	0.0003048



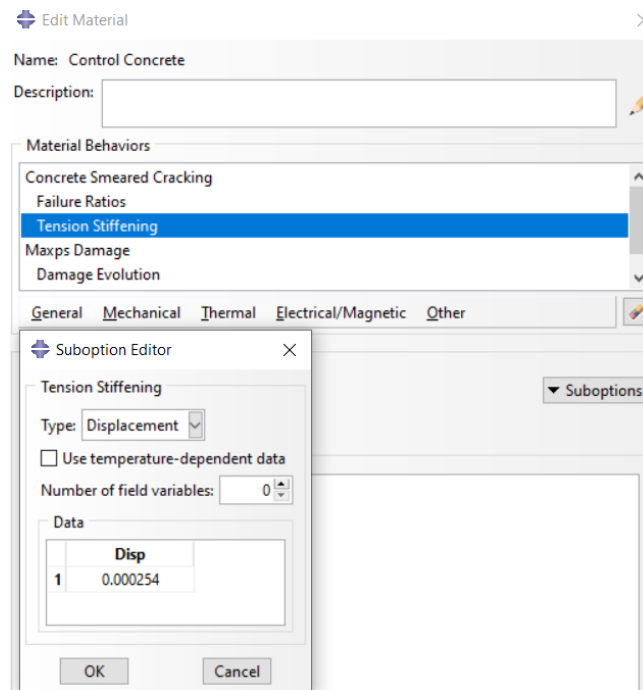


Figure 3.18: Defining tension stiffening for control concrete wall panel.

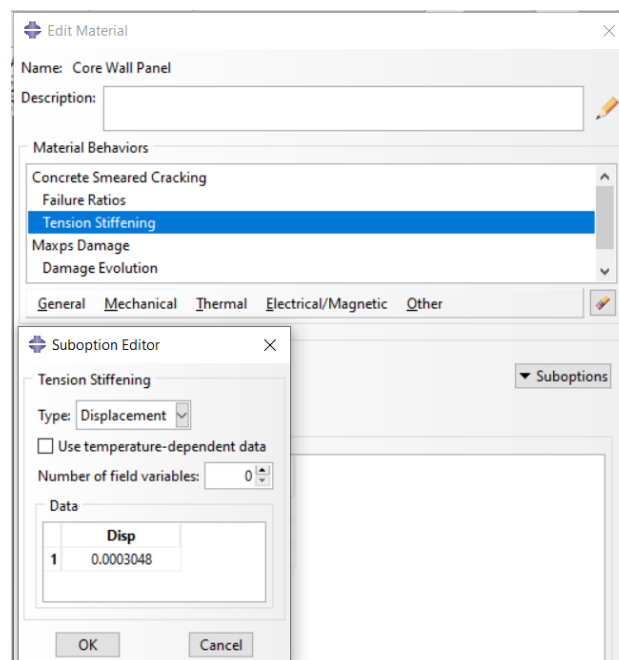


Figure 3.19: Defining tension stiffening for rubberized concrete wall panel.

### 3.9 Material Properties for Calcium Silicate Board

#### 3.9.1 Elastic Behaviour

The Young's Modulus of calcium silicate board has been extracted from catalogue under the brand name Promat. In general, Promat comprises three categories of calcium silicate board, which are high performance calcium silicate board, structural calcium silicate board and composite insulation boards (Promat, 2014). In this particular research, PROMINA structural calcium silicate board has been adopted and the given value for Young's Modulus is  $3.4E+09$  N/m<sup>2</sup>. Drobiec (2017) stated that the value of Poisson's Ratio for calcium silicate masonry block is 0.16 and the value is being adopted in this research. Figure 3.20 shows the definition of elastic behaviour for calcium silicate board under property module.

The screenshot shows the 'Edit Material' dialog box for 'Calcium Silicate Board'. The 'Material Behaviors' section has 'Elastic' selected. The 'Elastic' settings are as follows:

- Type: Isotropic
- Use temperature-dependent data:
- Number of field variables: 0
- Moduli time scale (for viscoelasticity): Long-term
- No compression:
- No tension:

The 'Data' table is shown below:

	Young's Modulus	Poisson's Ratio
1	3400000000	0.16

Figure 3.20: Input parameters for elastic behaviour of calcium silicate board.

### 3.9.2 Extended Finite Element Method (XFEM)

Even though ABAQUS does not have any built-in material constitutive model for calcium silicate board, there're numbers of material model for simulating the inelastic behaviour and failure pattern of calcium silicate board. Damage for traction-separation laws has been adopted among other material models available in ABAQUS due to its simplicity. This is because damage for traction-separation laws utilizes XFEM, which requires users to input two parameters only, which are damage initiation criteria and damage evolution.

#### 3.9.2.1 Damage Initiation Criteria

Maximum Principal Stress (MAXPS) is adopted for the damage initiation criteria for calcium silicate board and it is based on maximum flexural stress given in the catalogue for PROMINA structural calcium silicate board with the value of  $8E+06 \text{ N/m}^2$ . MAXPS can be represented in equation 3.1 and the initiation criteria will only be satisfied when the MAXPS ratio,  $f$  reaches value of 1 within predefined tolerance as illustrated in equation 3.2. According to user manual of ABAQUS, the default value for tolerance is 0.05. Even though the tolerance can be defined by user but the default value is adopted by this research for high accuracy purpose.

$$MAXPS = f = \left\{ \frac{\sigma_{max}}{\sigma_{max}^o} \right\} \quad (3.1)$$

where:

$\sigma_{max}^o$  = maximum allowable principal stress

$\sigma_{max}$  = principal stress

$$1.0 \leq f \leq 1.0 + f_{tol} \quad (3.2)$$

where:

$f_{tol}$  = predefined tolerance

Besides, MAXPS does not require users to specify the direction of crack propagation as all initiated cracks will always occur at right-angle of the direction of MAXPS (Dassault Systèmes, 2014). The remaining damage initiation criteria requires users to specify the direction of cracks to be orthogonal to local material axis. Figure 3.21 illustrates MAXPS value for calcium silicate board under property module.

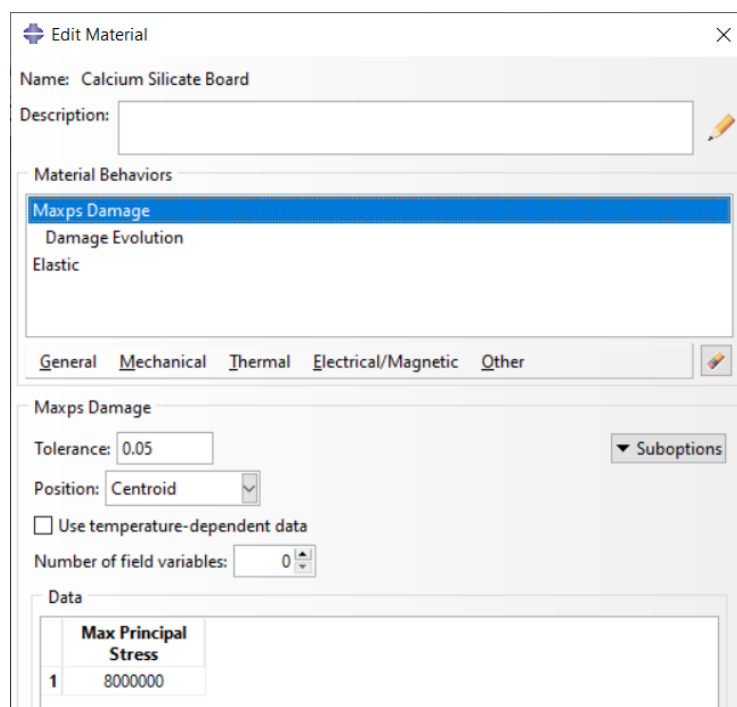


Figure 3.21: MAXPS value for calcium silicate board.

### 3.9.2.2 Damage Evolution

Energy type is adopted for defining the evolution of damage due to limited availability of experiments test conducted for assessing the maximum displacement failure of calcium silicate board. Yu, Hoogenboom and Rots (2021) had performed bending test on masonry wall made up of calcium silicate blocks and the fracture energy of calcium silicate wall was given as 0.015 N/mm and it can be converted to 15 N/m. Figure 3.22 shows the input value for defining damage evolution of calcium silicate board in ABAQUS.

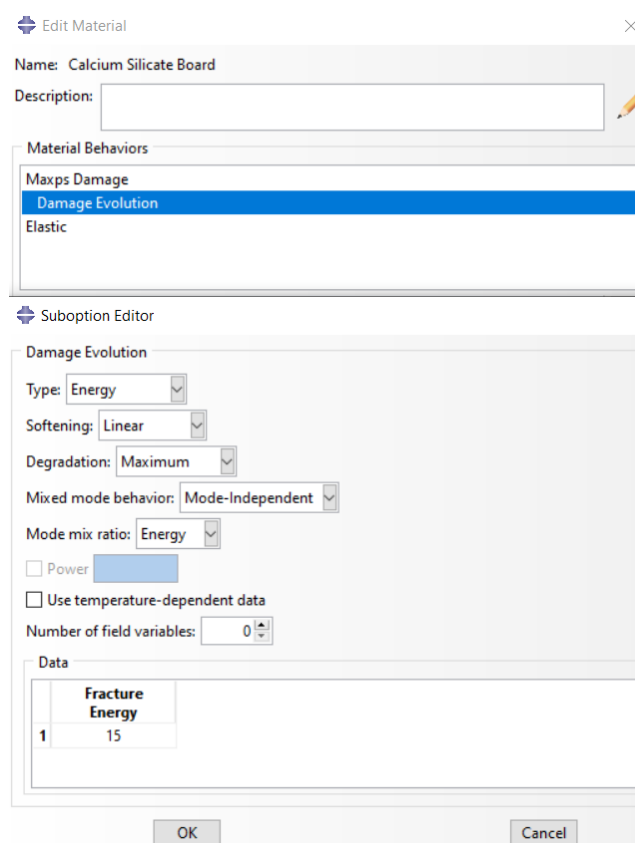


Figure 3.22: Defining damage evolution for calcium silicate board using fracture energy criterion.

### 3.10 Specify Steps and Field Output Request

Static, general is being applied for the entire analysis of this research because inertia effect is not taken into account for the simulation of wall panel subjected to compressive loading. Besides that, static, general takes into account the effects of non-linearities present in the model, which might arise from non-linear behaviour of concrete material and large displacement effects. Figure 3.23 shows that static, general has been defined under step module and Nlgeom has been turned on to include geometry non-linearity or large-displacement effects for respective step.

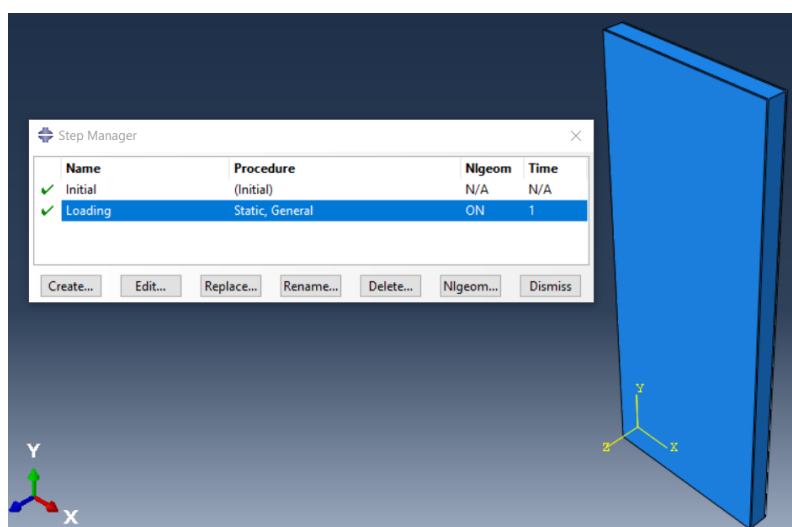


Figure 3.23: Both static, general and Nlgeom have been defined in step module.

The time period for the analysis in this research has been set to default, which is 5 seconds. Inside the incrementation tab, automatic control has been chosen as it could react to the non-linear response of the model and automatically select suitable increment size, which results in least computational time for obtaining convergent solution. The maximum number of increments has been set to 1000 increments to tackle the non-linear response, in which the analysis might takes more increment to converge. In general, the solution for a static, general model is being obtained in a series of increments, whereby each increment will iterate to reach equilibrium state. Therefore, it's vital to keep the incrementation size small as shown in Figure 3.24 for high accuracy modelling of non-linear response of concrete wall panel.

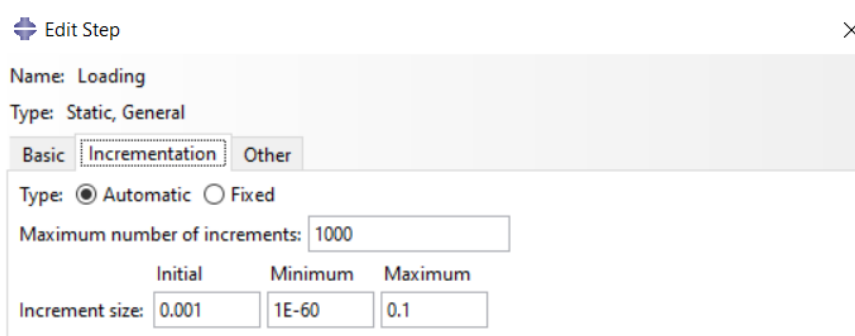


Figure 3.24: The increment size has been kept small with automatic control being selected.

By selecting automatic control, ABAQUS will automatically select suitable increment size between the range of minimum increment size and maximum increment size. However, analysis will be terminated if ABAQUS requires smaller increment size than specified minimum increment size. Therefore, the minimum increment size has been set to a very small value for reducing the number of trial and error in selecting suitable minimum increment size.

Once specifying the sequence of analysis, it's essential to specify the output request, whereby it defines which variables to be displayed for each analysis step. Since XFEM has been adopted to simulate initiation and propagation of cracks, it's vital to request output for both signed distance functions, PHILSM and PSILSM for showing the location of cracked elements in the enriched region, or else it will be invisible. Besides that, STATUSXFEM has been requested for showing the status of enriched element, whereby it'll show value of 1.0 if the element is completely cracked and 0.0 for element that does not crack. On the other hand, STATUSXFEM will show value between 0.0 and 1.0 for partially cracked element. Figure 3.25 shows that PHILSM, PSILSM and STATUSXFEM have been requested for showing cracked elements in output database.

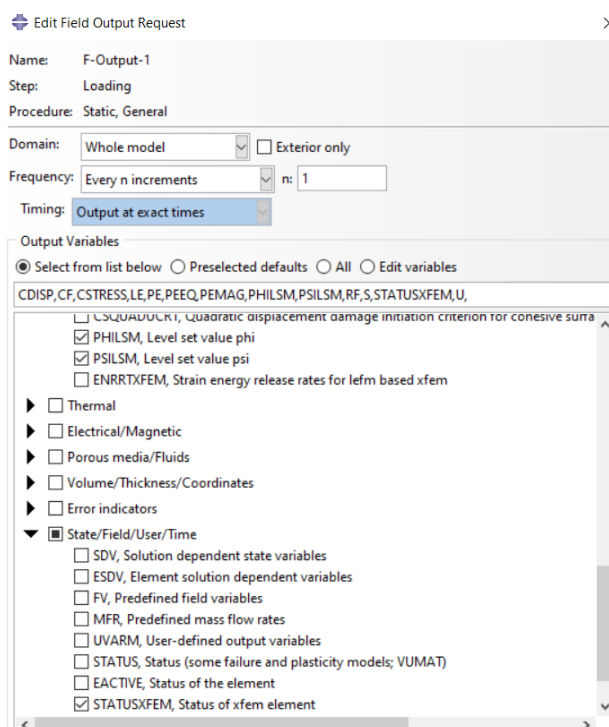


Figure 3.25: PHILSM, PSILSM and STATUSXFEM have been requested to output database.

### 3.11 Specify Interactions

Under interaction module, ABAQUS provides a list of contact algorithm for defining the interaction between surfaces or even edges. Both general contact and tie constraint have been utilized in this research.

#### 3.11.1 General Contact

Both tangential behaviour and normal behaviour have been defined for the interaction between concrete capping and top surface of wall panel. Tangential behaviour with penalty contact has been defined to simulate friction between the surfaces of concrete capping and wall panel as shown in Figure 3.26. According to EN 1992-1-1:2004, clause 6.2.5(2), it mentions that the friction coefficient between the interface of concrete layers is largely influenced by the degree of surface roughness. Since the interface between concrete capping and wall panel is assumed to be rough, the friction coefficient,  $\mu$  can be taken as 0.7 as shown in Figure 3.26.



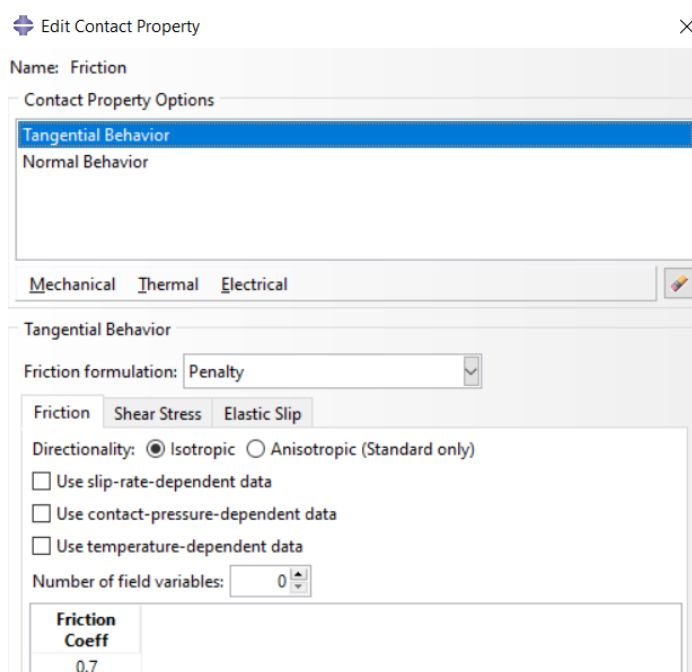


Figure 3.26: Input value for friction coefficient between concrete capping and wall panel.

Furthermore, the interaction between concrete capping and wall panel in the normal direction has been specified by normal behaviour as hard contact, which allows both surfaces to be separated by tensile force but it does not allow both surfaces to penetrate each other (Duarte, et al., 2016). Figure 3.27 shows that hard contact has been chosen for normal behaviour with allow separation after contact being toggled on.

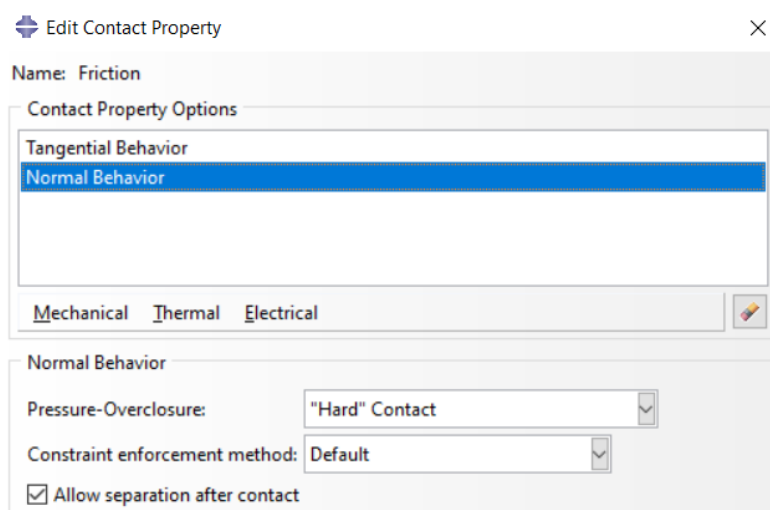


Figure 3.27: Definition of normal behaviour as hard contact between concrete capping and wall panel.

### 3.11.2 Tie Constraint

In general, both core panel and sheathing material are held together by tie connection, which is a type of mechanical connection that allows both core panel and sheathing material to act as a composite material (Gombeda, Quiel and Naito, 2019). In other words, it allows force or stress transfer between core panel and sheathing material. Surface-based tie constraint has been applied to tie the wall panels side-to-side to form a combined wall panel for 7.5 % Crumb-Comb Wall as shown in Figure 3.28. The same goes for 7.5 % Crumb-Wall + CS, whereby the calcium silicate board is being tied to the wall panel as shown in Figure 3.29. Surface-based tie constraint allows nodes on both surfaces to have the same translational and rotational motion. In short, surface-based tie constraint allows stress to be transferred between two tied surfaces. Moreover, it ties the two surfaces for the entire duration of simulation, which prevents slippage from occurring (Mohamad, et al., 2017).

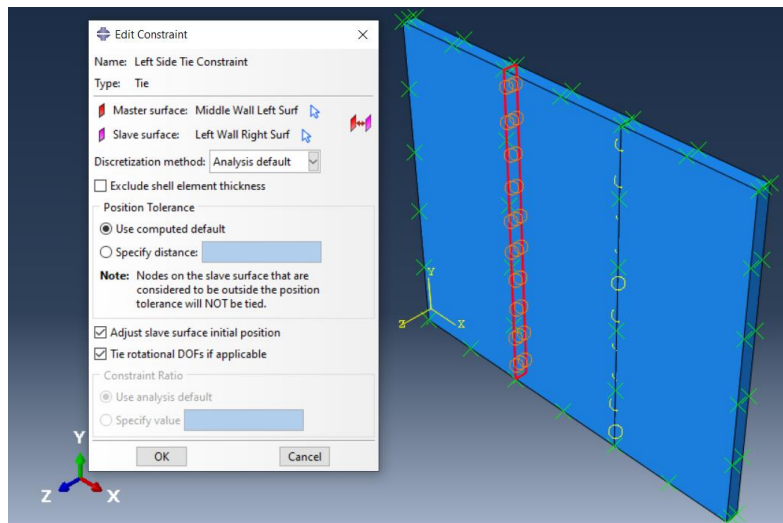


Figure 3.28: Defining tie constraint for tying wall panels side-by-side.

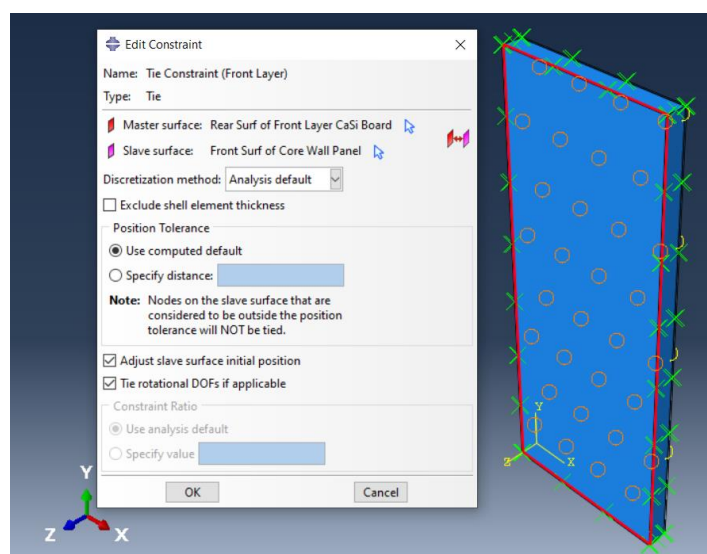


Figure 3.29: Defining tie constraint between the surfaces of calcium silicate board and core panel.

### 3.11.3 Define Enriched Region for XFEM

Besides defining damage initiation criteria and damage evolution for XFEM, it's vital to specify the enriched region, whereby the elements within this region will be enriched with additional functions for simulation of cracks initiation. Figures 3.30 show that calcium silicate board have been specified as enriched region. Since XFEM is capable of simulating multiple cracks in a specific enriched region without any initial defects or cracks present in the model, the crack location feature is not activated.

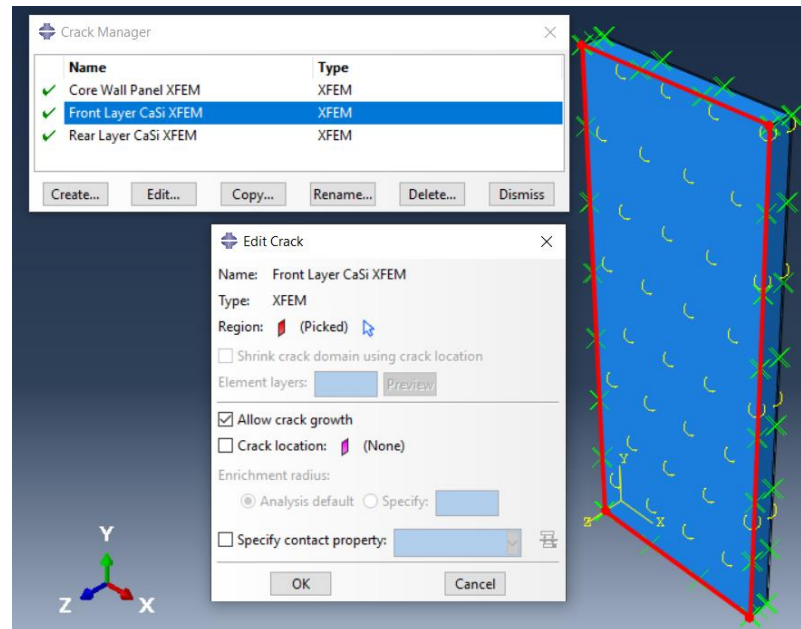


Figure 3.30: Specifying enriched region for calcium silicate board.

### 3.12 Specify Boundary Conditions

In this study, the bottom surface of the wall panel is defined as fixed support by restraining it from translational and rotational movement in x, y and z-axis. Thus, the bottom end of wall panel is restrained from any movement, which is similar to experimental test setup for ASTM E72-15 (Al-Fakih, et al., 2020). Figure 3.31 shows that the bottom end of the wall panel can be assigned as fixed support by selecting ENCASTRE, which constrains all degrees of freedom.

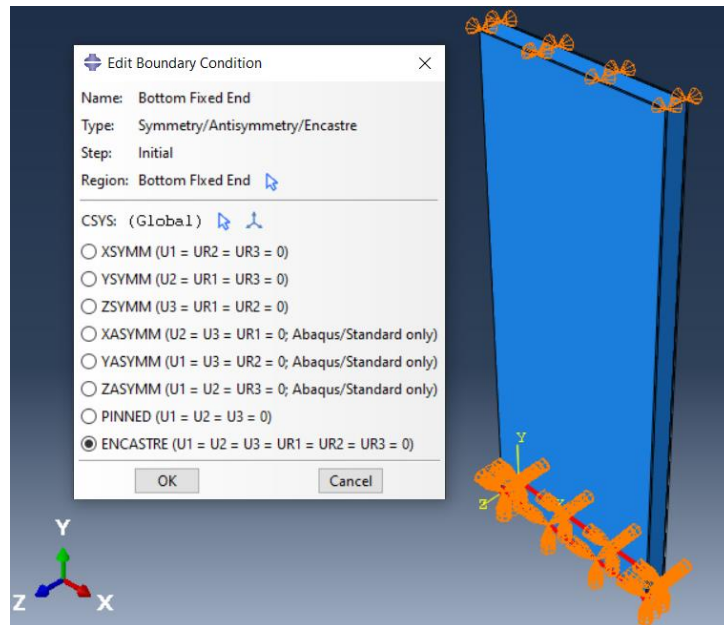


Figure 3.31: Defining ENCASTRE for bottom surface of wall panel.

Next, the top surface of wall panel is being treated as pinned support, which allows rotation along all three axes. However, the translations in both x and z-axis are being restrained as shown in Figure 3.32. Since loading will be applied on top surface of wall panel in y-direction, displacement or deformation will then occur along the direction of applied load. If translation in y-axis is being restrained, the analysis might end up with very small deformation value, which does not simulate the true behaviour of wall panel.

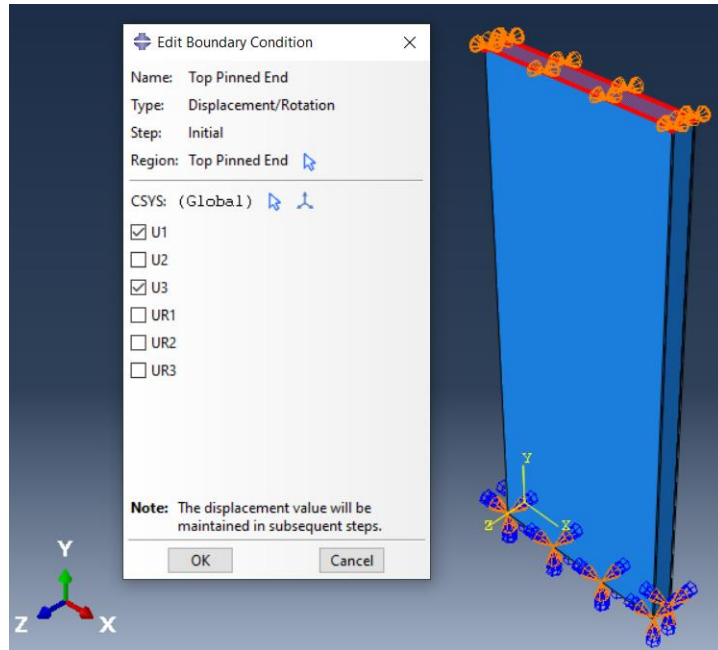


Figure 3.32: Defining top surface of wall panel as pinned support.

### 3.13 Specify Loading Conditions

Based on the setup for ASTM E72-15 in Figure 3.2, an I-beam is installed on top of wall panel to distribute point load into uniform pressure load across the entire top-loaded surface of tested panel. Inside the simulation, maximum pressure load is then applied on top of the wall panel to assess the actual stress-strain behaviour of wall panel under compressive loading. To obtain the maximum value of pressure load, simple calculations have been performed as follows.

The first step is to calculate the maximum compressive load that can be sustained by respective concrete grade used. Since the characteristic strength of concrete,  $f_{ck}$  used by Siringi (2012) is 30 MPa, the respective value for characteristic compressive cube strength,  $f_{ck, cube}$  is 37 MPa and is being defined in Equation 3.3.

$$f_{ck,cube} = 37 \text{ N/mm}^2 = \frac{F}{A} \quad (3.3)$$

where:

$F$  = maximum compressive load, N

$A$  = surface area of concrete cube subjected maximum compressive load,  $\text{mm}^2$

Under European Standard, characteristic compressive cube strength is tested with 150 mm size concrete cube and thus the surface area of concrete cube subjected to loading is taken as 150 mm x 150 mm. By substituting the surface area into Equation 3.3, the ultimate compressive load for C30/37 concrete is 832.5 kN.

The subsequent step is to determine the top surface area of a single wall panel subjected to loading, excluding the thickness of calcium silicate board. The top surface area of a single wall panel is found to be 0.0378 m<sup>2</sup>. Therefore, the value for maximum uniform pressure load can be obtained by dividing maximum compressive load, 832.5 kN with respective surface area, 0.0378 m<sup>2</sup>, which gives the value of 2.2E+07 N/m<sup>2</sup>.

Since the simulation in this research is static analysis, the loading is therefore independent of time and the rate of loading will not have any tremendous effect on the analysis. Hence, ramp function, which is the default amplitude has been specified as shown in Figure 3.33. Ramp function allows loading to be applied linearly with time throughout the step.

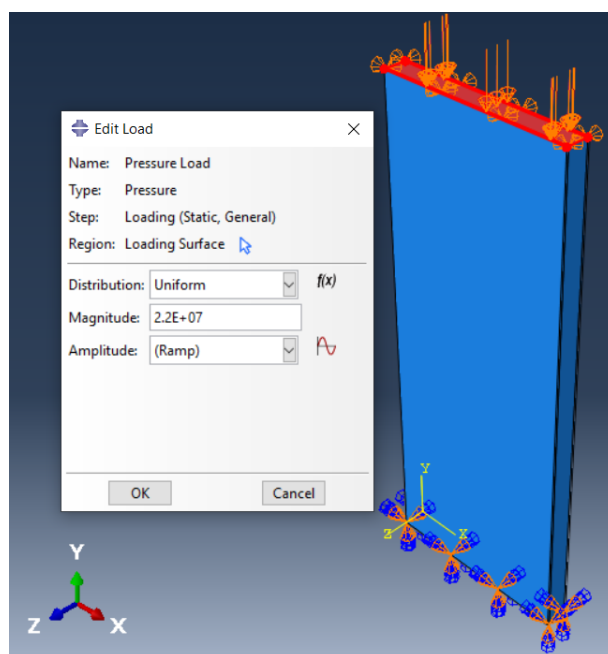


Figure 3.33: Applying maximum value of uniform pressure load on top surface of wall panel with linear ramp pattern.

### 3.14 Meshing

Under mesh module, it's essential to define the types of mesh elements before seeding the model. According to the user manual of ABAQUS, it's not recommended to use linear tetrahedral and wedge-shaped elements as these two elements are too stiff and might result in slow convergence rate of solution. However, both tetrahedral and wedge-shape elements can be utilized for meshing of a complex shape to capture stress concentration in those critical areas. For a regular shape model, like rectangular, a good mesh of hexahedral elements provides solution with almost same accuracy with lower computational cost compared to those using tetrahedral and wedge-shaped elements (Dassault Systèmes, 2014). Therefore, C3D8R, which is an 8-node linear hexahedral meshing element has been specified for all material parts, including wall panel, calcium silicate board and concrete capping as shown in Figure 3.34. Moreover, reduced integration has been specified to cut down the total running time by reducing the number of integration points within an element type. When it comes to defining seed density for respective part instance, approximate global size of 0.03 has been defined as shown in Figure 3.35.

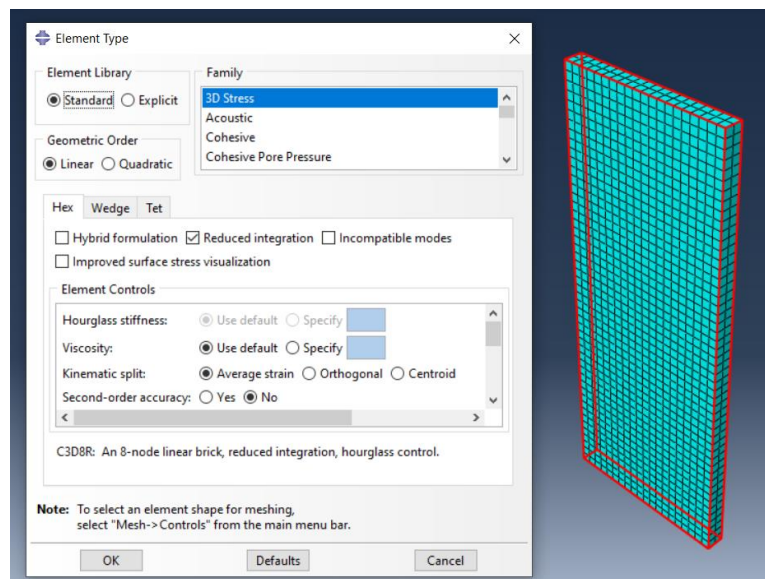


Figure 3.34: Specifying C3D8R as mesh elements under mesh module.



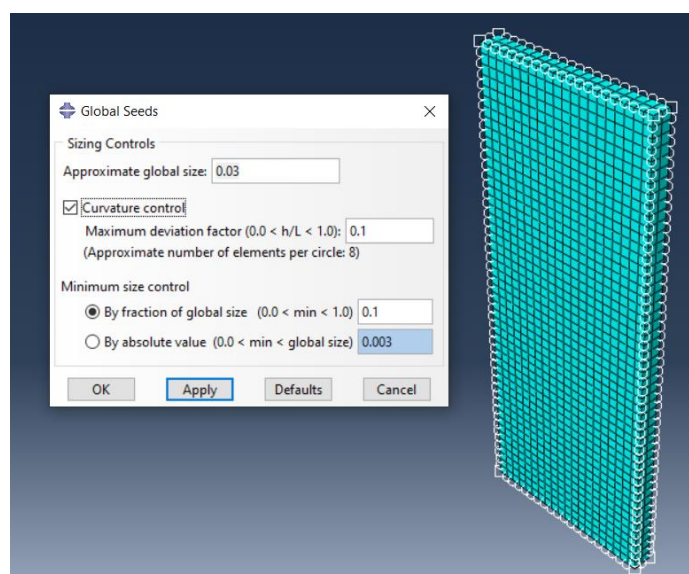


Figure 3.35: Defining seeding size of 0.03 for wall panel.

### 3.15 Summary

ABAQUS depends heavily on the input parameters for each material properties for solution convergence. Therefore, each input parameters should be evaluated carefully by considering the objectives of the research. Besides, it's vital to select suitable material constitutive for simulating different material properties. For instance, ABAQUS comprises three material models for simulating concrete beyond elastic range. This particular research has adopted concrete smeared cracking as the model is subjected to static monotonic loading and it takes into account both cracking and post-cracking behaviour. XFEM has been adopted for simulating inelastic behaviour for calcium silicate board as there's no built-in model for calcium silicate board. It is important to ensure that both boundary and loading conditions are correct and similar to actual experimental setup for getting desired results. Lastly, both incrementation size and meshing size should be kept as smaller as possible without compromising the computational efficiency.

## CHAPTER 4

### RESULTS AND DISCUSSION

#### 4.1 Introduction

This chapter examines the effect of crumb rubber as partial fine aggregate replacement on the compressive strength of precast concrete wall panel. Stress-strain graph for each model is generated and discussed in detail. This chapter also discusses the frictional and confining effect on rubberized concrete wall panel due to concrete capping and calcium silicate board. The last section of this chapter studies the mechanical behaviour of combined precast rubberized lightweight concrete wall panel.

#### 4.2 Control Sample for Concrete Wall Panel

##### 4.2.1 Influence of Slenderness Ratio

Slenderness ratio ( $H/t$ ) plays a vital role in determining the ultimate load capacity and failure mode of the wall panel. It can be calculated through Equation 4.1.

$$H/t = \frac{\text{Height of Wall Panel}}{\text{Thickness of Wall Panel}} \quad (4.1)$$

In general, a wall panel with a higher slenderness ratio tends to fail under buckling with large lateral deformation at the panel's mid-height. Mohamad, et al. (2017) reported that wall panel with  $H/t \leq 25$  tends to fail from crushing at either top or bottom half of the panel, while  $H/t \geq 25$  will result in buckling failure as mentioned earlier. The calculated slenderness ratio for Control-Wall was 23.81, and it was considered to be a non-slender wall. Figure 4.1 showed the failure mode for Control-Wall with the deformation scale factor of 80. Figure 4.1 highlighted the concrete bulging occurred at the corner of the panel's bottom. Thus, the Control-Wall tended to fail due to material failure rather than buckling failure.

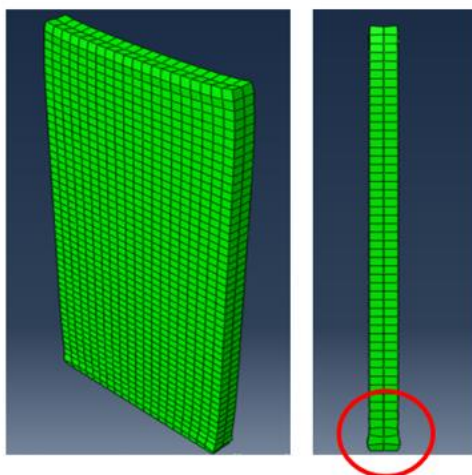


Figure 4.1: Failure mode for Control-Wall and the location of concrete bulging.

#### 4.2.2 Compressive Strength

In this study, von Mises stress was plotted against logarithmic strain (LE) to evaluate the compressive stress-strain behaviour of the model. Von mises stress was used to determine whether the given concrete material yielded, while LE strain was defined to evaluate large plastic deformation.

The compressive stress-strain graph for the control sample was presented in Figure 4.2. The first segment of the stress-strain graph showed that Control-Wall exhibited linear elastic behaviour where the deformation could be recoverable upon unloading. The yield stress of Control-Wall was 14.84 MPa, while the corresponding yield strain was 0.00013, as shown in Figure 4.2. The stress-strain curve for Control-Wall exhibited non-linear behaviour upon entering the plastic stage. Larger strains were recorded compared to initial elastic stage. The ultimate compressive stress for Control-Wall was 30.59 MPa, while the corresponding ultimate strain was 0.0017, as indicated in Figure 4.2. Moreover, the same graph showed that the Control-Wall exhibited sudden brittle failure right after reaching maximum compressive stress.

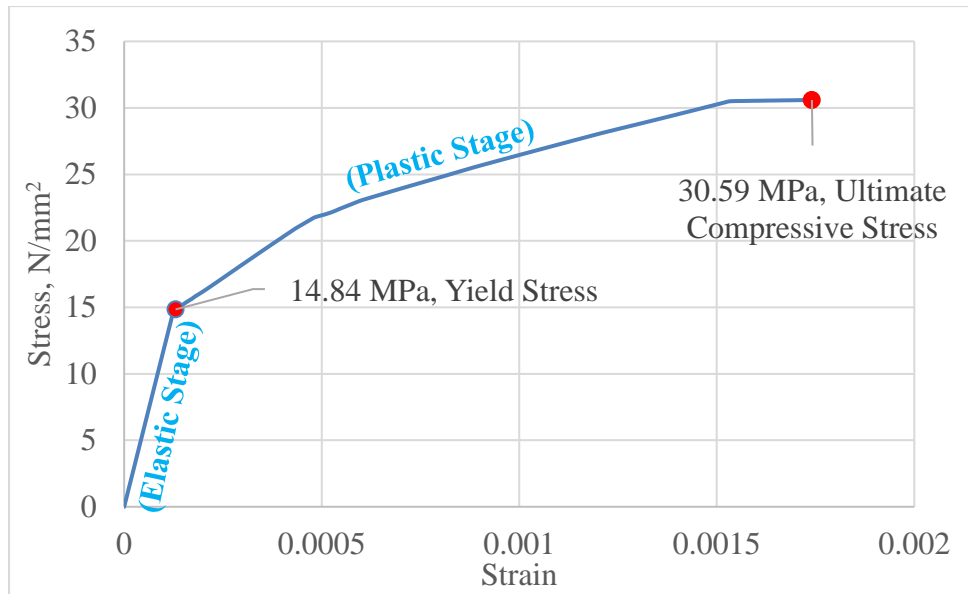


Figure 4.2: Numerical compressive stress-strain graph for Control-Wall.

From the study, it was identified that the percentage difference between the numerical value and the theoretical value of ultimate compressive stress for the Control-Wall was 2 %. Besides, it was vital to assess the accuracy of numerical prediction for the ultimate strain of Control-Wall. Equation 4.2 illustrates the formula for calculating the theoretical value for ultimate strain.

$$E = \frac{\sigma}{\varepsilon} \quad (4.2)$$

where:

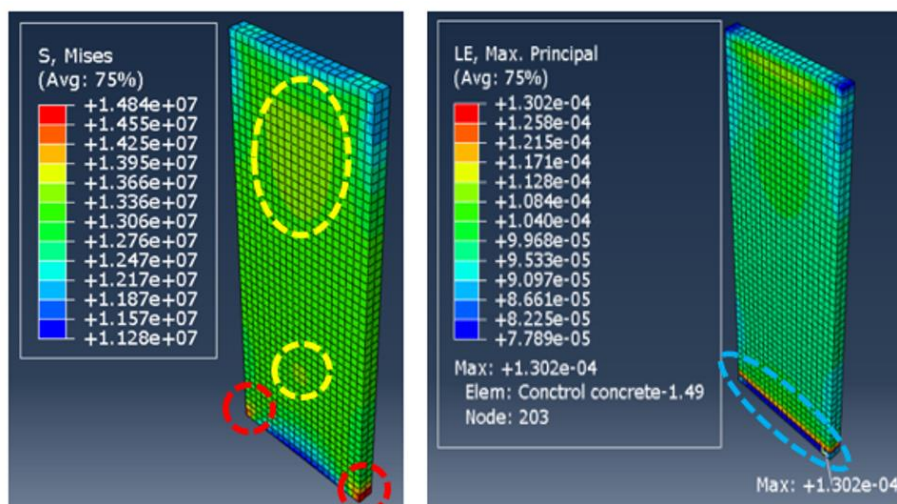
$E$  = Young's modulus,  $\text{N/mm}^2$

$\sigma$  = characteristic cylinder strength,  $\text{N/mm}^2$

$\varepsilon$  = theoretical value for ultimate strain

The elastic modulus defined in the model for Control-Wall was  $24700 \text{ N/mm}^2$ . Based on Equation 4.2, it was reported that the theoretical value for the ultimate strain was 0.0012, and the corresponding percentage difference was about 42 %.

The position of critical yield stress (14.84 MPa) for Control-Wall was indicated by the red circles in Figure 4.3 (a). The blue circle in Figure 4.3 (b) illustrated the maximum yield strain of 0.00013 that occurred near the panel's bottom end. The magnified view for the location of maximum yield strain for Control-Wall was illustrated in Figure 4.4. Since the bottom end of the panel was restrained from translational and rotational movement along all axes, the increasing load will result in maximum stress and strain at the panel's bottom corner. Figure 4.3 (a) showed that Control-Wall displayed high von Mises stress of 13.95 MPa at the top and bottom half of the panel, as indicated by the yellow circles. A plausible explanation is that the highlighted regions are under compression, which are responsible to sustain the applied load from the top surface. It should be noted that the lowest von Mises stress occurred at the bottom end of the panel in Figure 4.3 (a), represented by a dark-blue contour plot with a magnitude of 11.28 MPa. A possible explanation is that most of the applied force has been taken by the concrete at the top region of the panel, resulting in lower stress magnitude at the bottom end.



(a) Von Mises Stress

(b) LE Strain

Figure 4.3: Contour plot for Control-Wall at the yield point.

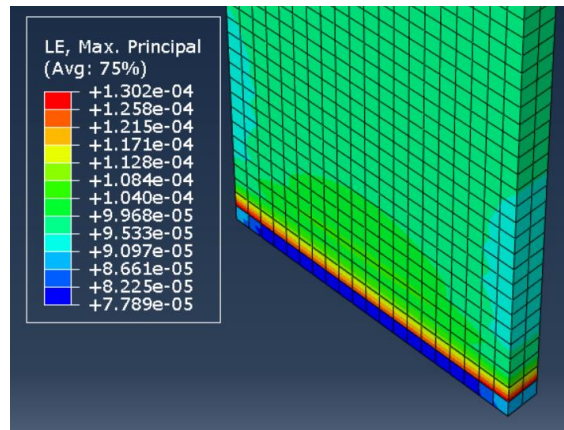


Figure 4.4: Magnified view for showing the location of critical yield strain for Control-Wall.

Figures 4.5 (a) and (b) showed the location for ultimate compressive stress (30.59 MPa) and ultimate strain (0.0017) for Control-Wall, respectively. The ultimate compressive stress and strain developed at the bottom corner of the Control-Wall could be attributed to the bottom support's restraining effect. The yellow circle in Figure 4.5 (a) depicted that the top half of the Control-Wall was highly stressed with a magnitude of 28.98 MPa. Furthermore, it can be observed that the bottom end of Control-Wall exhibited the lowest von Mises stress of 20.90 MPa. Overall, it can be concluded that the location indicated by the red dotted circles for Control-Wall in Figure 4.5 (a) were prone to concrete crushing upon reaching ultimate compressive stress.

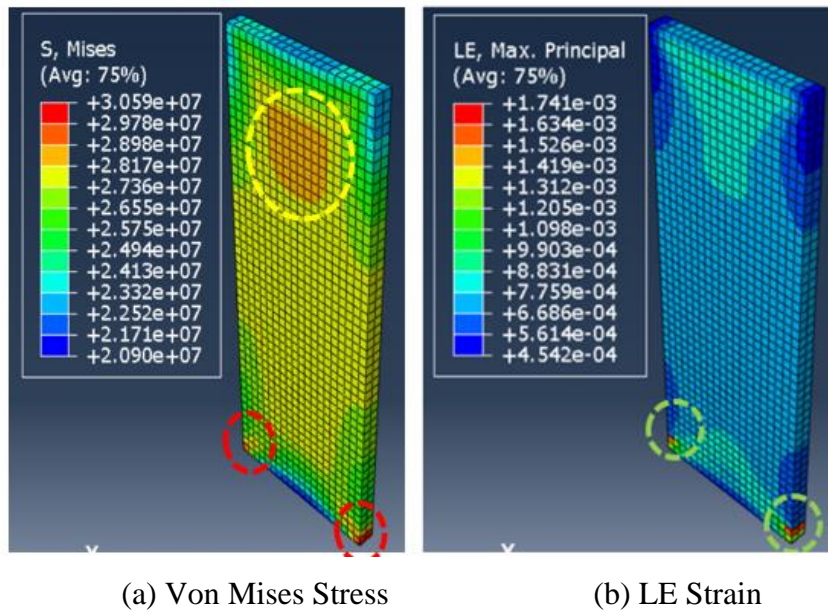


Figure 4.5: Contour plot for Control-Wall before failure.

### 4.3 Precast Rubberized Lightweight Concrete Wall Panel

#### 4.3.1 Influence of Slenderness Ratio

The failure mode for 7.5 % Crumb-Wall upon reaching ultimate compressive stress was illustrated in Figure 4.6. The 7.5 % Crumb-Wall had considerable convexity at the lower end compared to Control-Wall, as indicated in Figure 4.6. It tended to fail at crushing at the lower end corner rather than the local buckling effect at the panel's mid-height.

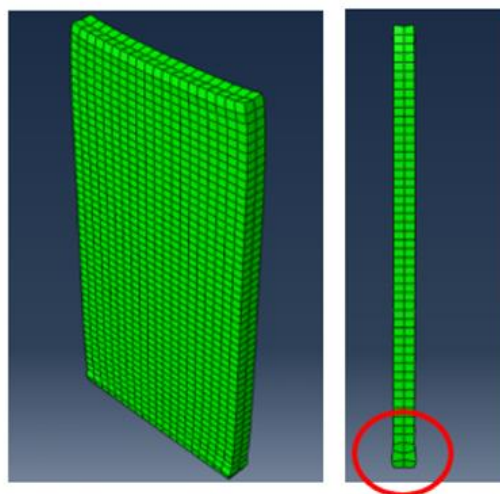


Figure 4.6: Failure mode for 7.5 % Crumb-Wall and the location of concrete bulging.

### 4.3.2 Compressive Strength

The compressive stress-strain graph for 7.5 % Crumb-Wall was presented in Figure 4.7. The first segment of the stress-strain graph showed that 7.5 % Crumb-Wall exhibited linear elastic behaviour where the deformation could be recoverable upon unloading. The yield stress of 7.5 % Crumb-Wall was 12.70 MPa, while the corresponding yield strain was 0.00013, as shown in Figure 4.7. The stress-strain curve for 7.5 % Crumb-Wall exhibited non-linear behaviour upon entering the plastic stage. Larger strains were recorded compared to initial elastic behaviour. The ultimate compressive stress for 7.5 % Crumb-Wall was 26.57 MPa, and the corresponding ultimate strain was 0.0018, as shown in Figure 4.7. Similar to Control-Wall, the 7.5 % Crumb-Wall exhibited sudden brittle failure as there was no plastic deformation after reaching maximum compressive stress.

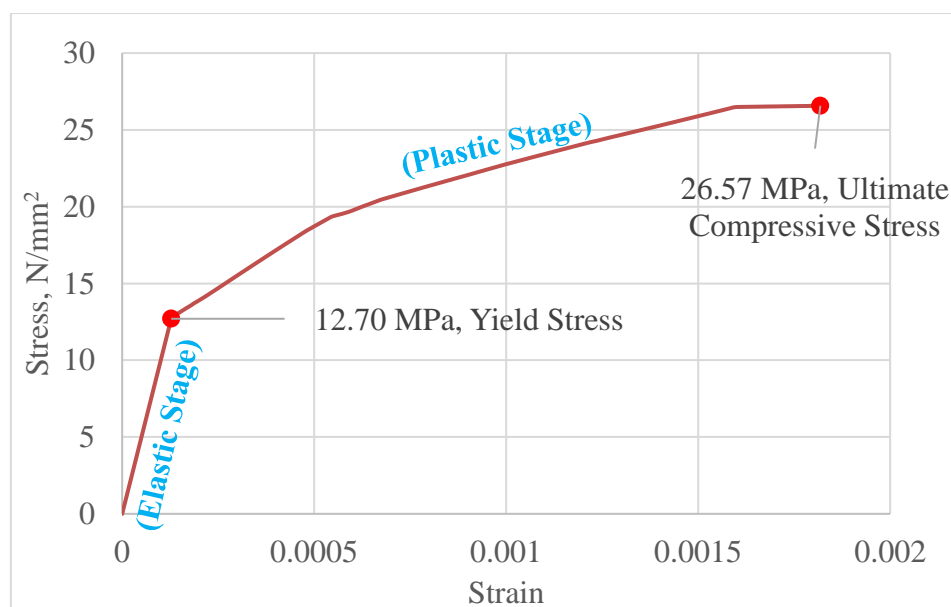


Figure 4.7: Numerical compressive stress-strain graph for 7.5 % Crumb-Wall.

From the study, it was identified that the percentage difference between the numerical value and the theoretical value of ultimate compressive stress for the 7.5 % Crumb-Wall was 11.43 %. The difference may be attributed to low elastic modulus of crumb rubber that significantly degrades its load-carrying capacity compared to mineral aggregates.



The elastic modulus defined in the model for 7.5 % Crumb-Wall was 20800 N/mm<sup>2</sup>. Based on Equation 4.2, it was identified that the theoretical value for the ultimate strain was 0.0014, and the percentage difference was about 22 %.

The position of critical yield stress (12.70 MPa) for 7.5 % Crumb-Wall was indicated by the red circles in Figure 4.8 (a). The blue circle in Figure 4.8 (b) illustrated the maximum yield strain of 0.00013 that occurred near the panel's bottom end. The magnified view for the location of maximum yield strain for 7.5 % Crumb-Wall was illustrated in Figure 4.9. The maximum yield stress and strain developed at the bottom corner of 7.5 % Crumb-Wall could be attributed to the bottom support's restraining effect. Figure 4.8 (a) showed that 7.5 % Crumb-Wall displayed high von Mises stress of 11.93 MPa at the top half of the panel, as indicated by the yellow circle. A plausible explanation is that the top region of the panel is under compression, which is responsible for sustaining the load from the top surface. It should be noted that the lowest von Mises stress occurred at the bottom end of the panel in Figure 4.8 (a), represented by a dark-blue contour plot with a magnitude of 9.60 MPa. A possible reason is that most of the applied force has been taken by the concrete at the top region of the panel, resulting in lower stress magnitude at the bottom end.

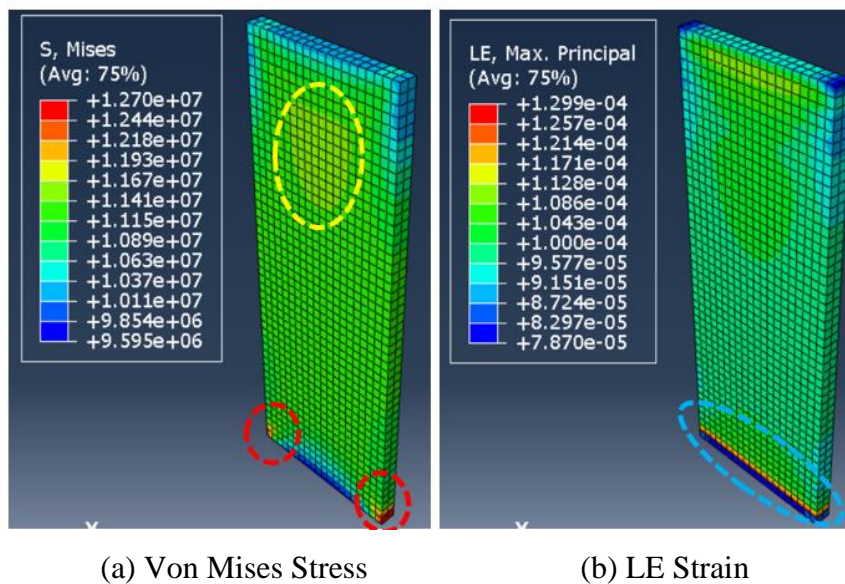


Figure 4.8: Contour plot for 7.5% Crumb-Wall at the yield point.

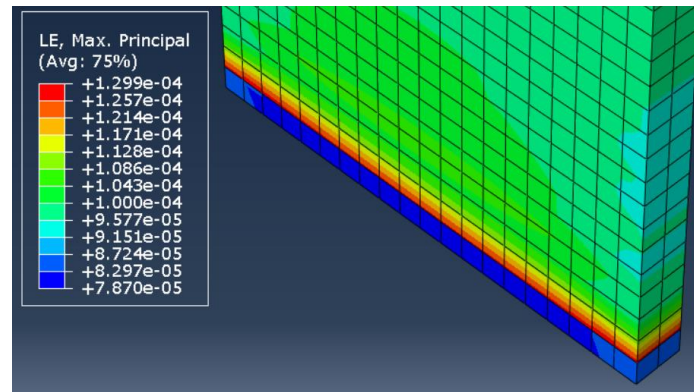
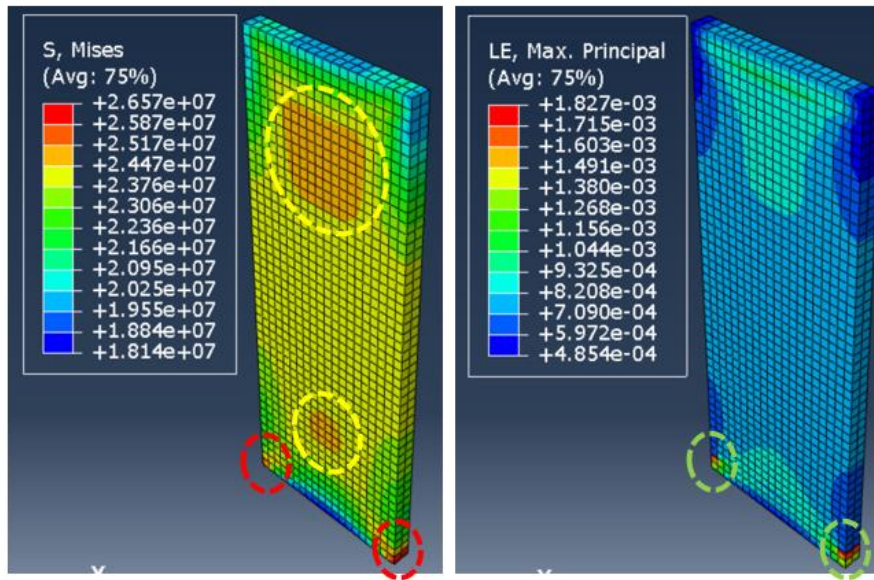


Figure 4.9: Magnified view for showing the location of critical yield strain for 7.5% Crumb-Wall.

Figures 4.10 (a) and (b) showed the location for ultimate compressive stress (26.57 MPa) and ultimate strain (0.0018) for 7.5% Crumb-Wall, respectively. The yellow circles in Figure 4.10 (a) depicted that both the top and bottom half of 7.5 % Crumb-Wall were highly stressed with a magnitude of 25.17 MPa. A possible explanation is that the increasing load beyond the yield strength of concrete leads to crack propagation, which results in lower stiffness of the concrete material at the top region of the panel. Thus, high stress concentration developed at the lower region of 7.5 % Crumb-Wall as there was less material available to sustain the stress caused by the applied force. Furthermore, it can be observed that the bottom end of 7.5 % Crumb-Wall exhibited the lowest von Mises stress of 18.14 MPa. Overall, it can be concluded that the location indicated by the red circles for 7.5 % Crumb-Wall in Figure 4.10 (a) were prone to concrete crushing upon reaching ultimate compressive stress.



(a) Von Mises Stress (b) LE Strain  
 Figure 4.10: Contour plot for 7.5 % Crumb-Wall before failure.

#### 4.4 Precast Rubberized Lightweight Concrete Wall Panel with Calcium Silicate Board

##### 4.4.1 Influence of Slenderness Ratio

Since the rubberized concrete core panel of 7.5 % Crumb-Wall + CS was insulated with calcium silicate board on both sides, it had a total thickness of 75 mm. The calculated slenderness ratio for 7.5 % Crumb-Wall + CS was 20, and it was considered to be a non-slender wall. Figure 4.11 depicted the failure mode for 7.5 % Crumb-Wall + CS upon reaching ultimate compressive stress. The 7.5 % Crumb-Wall + CS had considerable convexity at the lower end compared to 7.5 % Crumb-Wall. It tended to fail at crushing at the lower end corner rather than the local buckling effect at the panel's mid-height.

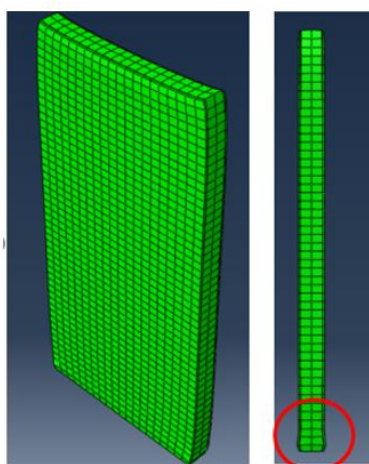


Figure 4.11: Failure mode for 7.5 % Crumb-Wall + CS and the location of concrete bulging.

##### 4.4.2 Compressive Strength

The compressive stress-strain graph for 7.5 % Crumb-Wall + CS was presented in Figure 4.12. The first segment of the stress-strain graph showed that 7.5 % Crumb-Wall + CS exhibited linear elastic behaviour where the deformation could be recoverable upon unloading. The yield stress of 7.5 % Crumb-Wall + CS was 12.69 MPa while the corresponding yield strain was 0.00013, as shown in Figure 4.12. The stress-strain graph for 7.5 % Crumb-Wall + CS exhibited non-linear behaviour upon entering the plastic stage. Larger strains were recorded compared to initial elastic stage. The ultimate compressive stress for 7.5 % Crumb-Wall + CS was 26.51 MPa, and the

corresponding ultimate strain was 0.0016, as shown in Figure 4.12. Similar to 7.5 % Crumb-Wall, the 7.5 % Crumb-Wall + CS exhibited sudden brittle failure upon reaching the ultimate compressive stress.

From the study, it was identified that the percentage difference for the ultimate compressive stress and ultimate strain of 7.5 % Crumb-Wall + CS was 11.63 % and 14.29 %, respectively.

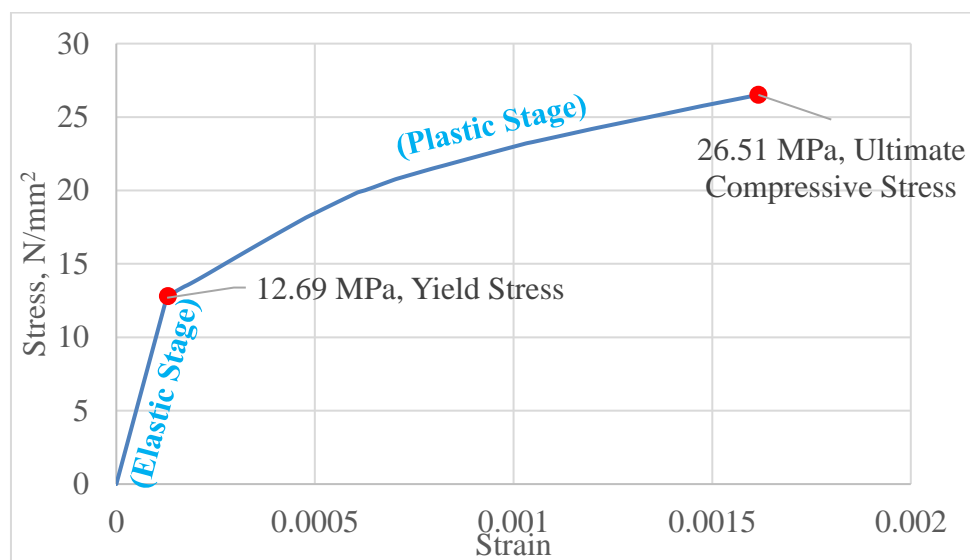
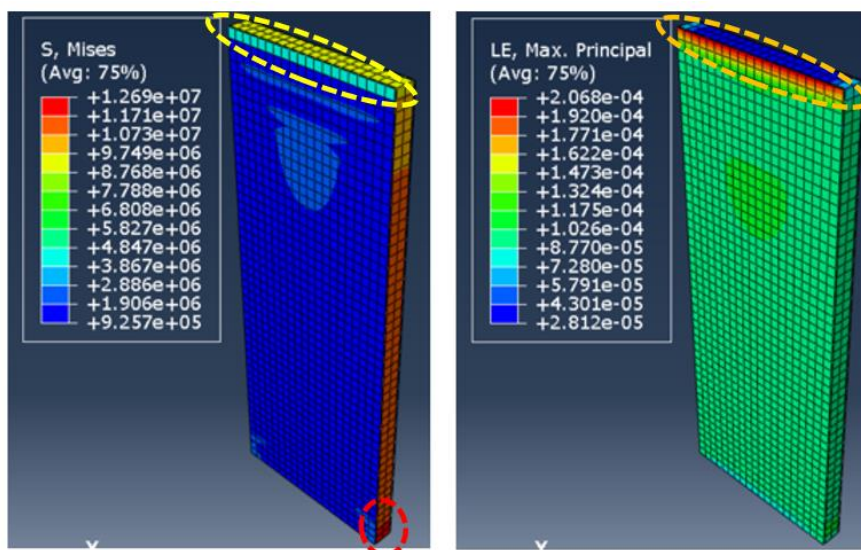


Figure 4.12: Numerical compressive stress-strain curve for 7.5 % Crumb-Wall + CS.

The position of critical yield stress (12.69 MPa) for the rubberized concrete core panel of 7.5 % Crumb-Wall + CS was indicated by the red circle in Figure 4.13 (a). Besides, Figure 4.13 (a) showed that the calcium silicate board displayed significantly lower critical yield stress of 3.87 MPa at the top edge of the board, as indicated by the yellow circle. A possible explanation is that the low Young's Modulus of calcium silicate board (3.4 GPa) results in lower stiffness or load-carrying capacity. Thus, the rubberized concrete core panel will carry most of the loading applied due to its higher Young's Modulus (20.8 GPa). The orange circle in Figure 4.13 (b) illustrated the maximum yield strain of 0.0002 that occurred at the calcium silicate board's top edge. The reason might be attributed to the low stiffness of the calcium silicate board compared to that of the core panel.



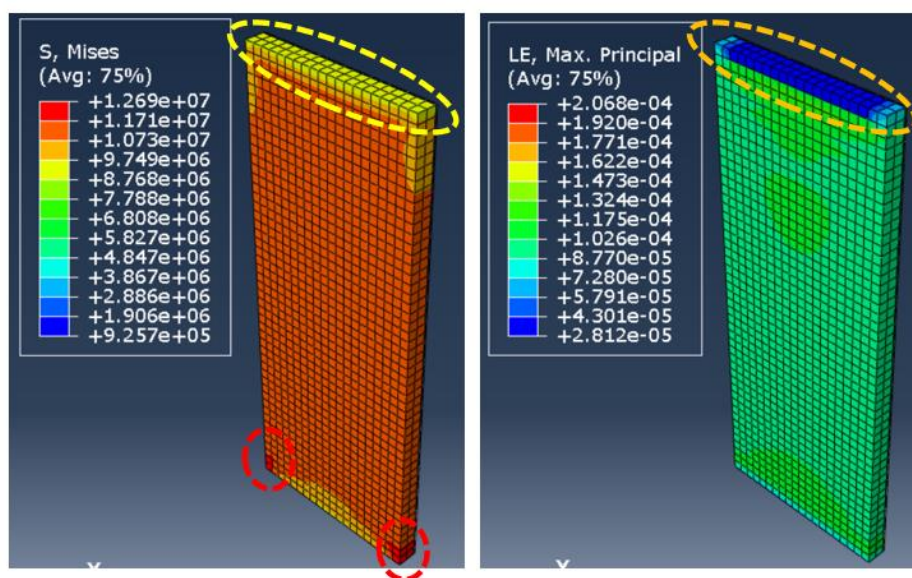
(a) Von Mises Stress

(b) LE Strain

Figure 4.13: Contour plot for the calcium silicate board of 7.5 % Crumb-Wall + CS at the yield point.

Since this research aimed to study the confining effect of calcium silicate board, the front layer calcium silicate board was hidden for having a more precise insight of the stress concentration within the rubberized concrete core panel. As illustrated in Figure 4.14 (a), the red circles denoted the critical yield stress of 12.69 MPa for the rubberized concrete core panel, as mentioned earlier. Figure 4.14 (a) showed that the entire core panel of 7.5 % Crumb-Wall + CS displayed a uniform stress distribution of 11.71 MPa, represented by the red contour plot. A possible explanation may be attributed to the confinement effect of calcium silicate board, which aids in redistributing the stress. The yellow circle in Figure 4.14 (a) indicated that the rubberized concrete core panel exhibited the lowest von Mises stress of 9.75 MPa at the top surface. A possible explanation is that the top surface of the rubberized concrete core panel is not fully restrained, resulting in lowest stress concentration and also lowest strain, as shown in Figure 4.14 (b).





(a) Von Mises Stress

(b) LE Strain

Figure 4.14: Contour plot for the rubberized concrete core panel of 7.5 % Crumb-Wall + CS at the yield point.

The blue circles in Figure 4.15 (a) depicted the location for ultimate compressive stress (9.20 MPa) for the calcium silicate board. The maximum compressive stress developed at the bottom corner of the calcium silicate board could be attributed to the bottom support's restraining effect; the maximum compressive stress developed at the top edge of the calcium silicate board may due to direct contact with the applied loading.

The front layer calcium silicate board was hidden to assess the rubberized concrete core panel's confining effect, as shown in Figure 4.16. Figures 4.16 (a) and (b) showed the location for ultimate compressive stress (26.51 MPa) and ultimate strain (0.0016) for the rubberized concrete core panel of 7.5 % Crumb-Wall + CS. The yellow circles in Figure 4.16 (a) depicted that both the top and bottom half of the core panel were highly stressed with a magnitude of 24.59 MPa. A possible explanation is that the increasing load beyond the yield strength of concrete leads to crack propagation, which results in lower stiffness of the concrete material at the top region of the panel. Thus, high stress concentration developed at the lower region of the core panel as there was less material available to sustain the stress caused by the applied force. Overall, it can be concluded that the location indicated by the red circles for 7.5 % Crumb-Wall + CS in Figure

4.16 (a) were prone to concrete crushing upon reaching ultimate compressive stress.

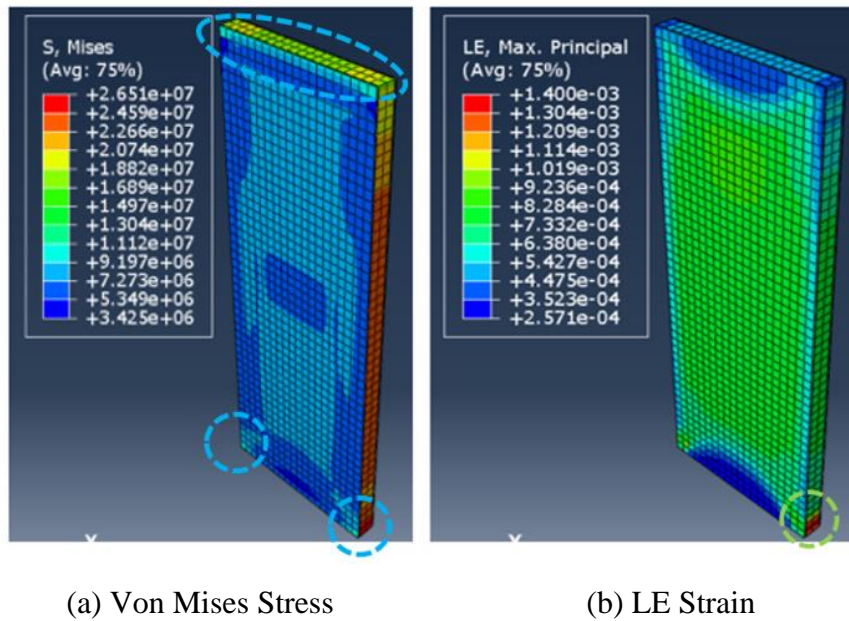


Figure 4.15: Contour plot for the calcium silicate board of 7.5 % Crumb-Wall + CS before failure.

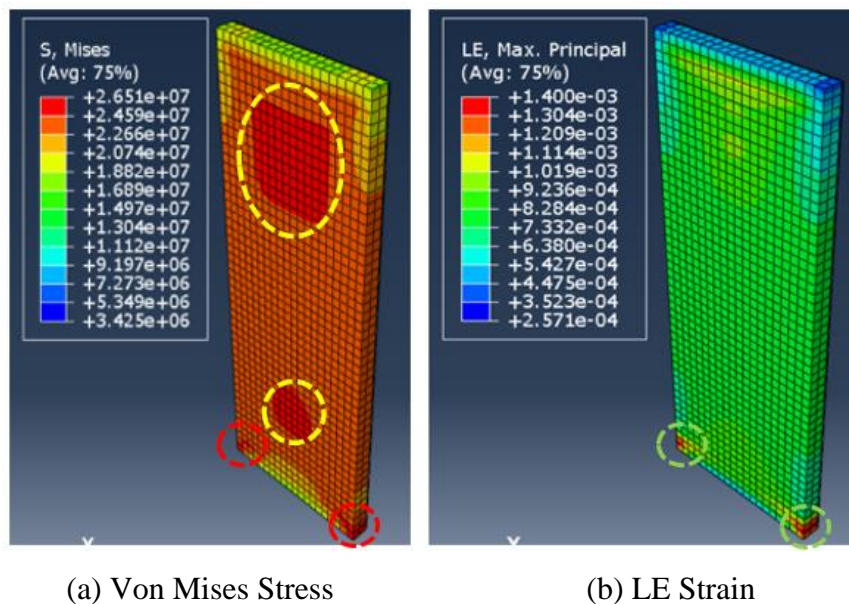


Figure 4.16: Contour plot for the rubberized concrete core panel of 7.5 % Crumb-Wall + CS before failure.



## **4.5 Comparative Study between Control-Wall, 7.5 % Crumb-Wall and 7.5 % Crumb-Wall + CS**

### **4.5.1 Suitability of Concrete Constitutive Model**

Table 4.1 summarised the percentage difference for each model in terms of ultimate compressive stress and ultimate strain. Based on Table 4.2, it appeared that the constitutive model used, concrete smeared cracking, overestimated the ultimate strain for each model. However, the overestimation was due to the use of Nlgeom, as mentioned in previous Chapter 3, to account for material non-linearity and large deformation. The stiffness matrix for a given FE model will be updated constantly after each loading increment. Thus, the numerical value for each model's ultimate strain was more accurate and resembled the model's true nature. According to EN 1992-1-1:2004, Table 3.1, the ultimate strain for normal concrete ( $f_{ck} < 50$  MPa) is given as 0.002. Thus, the numerical value for each model's ultimate strain was deemed valid as it did not exceed 0.002.

The numerical simulation for Control-Wall showed a discrepancy of 2 % for ultimate compressive stress. However, 7.5 % Crumb-Wall exhibited a high percentage discrepancy of 11.43 % in ultimate compressive stress. The high discrepancy was attributed to the low elastic modulus of crumb rubber, which lowered the concrete compressive strength from 30 MPa to 26.57 MPa. The same goes for 7.5 % Crumb-Wall + CS. In other words, concrete smeared cracking was capable of simulating the behaviour of rubberized concrete.

In conclusion, concrete smeared cracking was proven to be a suitable constitutive model together with the use of Nlgeom to simulate the actual mechanical behaviour of precast rubberized lightweight concrete wall panel.

Table 4.1: Percentage difference between numerical and theoretical value for ultimate compressive stress and ultimate strain.

Model	Percentage Difference for Ultimate Compressive Stress (%)	Percentage Difference for Ultimate Strain (%)
Control-Wall	2.00	42.00
7.5 % Crumb-Wall	11.43	22.00
7.5 % Crumb-Wall + CS	11.63	14.29

Table 4.2: Summary of numerical and theoretical value in terms of ultimate compressive stress and ultimate strain.

Model	Numerical Results		Theoretical Results	
	Ultimate Compressive Stress (MPa)	Ultimate Strain	Ultimate Compressive Stress (MPa)	Ultimate Strain
Control-Wall	30.59	0.0017	30.00	0.0012
7.5 % Crumb-Wall	26.57	0.0018	30.00	0.0014
7.5 % Crumb-Wall + CS	26.51	0.0016	30.00	0.0014

#### 4.5.2 Compressive Stress-Strain Behaviour

The compressive stress-strain curve for Control-Wall, 7.5 % Crumb-Wall and 7.5 % Crumb-Wall + CS were presented in Figure 4.17. It was identified that 7.5 % Crumb-Wall had a lower yield stress of 12.7 MPa, but similar yield strain of 0.00013 compared to Control-Wall. The reduction in yield stress was mainly due to extremely low Young's Modulus of crumb rubber compared to mineral aggregates, such as sand and gravel. Siringi (2012) reported that Young's Modulus of crumb rubber generally ranged from 1.24 MPa to 5.17 MPa, which tended to deform more easily. Thus, 7.5 % Crumb-Wall had a lower load-carrying capacity as irrecoverable plastic deformation can occur with lower stress.

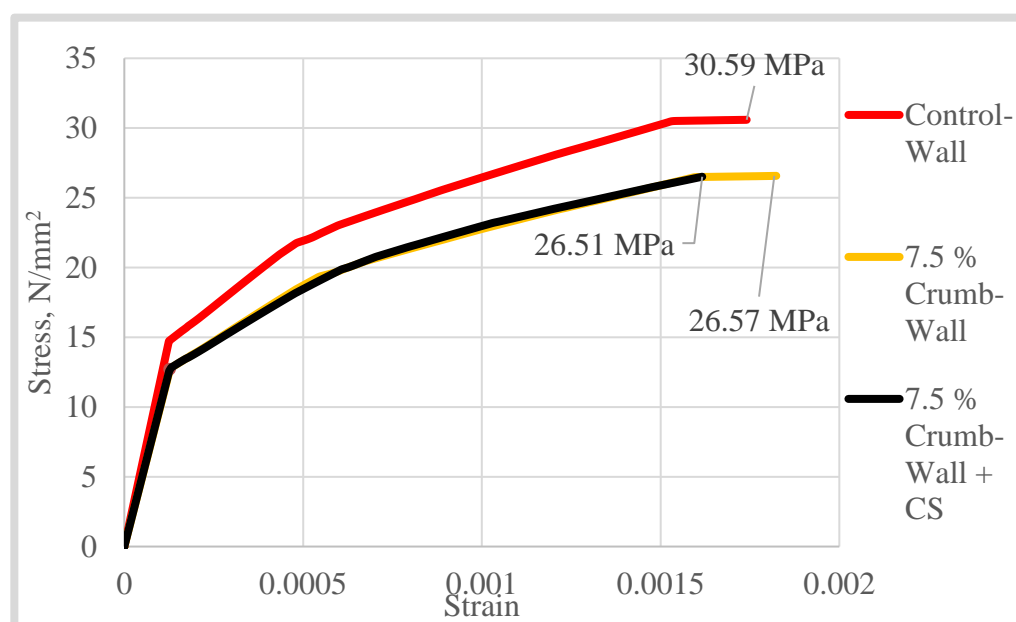


Figure 4.17: Numerical compressive stress-strain graph for Control-Wall, 7.5 % Crumb-Wall and 7.5 % Crumb-Wall + CS.

Figure 4.17 showed that the ultimate compressive stress of 7.5 % Crumb-Wall was 26.57 MPa, which was about 13 % lower than that of Control-Wall, 30.59 MPa. The results proved that the reduction in compressive strength was unavoidable due to the lower elastic modulus of crumb rubber. It should be noted that the ultimate strain of 7.5 % Crumb-Wall in Figure 4.17 was 0.0018, which was 5 % higher than Control-Wall, 0.0017. The results showed good agreement with Hassanli, Youssf and Mills (2017)

findings, whereby the compressive strain capacity of concrete will increase by incorporating crumb rubber. Therefore, 7.5 % Crumb-Wall had reduced compressive strength but improved ductility, whereby it could undergo more considerable plastic deformation without failing.

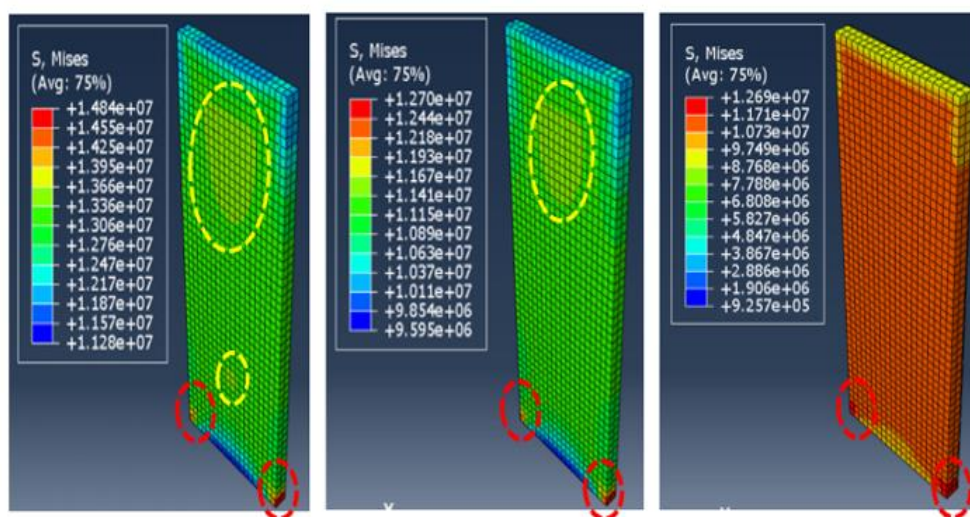
Figure 4.17 showed that both 7.5 % Crumb-Wall and 7.5 % Crumb-Wall + CS had similar yield strength (12.7 MPa) and yield strain (0.00013). The results proved that the yield strength of 7.5 % Crumb-Wall was unaffected despite the calcium silicate board's presence. Figure 4.17 showed that the ultimate compressive stress for 7.5 % Crumb-Wall + CS was 26.51 MPa, which was slightly lower than 7.5 % Crumb-Wall, 26.57 MPa. The reduction in ultimate compressive stress for 7.5 % Crumb-Wall + CS was less than 1 % and can be neglected. Nevertheless, 7.5 % Crumb-Wall + CS had a relatively lower ultimate strain of 0.0016, which was 11 % lower than 7.5 % Crumb-Wall, 0.0018. The reduction in ultimate strain may be attributed to the presence of calcium silicate board, which increased the panel's overall stiffness. Thus, it can be deduced that incorporating calcium silicate board as insulation material can provide moisture protection and insulating effects while retaining rubberized concrete wall panel strength.

### 4.5.3 Stress Distribution

The location of critical yield stress for each model was indicated by the red circles in Figures 4.18 (a), (b) and (c), respectively. As mentioned earlier, the maximum yield stress at the bottom corner may be attributed to the bottom fixed support's restraining effect. The yellow circles in Figure 4.18 (a) depicted that both the top and bottom half of Control-Wall were highly stressed with a magnitude of 13.95 MPa. On the other hand, the yellow circle in Figure 4.18 (b) showed that only the top half of 7.5 % Crumb-Wall was highly stressed with a magnitude of 11.93 MPa. A plausible explanation is that Control-Wall has a higher elastic modulus of 24700 N/mm<sup>2</sup> compared to 7.5 % Crumb-Wall, 20800 N/mm<sup>2</sup>. Thus, the Control-Wall required more stress to create the same amount of strain as 7.5 % Crumb-Wall, resulting in high stress distribution at the lower region of the panel.

Unlike Control-Wall and 7.5 % Crumb-Wall, the entire core panel of 7.5 % Crumb-Wall + CS displayed a uniform stress distribution of 11.71 MPa,

represented by the red contour in Figure 4.18 (c). A possible explanation may be due to the confinement effect of calcium silicate board, which aids in redistributing the stress. Furthermore, it can be observed that the stress concentration at the bottom end of 7.5 % Crumb-Wall + CS (10.73 MPa) was slightly larger than 7.5 % Crumb-Wall (9.60 MPa). A plausible explanation is that the bottom end of 7.5 % Crumb-Wall + CS is stiffer due to the restraining effect of calcium silicate board and bottom fixed support.



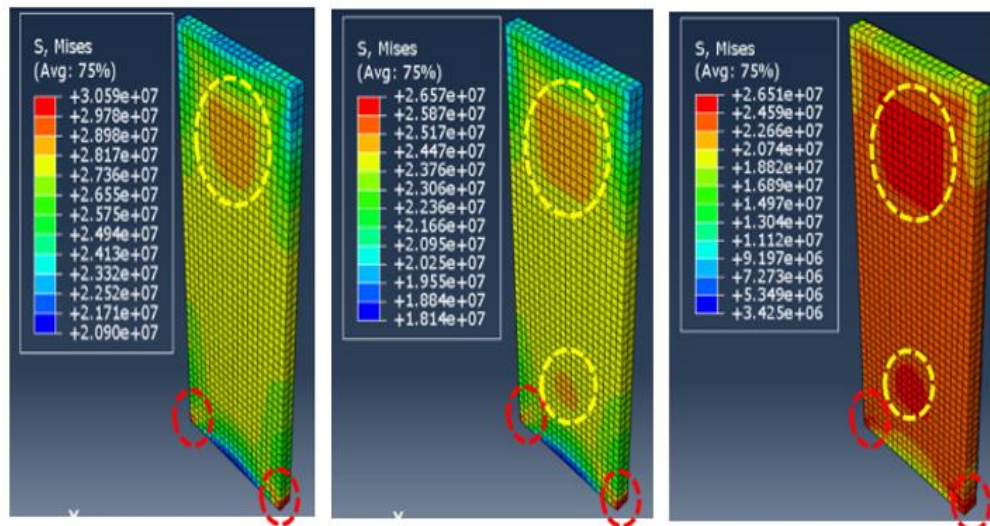
(a) Control-Wall      (b) 7.5 % Crumb-Wall      (c) 7.5 % Crumb-Wall + CS  
Figure 4.18: Contour plot of von Mises stress for each model at the yield point.

The position of ultimate compressive stress for each model was indicated by the red circles in Figures 4.19 (a), (b) and (c), respectively. Since each model had a similar slenderness ratio of 23.81, it was considered to be a non-slender wall, whereby it will collapse due to material failure without undergoing significant lateral deformation. Figures 4.19 (a), (b) and (c) further proved that each model tended to fail at crushing at the lower end corner rather than buckling failure.

Figure 4.19 (a) showed that Control-Wall displayed high von Mises stress of 28.98 MPa at the top half of the panel, as indicated by the yellow circle. However, it should be noted that both the top and bottom half of 7.5 % Crumb-Wall in Figure 4.19 (b) were highly stressed with a magnitude of 25.17 MPa, as represented by the yellow circles. A possible reason is that 7.5 % Crumb-Wall has a lower Young's modulus of 20800 N/mm<sup>2</sup> than Control-

Wall, 24700 N/mm<sup>2</sup>. Therefore, 7.5 % Crumb-Wall tended to deform more compared to Control-Wall under the same amount of stress, resulting in high stiffness degradation of the concrete material at the upper part of the panel. Hence, the lower part of 7.5 % Crumb-Wall experienced high stress as there was less material available to sustain the applied force.

The yellow circles in Figure 4.19 (c) denoted that both the top and bottom half of the core panel of 7.5 % Crumb-Wall + CS were highly stressed, but with a lower magnitude of 24.59 MPa compared to 7.5 % Crumb-Wall, 25.17 MPa. Since a small portion of the applied load had been carried by the calcium silicate board, the core panel exhibited slightly lower stress magnitude compared to 7.5 % Crumb-Wall. However, it should be noted that the stress developed at the bottom end of the core panel for 7.5 % Crumb-Wall + CS (20.74 MPa) was slightly larger than 7.5 % Crumb-Wall (18.14 MPa).



(a) Control-Wall      (b) 7.5 % Crumb-Wall      (c) 7.5 % Crumb-Wall + CS

Figure 4.19: Contour plot of von Mises stress for each model before failure.

## 4.6 Precast Rubberized Lightweight Concrete Wall Panel with Concrete Capping

### 4.6.1 Influence of Slenderness Ratio

The failure mode for 7.5 % Crumb-Wall + CAP upon reaching ultimate compressive stress was presented in Figure 4.20. The 7.5 % Crumb-Wall + CAP exhibited considerable convexity at the lower end compared to 7.5 % Crumb-Wall, as indicated in Figure 4.20. It tended to fail at crushing at the lower end corner rather than the local buckling effect at the panel's mid-height.

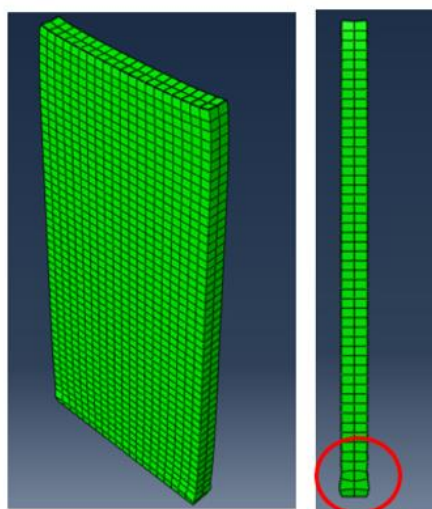


Figure 4.20: Failure model for 7.5 % Crumb-Wall + CAP and the location of concrete bulging.

### 4.6.2 Compressive Strength

The compressive stress-strain graph for both 7.5 % Crumb-Wall and 7.5 % Crumb-Wall + CAP were presented in Figure 4.21. It was identified that the stress-strain curve for both panels exhibited linear elastic behaviour before entering the plastic stage. Figure 4.21 provided clear evidence that both 7.5 % Crumb-Wall and 7.5 % Crumb-Wall + CAP had similar yield strength (12.70 MPa) and yield strain (0.00013). Next, it can be observed that both stress-strain curves became non-linear upon entering the plastic stage. Figure 4.21 showed that the ultimate compressive stress of 7.5 % Crumb-Wall + CAP was 26.53 MPa, where the difference was insignificant compared to that of 7.5 % Crumb-Wall, 26.57 MPa. The drop in ultimate compressive stress for 7.5 % Crumb-Wall + CAP could be attributed to friction losses, which is a

consequence of the rough surface defined between the concrete capping and the panel. Figure 4.21 depicted that the ultimate strain for 7.5 % Crumb-Wall + CAP was 0.0017, which was 5.5 % lower than 7.5 % Crumb-Wall, 0.0018. The lower compressive strain can be attributed to the presence of concrete capping, which slightly increases the panel's overall stiffness. Similar to 7.5 % Crumb-Wall, the 7.5 % Crumb-Wall + CAP exhibited sudden brittle failure upon reaching ultimate compressive stress.

From the study, it was identified that the percentage difference for ultimate compressive stress and ultimate strain of 7.5 % Crumb-Wall + CAP was 11.57 % and 21.43 %, respectively. The difference for the ultimate compressive stress may be attributed to low elastic modulus of crumb rubber that significantly degrades its load-carrying capacity compared to mineral aggregates; the difference for the ultimate strain may due to the use of NIgeom, where the stiffness matrix of the FE model constantly updated.

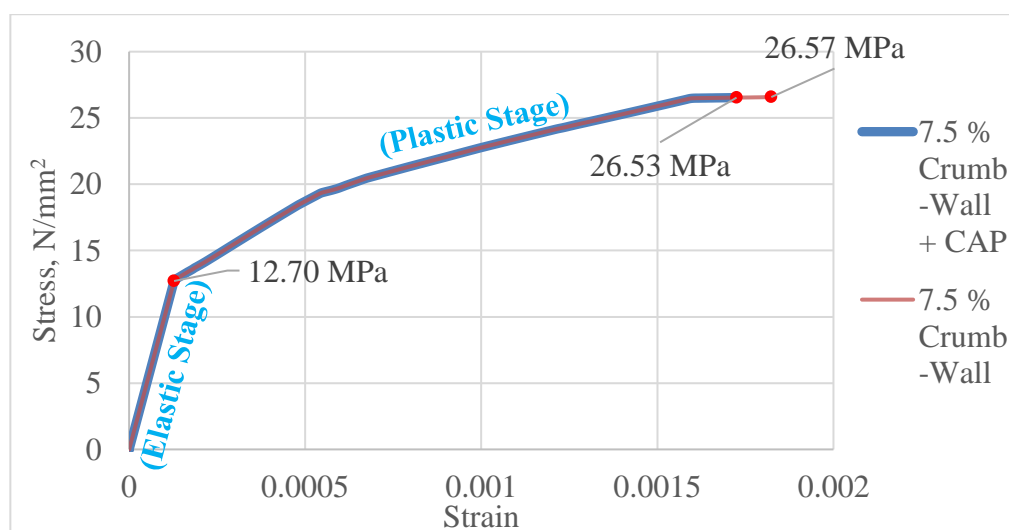


Figure 4.21: Numerical compressive stress-strain curve for 7.5 % Crumb-Wall and 7.5 % Crumb-Wall + CAP.

The position of critical yield stress (12.70 MPa) for 7.5 % Crumb-Wall + CAP was indicated by the red circles in Figure 4.22 (a). The blue circle in Figure 4.22 (b) illustrated the maximum yield strain of 0.00013 that occurred near the panel's bottom end. The maximum yield stress and strain developed at the bottom corner of 7.5 % Crumb-Wall + CAP could be attributed to the bottom support's restraining effect. Figure 4.22 (a) showed that 7.5 % Crumb-



Wall + CAP displayed high von Mises stress of 11.73 MPa at the top half of the panel, as indicated by the yellow circle. A plausible explanation is that the top region of the panel is under compression, which is responsible for sustaining the load from the top surface. Since the concrete capping acted as a medium for transferring the applied load, it appeared to exhibit the slightest pressure of 8 MPa, represented by a dark-blue contour in Figure 4.22 (a).

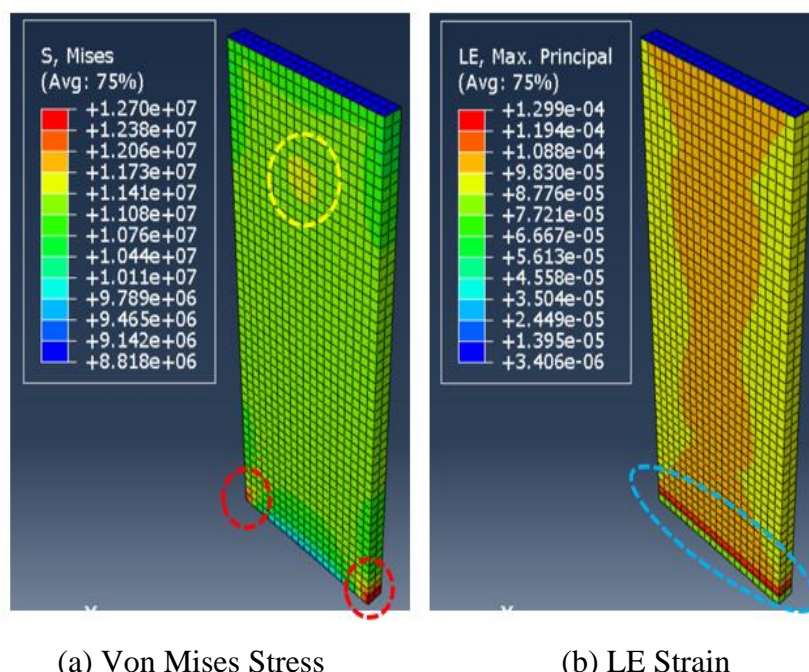
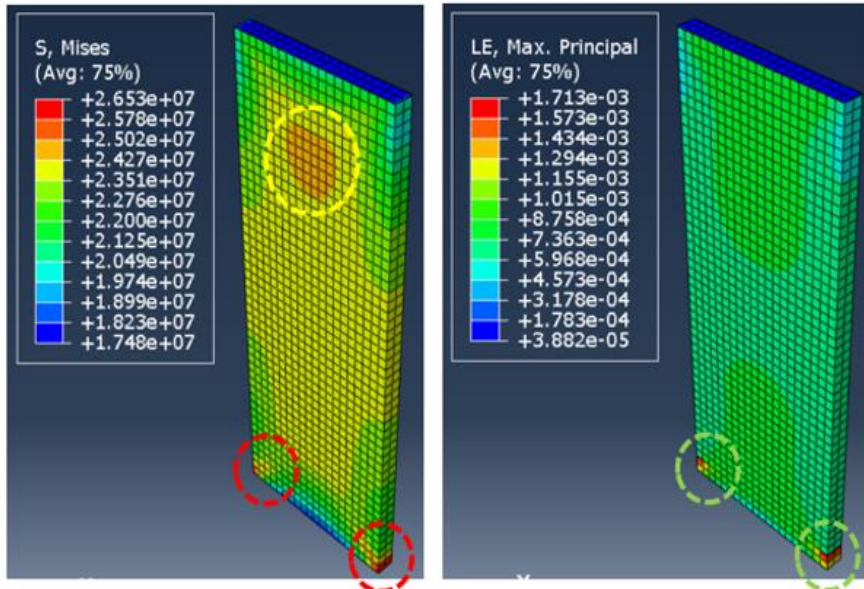


Figure 4.22: Contour plot for 7.5 % Crumb-Wall + CAP at the yield point.

Figures 4.23 (a) and (b) showed the location for ultimate compressive stress (26.53 MPa) and ultimate strain (0.0017) for 7.5 % Crumb-Wall + CAP, respectively. The yellow circle in Figure 4.23 (a) depicted that the top half of 7.5 % Crumb-Wall + CAP was highly stressed with a magnitude of 25 MPa. Furthermore, it can be noticed that both concrete capping and bottom end of 7.5 % Crumb-Wall + CAP exhibited the lowest von Mises stress of 17.48 MPa. A plausible explanation for the lowest stress magnitude at the bottom end may be due to most of the applied force has been taken by the concrete at the top region of the panel. Overall, it can be concluded that the location indicated by the red circles for 7.5 % Crumb-Wall + CAP in Figure 4.23 (a) were prone to concrete crushing upon reaching ultimate compressive stress.

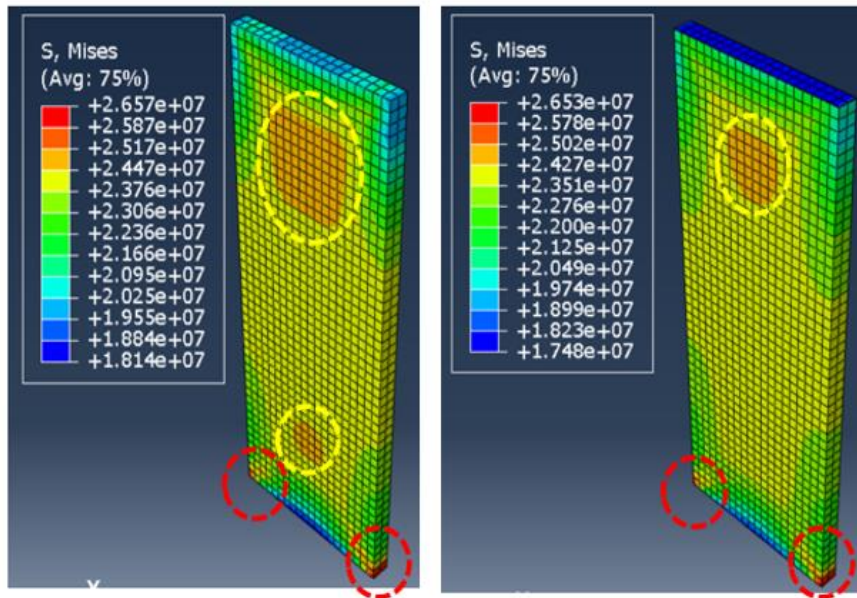


(a) Von Mises Stress

(b) LE Strain

Figure 4.23: Contour plot for 7.5 % Crumb-Wall + CAP before failure.

Figures 4.24 (a) and (b) demonstrated that both panels exhibited ultimate compressive stress at the bottom corner. The yellow circles in Figure 4.24 (a) indicated that both the top and bottom half of 7.5 % Crumb-Wall were highly stressed with a magnitude of 25.17 MPa. It should be noted that only the top half of 7.5 % Crumb-Wall + CAP exhibited high von Mises stress of 25 MPa, as indicated by the yellow circle in Figure 4.24 (b). A plausible explanation is that part of the applied force has been absorbed by the concrete capping or lost due to friction losses, which results in a lower magnitude of stress distribution at the lower part of the panel.



(a) 7.5 % Crumb-Wall

(b) 7.5 % Crumb-Wall + CAP

Figure 4.24: Contour plot of ultimate von Mises stress before failure.

## 4.7 Combination of Three Precast Rubberized Lightweight Concrete Wall Panel

### 4.7.1 Influence of Slenderness Ratio

The failure mode for 7.5 % Crumb-Comb Wall upon reaching ultimate compressive stress was illustrated in Figure 4.25. The 7.5 % Crumb-Comb Wall had considerable convexity at the lower end compared to 7.5 % Crumb-Wall, as indicated in Figure 4.25. It tended to fail at crushing at the lower end corner rather than the local buckling effect at the panel's mid-height.

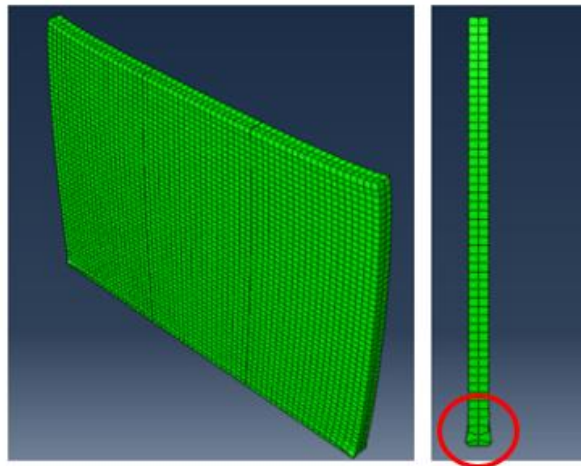


Figure 4.25: Failure mode for 7.5 % Crumb-Comb Wall and the location of concrete bulging.

#### 4.7.2 Compressive Strength

The compressive stress-strain curve for both 7.5 % Crumb-Wall and 7.5 % Crumb-Comb Wall were presented in Figure 4.26. It was identified that both panels exhibited linear elastic behaviour before entering the plastic stage. Figure 4.26 provided clear evidence that both panels had similar yield strength (12.70 MPa) and yield strain (0.00013). Next, it can be observed that both stress-strain curves became non-linear upon entering the plastic stage. Figure 4.26 showed that the ultimate compressive stress for 7.5 % Crumb-Comb Wall was 26.88 MPa, which was slightly higher than 7.5 % Crumb-Wall, 26.57 MPa. The slight increase in the ultimate compressive stress for 7.5 % Crumb-Comb Wall may be attributed to the increased stiffness of the entire combined panel. Figure 4.26 depicted that the ultimate strain for 7.5 % Crumb-Comb Wall had improved from 0.0018 to 0.0027. Similar to 7.5 % Crumb-Wall, the 7.5 % Crumb-Comb Wall exhibited sudden brittle failure upon reaching ultimate compressive stress.

From the study, it was identified that the percentage difference for ultimate compressive stress and ultimate strain of 7.5 % Crumb-Comb Wall was 10.4 % and 43 %, respectively. The difference for the ultimate compressive stress may be attributed to low elastic modulus of crumb rubber that significantly degrades its load-carrying capacity compared to mineral aggregates; the difference for the ultimate strain may due to the use of NIgeom, where the stiffness matrix of the FE model constantly updated.

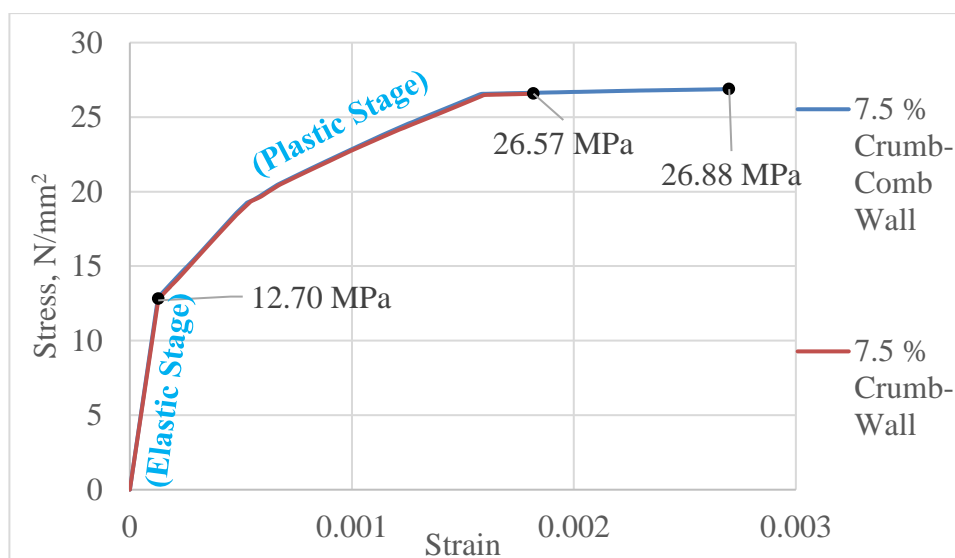
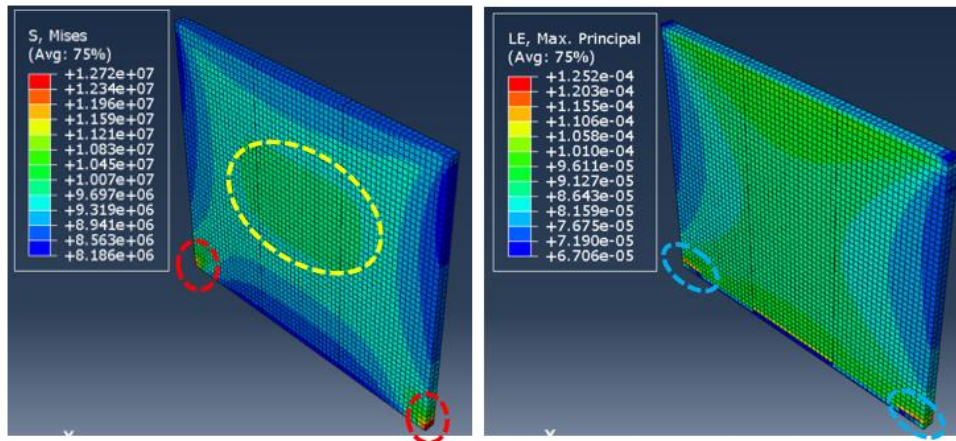


Figure 4.26: Numerical compressive stress-strain curve for 7.5 % Crumb-Wall and 7.5 % Crumb-Comb Wall.

The position of critical yield stress (12.72 MPa) for 7.5 % Crumb-Comb Wall was indicated by the red circles in Figure 4.27 (a). The blue circles in Figure 4.27 (b) illustrated the maximum yield strain of 0.00013 that occurred near the panel's bottom end. The maximum yield stress and strain developed at the bottom corner of 7.5 % Crumb-Wall could be attributed to the bottom support's restraining effect. Figure 4.27 (a) showed that the middle panel of 7.5 % Crumb-Comb Wall displayed high von Mises stress at the mid-height, as indicated by the yellow circle, ranging from 9.32 MPa to 11.21 MPa. A plausible explanation is that the middle panel has a higher lateral stiffness due to the restraining effect by the side panels. It should be noted that lowest von Mises stress occurred at the sides and top and bottom surfaces of 7.5 % Crumb-Comb Wall, represented by a dark-blue contour plot with a magnitude of 8.19 MPa. A plausible explanation is that most of the applied force has been taken by the middle panel, resulting in lower stress magnitude at the highlighted areas.



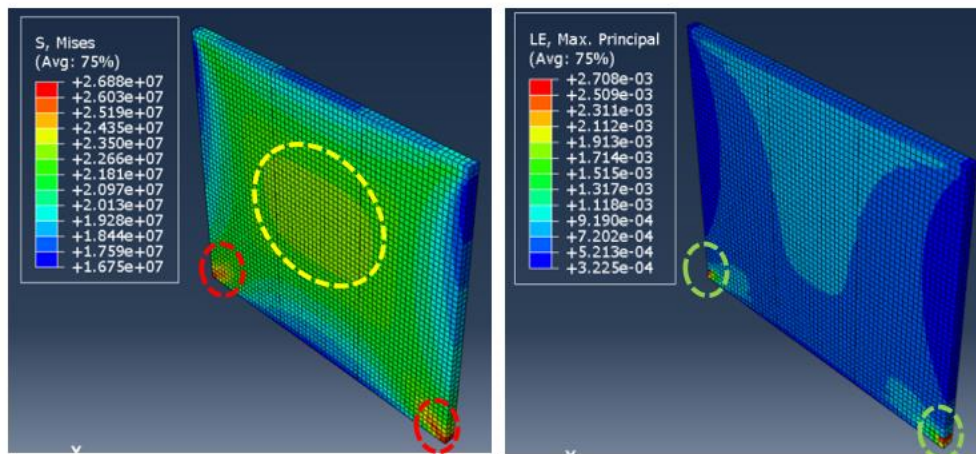


(a) Von Mises Stress

(b) LE Strain

Figure 4.27: Contour plot for 7.5 % Crumb-Comb Wall at the yield point.

Figures 4.28 (a) and (b) showed the location for ultimate compressive stress (26.88 MPa) and ultimate strain (0.0027) for 7.5 % Crumb-Comb Wall, respectively. The yellow circle in Figure 4.28 (a) depicted that the middle panel of 7.5 % Crumb-Comb Wall displayed high von Mises stress of 24.35 MPa at the mid-height. It was identified that the side panels were more crucial than the middle panels as the side panels exhibited concrete crushing failure at the bottom corner upon reaching the ultimate load. Figure 4.28 (a) proved that 7.5 % Crumb-Comb Wall did not collapse due to connection failure but crushing failure at the bottom corner. Although the simulation showed that the connections between panels behaved satisfactorily, the wall panels need to be appropriately tied during construction.



(a) Von Mises Stress

(b) LE Strain

Figure 4.28: Contour plot for 7.5 % Crumb-Comb Wall before failure.

#### **4.8 Summary**

In summary, the comparison between numerical and theoretical results demonstrate that concrete smeared cracking is capable of simulating both plain concrete and rubberized concrete under elastic and plastic range. However, the large discrepancy associated to ultimate strain is attributed to the use of Nlgeom, whereby the stiffness matrix of a given FE model will be constantly updated, results in higher ultimate strain. Next, a comparative study is conducted to determine the effect of crumb rubber as partial fine aggregate replacement on the compressive strength of precast concrete wall panel. Furthermore, separate rubberized concrete wall panel with calcium silicate board and concrete capping are modelled to evaluate the confining effect. Lastly, a combined wall panel is modelled, which comprises three single rubberized concrete wall panels to assess its actual behaviour in real-life practice.

## CHAPTER 5

### CONCLUSION AND RECOMMENDATIONS

#### 5.1 Conclusion

Based on the FEA results generated from ABAQUS, the following conclusions can be made corresponding to the objectives of the study.

The first objective is to determine suitable constitutive model for simulating the actual mechanical behaviour of precast rubberized lightweight concrete wall panel. Concrete smeared cracking was proven to be a suitable constitutive model together with the use of Nlgeom.

The second objective is to study the effect of crumb rubber as partial fine aggregate replacement on the compressive strength of precast concrete wall panel. It was identified that at 7.5 % crumb rubber replacement, the ultimate compressive strength reduced by 13 %, followed by an improvement in ultimate strain by 5 %. Both control sample and rubberized concrete wall panel exhibited concrete crushing failure at the bottom corner upon reaching ultimate compressive stress. Besides, the top and bottom half of the rubberized concrete wall panel were also highly stressed, unlike the control sample, which had only the top half of the panel with high-stress concentration. Overall, it can be concluded that the precast concrete wall panel with 7.5 % of crumb rubber as partial fine aggregate replacement had reduced compressive strength but improved ductility, whereby it could sustain more plastic deformation before failing.

The third objective is to evaluate the confinement effect on precast rubberized lightweight concrete wall panel by modelling separate rubberized concrete wall panels with concrete capping and calcium silicate board. Both the rubberized concrete wall panel yield stress and yield strain were unaffected despite the calcium silicate board's presence. However, there was a slight drop in ultimate compressive strength from 26.57 MPa to 26.51 MPa. Thus, the reduction in ultimate compressive strength was less than 1 % and can be neglected. Moreover, there was also an 11 % reduction in ultimate strain from 0.0018 to 0.0016. Upon reaching ultimate compressive stress, the rubberized



concrete core panel exhibited concrete crushing failure at the bottom corner. Although both the top and bottom half of the core panel were also highly stressed but with a lower stress magnitude than 7.5 % Crumb-Wall. Since a small portion of the applied load had been carried by the calcium silicate board, the core panel exhibited slightly lower stress magnitude. The bottom end of the core panel for 7.5 % Crumb-Wall + CS exhibited a larger stress magnitude than 7.5 % Crumb-Wall.

Next, both the rubberized concrete wall panel yield stress and yield strain were unaffected despite the concrete capping's presence. However, there was a slight drop in ultimate compressive strength from 26.57 MPa to 26.53 MPa. The reduction in ultimate compressive strength was less than 1 % and can be neglected. The presence of concrete capping had also led to a drop in ultimate strain by 5 %. Upon reaching ultimate compressive stress, 7.5 % Crumb-Wall + CAP exhibited concrete crushing failure at the bottom corner. Besides, the top half of 7.5 % Crumb-Wall + CAP was also highly stressed, unlike 7.5 % Crumb-Wall.

The last objective is to evaluate the mechanical behaviour of combined precast rubberized lightweight concrete wall panel. It was identified that both yield stress and yield strain for 7.5 % Crumb-Comb Wall remained the same as 7.5 % Crumb-Wall. The numerical results underlined that combined rubberized concrete wall panels had led to an improvement in ultimate strain from 0.0018 to 0.0027. Besides, there was also a slight increase in ultimate compressive strength of 7.5 % Crumb-Comb Wall from 26.57 MPa to 26.88 MPa. The side panels were more crucial than the middle panels as the side panels exhibited concrete crushing failure at the bottom corner upon reaching the ultimate load. Lastly, 7.5 % Crumb-Comb Wall did not collapse due to connection failure but crushing failure at the bottom corner.

Overall, this research has highlighted that ABAQUS is a powerful numerical tool that allows in-depth understanding on the stress distribution and the failure mechanism of precast rubberized lightweight concrete wall panel.

## **5.2 Limitations and Recommendations for Future Research**

Due to the ongoing Covid-19 pandemic, the material parameters for both plain concrete and rubberized concrete were extracted from Siringi (2012). Thus, this study did not consider crumb rubber replacement beyond 7.5 %. Further FE modelling of the rubberized concrete wall panel with a higher crumb rubber replacement rate would then be required.

Next, it is recommended to conduct further study on wall panel with different slenderness ratio. It should be noted that the current study only focused on the non-slender wall panel, whereby the failure mode is governed by material failure rather than buckling failure. Thus, the impact of crumb rubber on the failure mode of slender wall panel was not taken into account.

Since the wall panels in actual practice are constantly subjected to wind load, the transverse load test could be carried out for precast rubberized lightweight concrete wall panel to assess its lateral load capacity.

## REFERENCES

- Al-Azzawi, A.A., Shakir, D. and Saad, N., 2018. Flexural behavior of rubberized reinforced concrete beams. *International Journal of Engineering & Technology*, 7(4.20), pp.316-320.
- Al-Fakih, A., Wahab, M.M.A., Mohammed, B.S., Liew, M.S., Zawawi, N.A.W.A. and As'ad, S., 2020. Experimental study on axial compressive behavior of rubberized interlocking masonry walls. *Journal of Building Engineering*, [e-journal] 29, pp.101-107. <https://doi.org/10.1016/j.jobe.2019.101107> .
- Al-Shwaiter, A. and Al-Gaboby, Z., 2019. Behavior of rubberized concrete-filled square steel tube under axial loading. *Journal of Science and Technology*, [e-journal] 24(1), pp.23–39. <https://doi.org/10.20428/JST.24.1.2> .
- American Society for Testing and Materials, 2015. *ASTM E72 : Standard test methods of conducting strength tests of panels for building construction*. Conshohocken, Pennsylvania, United States: ASTM International.
- Azmi, A.A., Abdullah, M.M.A.B., Ghazali, C.M.R., Sandu, A.V. and Hussin, K., 2015. A review - manufacturing on rubberized concrete filled recycled tire rubber. *Key Engineering Materials*, [e-journal] 660(October), pp.249–253. <https://doi.org/10.4028/www.scientific.net/KEM.660.249> .
- Batayneh, M.K., Marie, I. and Asi, I., 2008. Promoting the use of crumb rubber concrete in developing countries. *Waste Management*, [e-journal] 28(11), pp.2171–2176. <https://doi.org/10.1016/j.wasman.2007.09.035> .
- Bing, C. and Ning, L., 2014. Experimental research on properties of fresh and hardened rubberized concrete. *Journal of Materials in Civil Engineering*, [e-journal] 26(8), pp.1–8. [https://doi.org/10.1061/\(ASCE\)MT.1943-5533.0000923](https://doi.org/10.1061/(ASCE)MT.1943-5533.0000923) .
- Chaudhari, S.V. and Chakrabarti, M.A., 2012. Modeling of concrete for nonlinear analysis using finite element code ABAQUS. *International Journal of Computer Applications*, 44(7), pp.14–18.
- Chiew, S.M., Ibrahim, I.S., Sarbini, N.N., Mohamed, R.N. and Jamaluddin, N., 2019. Comparison of biaxial tensile behaviour of plain and steel fibre reinforced concrete (SFRC) with different testing techniques. *Malaysian Construction Research Journal*, 6(1), pp.193–203.
- Dassault Systèmes, 2014. *ABAQUS 6.14 analysis user's guide volume III: materials*.

Drobiec, Ł., 2017. FEM model of the masonry made of hollow calcium silicate units. *Procedia Engineering*, [e-journal] 193, pp.462–469. <http://dx.doi.org/10.1016/j.proeng.2017.06.238> .

Duarte, A.P.C., Silva, B.A., Silvestre, N., De Brito, J. and Júlio, E., 2015. Mechanical characterization of rubberized concrete using an image-processing/XFEM coupled procedure. *Composites Part B: Engineering*, [e-journal] 78, pp.214–226. <http://dx.doi.org/10.1016/j.compositesb.2015.03.082> .

Duarte, A.P.C., Silva, B.A., Silvestre, N., De Brito, J., Júlio, E. and Castro, J.M., 2016. Finite element modelling of short steel tubes filled with rubberized concrete. *Composite Structures*, [e-journal] 150, pp.28–40. <http://dx.doi.org/10.1016/j.compstruct.2016.04.048> .

Duarte, A.P.C., Silvestre, N., De Brito, J. and Júlio, E., 2017. Numerical study of the compressive mechanical behaviour of rubberized concrete using the Extended Finite Element Method (XFEM). *Composite Structures*, [e-journal] 179, pp.132–145. <http://dx.doi.org/10.1016/j.compstruct.2017.07.048> .

Ekaputri, J.J., Triwulan, T., Brahmantyo, D. and Nasir, F.R.S., 2013. Optimization of pressure and curing time in producing autoclaved aerated concrete. *6th Civil Engineering Conference in Asia Region: Embracing the Future through Sustainability*, [e-journal], pp.51–56. <http://dx.doi.org/10.13140/2.1.2505.6964> .

Eltayeb, E., Ma, X., Zhuge, Y., Osama, Y. and Mills, J.E., 2020. Influence of rubber particles on the properties of foam concrete. *Journal of Building Engineering*, [e-journal] 30, pp.1–13. <https://doi.org/10.1016/j.jobe.2020.101217> .

European Committee for Standardization, 2016. *EN 13055:2016 Lightweight Aggregates*.

European Committee for Standardization, 2004. *EN 1992-1-1:2004 Design of concrete structures - part 1-1: general rules and rules for buildings*.

Fiore, A., Marano, G.C., Marti, C. and Molfetta, M., 2014. On the fresh/hardened properties of cement composites incorporating rubber particles from recycled tires. *Advances in Civil Engineering*, [e-journal] 2014, pp.1–12. <http://dx.doi.org/10.1155/2014/876158> .

Gombeda, M.J., Quiel, S.E. and Naito, C.J., 2019. Development and performance of a ductile shear tie for precast concrete insulated wall panels. *Journal of Building Engineering*, [e-journal], pp.1–45. <https://doi.org/10.1016/j.jobe.2019.101084> .

Gregori, A., Castoro, C., Mercuri, M. and Angiolilli, M., 2021. Numerical modelling of the mechanical behaviour of rubbercrete. *Computers and Structures*, [e-journal] 242, pp.1–12. <https://doi.org/10.1016/j.compstruc.2020.106393> .

Hassanli, R., Youssf, O. and Mills, J.E., 2017. Experimental investigations of reinforced rubberized concrete structural members. *Journal of Building Engineering*, [e-journal] 10, pp.149–165. <http://dx.doi.org/10.1016/j.jobte.2017.03.006> .

Hoff, G.C., 2002. *Guide for the use of low-density concrete in civil works projects*.

Hofko, B., Eberhardsteiner, L., Füssl, J., Grothe, H., Handle, F., Hospodka, M., Grossegger, D., Nahar, S.N., Schmets, A.J.M. and Scarpas, A., 2016. Impact of maltene and asphaltene fraction on mechanical behavior and microstructure of bitumen. *Materials and Structures*, [e-journal] 49(3), pp.829–841. <http://dx.doi.org/10.1617/s11527-015-0541-6> .

Ibrahim, M.R., Katman, H.Y., Karim, M.R., Koting, S. and Mashaan, N.S., 2013. A review on the effect of crumb rubber addition to the rheology of crumb rubber modified bitumen. *Advances in Materials Science and Engineering*, [e-journal] 2013, pp.1-8. <http://dx.doi.org/10.1155/2013/415246> .

Jalal, M., Tanveer, A., Jagdeesh, K. and Ahmed, F., 2017. Foam Concrete. *International Journal of Civil Engineering Research*, 8(1), pp.1–14.

Kumaran, G.S., Mushule, N. and Lakshmipathy, M., 2008. A review on construction technologies that enables environmental protection : rubberized concrete. *American J. of Engineering and Applied Sciences*, 1(1), pp.40–44.

Li, L., Ruan, S. and Zeng, L., 2014. Mechanical properties and constitutive equations of concrete containing a low volume of tire rubber particles. *Construction and Building Materials*, [e-journal] 70, pp.291–308. <http://dx.doi.org/10.1016/j.conbuildmat.2014.07.105> .

Ling, T.C., 2011. Prediction of density and compressive strength for rubberized concrete blocks. *Construction and Building Materials*, [e-journal] 25(11), pp.4303–4306. <http://dx.doi.org/10.1016/j.conbuildmat.2011.04.074> .

Mohamad, N., Goh, W.I., Abdullah, R., Samad, A.A.A., Mendis, P. and Sofi, M., 2017. Structural performance of FCS wall subjected to axial load. *Construction and Building Materials*, [e-journal] 134, pp.185–198. <http://dx.doi.org/10.1016/j.conbuildmat.2016.12.133> .

Newman, J. and Choo, B.S., 2003. *Advanced Concrete Technology Processes*. [e-book] Great Britain: Butterworth-Heinemann. Available at: Google Books <[https://books.google.com.my/books?hl=en&lr=&id=wTqMFyczxngC&oi=fnd&pg=PP1&dq=Advanced+Concrete+Technology+Processes+newman&ots=8jBEw7HD7f&sig=ZYuQa9CPAzU9F5IIV4XQVeiCFE&redir\\_esc=y#v=onepage&q=Advanced%20Concrete%20Technology%20Processes%20newman&f=false](https://books.google.com.my/books?hl=en&lr=&id=wTqMFyczxngC&oi=fnd&pg=PP1&dq=Advanced+Concrete+Technology+Processes+newman&ots=8jBEw7HD7f&sig=ZYuQa9CPAzU9F5IIV4XQVeiCFE&redir_esc=y#v=onepage&q=Advanced%20Concrete%20Technology%20Processes%20newman&f=false)> [Accessed 8 August 2020].

Panda, K.C., Parhi, P.S. and Jena, T., 2012. Scrap-Tyre-Rubber replacement for aggregate in cement concrete: Experimental study. *International Journal of Earth Sciences and Engineering*, 5(06(01)), pp.1692–1701.

- Panesar, D.K., 2013. Cellular concrete properties and the effect of synthetic and protein foaming agents. *Construction and Building Materials*, [e-journal] 44, pp.575–584. <http://dx.doi.org/10.1016/j.conbuildmat.2013.03.024> .
- Promat, 2014. *Calcium silicate insulation*. Malaysia: ETEX.
- Saand, A., Tariq, A., Ali Keerio, M. and Khan Bangwar, D., 2019. Experimental study on the use of rice husk ash as partial cement replacement in aerated concrete. *Engineering, Technology & Applied Science Research*, 9(4), pp.4534–4537.
- Segre, N. and Joekes, I., 2000. Use of tire rubber particles as addition to cement paste. *Cement and Concrete Research*, 30(9), pp.1421–1425.
- Sgobba, S., Marano, G.C., Borsa, M. and Molfetta, M., 2010. Use of rubber particles from recycled tires as concrete aggregate for engineering applications. *2nd International Conference on Sustainable Construction Materials and Technologies*, (January), pp.465–475.
- Siringi, G.M., 2012. *Properties of concrete with tire derived aggregate and crumb rubber as lightweight substitute for mineral aggregates in the concrete mix*. PhD. The University of Texas At Arlington.
- Sofi, A., 2018. Effect of waste tyre rubber on mechanical and durability properties of concrete – a review. *Ain Shams Engineering Journal*, [e-journal] 9(4), pp.2691–2700. <https://doi.org/10.1016/j.asej.2017.08.007> .
- Sol-Sánchez, M., Thom, N., Moreno-Navarro, F., Rubio-Gámez, M. and Airey, G., 2015. A study into the use of crumb rubber in railway ballast. *Construction and Building Materials*, [e-journal] 75, pp.19–24. <http://dx.doi.org/10.1016/j.conbuildmat.2014.10.045> .
- Strukar, K., Šipoš, T.K., Dokšanović, T. and Rodrigues, H., 2018. Experimental study of rubberized concrete stress-strain behavior for improving constitutive models. *Materials*, [e-journal] 11(11), pp.1-23. <https://doi.org/10.3390/ma11112245> .
- Thomas, B.S., Gupta, R.C. and Panicker, V.J., 2015. Experimental and modelling studies on high strength concrete containing waste tire rubber. *Sustainable Cities and Society*, [e-journal] 19, pp.68–73. <http://dx.doi.org/10.1016/j.scs.2015.07.013> .
- Vaghei, R., Hejazi, F., Taheri, H., Jaafar, M.S. and Ali, A.A.A., 2014. Evaluate Performance of Precast Concrete Wall to Wall Connection. *APCBEE Procedia*, [e-journal] 9, pp.285–290. <http://dx.doi.org/10.1016/j.apcbec.2014.01.051> .
- Wang, R., Gao, P., Tian, M. and Dai, Y., 2019. Experimental study on mechanical and waterproof performance of lightweight foamed concrete mixed with crumb rubber. *Construction and Building Materials*, [e-journal] 209, pp.655–664. <https://doi.org/10.1016/j.conbuildmat.2019.03.157> .

Xu, X., Zhang, Z., Hu, Y. and Wang, X., 2020. Bearing strength of crumb rubber concrete under partial area loading. *Materials*, [e-journal] 13(11), pp.1–26. <https://doi.org/10.3390/MA13112446> .

Yu, C., Hoogenboom, P. and Rots, J., 2021. Extension of incremental sequentially linear analysis to geometrical non-linearity with indirect displacement control. *Engineering Structures*, [e-journal] 229. <https://doi.org/10.1016/j.engstruct.2020.111562> .

Zheng, L., Huo, X.S. and Yuan, Y., 2008. Strength, modulus of elasticity, and brittleness index of rubberized concrete. *Journal of Materials in Civil Engineering*, [e-journal] 20(11), pp.692–699. [https://doi.org/10.1061/\(ASCE\)0899-1561\(2008\)20](https://doi.org/10.1061/(ASCE)0899-1561(2008)20) .